Czech Technical University in Prague
Faculty of Nuclear Sciences and Physical Engineering

Department of Physics
Field of Study: Experimental Nuclear and Particle Physics

Multiplicity fluctuations and resonances in heavy-ion collisions

MASTER'S THESIS

Author: Bc. Josef Uchytil
Supervisor: prof. Dr. Boris Tomášik
Academic Year: 2018/2019

České vysoké učení technické v Praze
Fakulta jaderná a fyzikálně inženýrská

Katedra fyziky
Obor: Experimentální jaderná a částicová fyzika

Fluktuace multiplicity a rezonance ve srážkách těžkých iontů

DIPLOMOVÁ PRÁCE

Vypracoval: Bc. Josef Uchytil
Vedoucí práce: prof. Dr. Boris Tomášik

Akademický rok: 2018/2019

PŘEDNÍ STRANA ZADÁNÍ

ZADNÍ STRANA ZADÁNÍ

Prohlášení

Prohlašuji, že jsem svou diplomovou práci vypracoval samostatně a použil jsem pouze podklady (literaturu, projekty) uvedené v přiloženém seznamu.

Nemám závažný důvod proti použití tohoto školního díla ve smyslu § 60 Zákona č. 121/200 Sb., o právech souvisejících s právem autorským a o změně některých zákonů (autorský zákon).

V Praze dne 7. 1. 2019

....
Bc. Josef Uchytil

Poděkování

Děkuji prof. Dr. Borisi Tomášikovi za vedení mé diplomové práce a podnětné návrhy, které ji obohatily.

Bc. Josef Uchytil

Title:
Multiplicity fluctuations and resonances in heavy-ion collisions

Author: Bc. Josef Uchytil

Field of Study: Experimental Nuclear and Particle Physics
Kind of paper: Master's Thesis

Supervisor: prof. Dr. Boris Tomášik
Katedra fyziky, Fakulta jaderná a fyzikálně inženýrská, České vysoké učení technické v Praze

Abstract:
The number of particles produced in ultra-relativistic nucleus-nucleus collisions is well described by the statistical model. In this model, the particle yields depend on temperature and chemical potential. However, statistical physics can also predict multiplicity fluctuations, which can subsequently be compared to experimental data. The aim of this thesis is to provide information on how to compute multiplicity fluctuations along with higher moments of the multiplicity distribution using the central statistical moments. Furthermore, said moments of the multiplicity distribution in a hadron resonance gas model will be investigated for both the chemical equilibrium and the chemical non-equilibrium, where the generation of temperature-dependent chemical potentials for each stable particle species is assumed. Finally, the results in form of the temperature dependence of the moments of the proton number distribution at chemical non-equilibrium will be introduced for relevant cool-down scenarios based on the data from the RHIC BES programme.

Key words: Heavy-ion collisions, Statistical model, Central moments, Multiplicity fluctuations, Chemical non-equilibrium

Název práce:
Fluktuace multiplicity a rezonance ve srážkách těžkých iontů

Autor: Bc. Josef Uchytil

Obor: Experimentální jaderná a částicová fyzika
Druh práce: Diplomová práce

Vedoucí práce: prof. Dr. Boris Tomášik
Katedra fyziky, Fakulta jaderná a fyzikálně inženýrská, České vysoké učení technické v Praze

Abstrakt:
Počty částic produkované v ultrarelativistických jaderných srážkách jsou dobře popsány statistickým modelem. V tomto modelu závisí výtěžky na teplotě a chemickém potenciálu. Statistická fyzika však dokáže předpovědět i fluktuace multiplicity. Ty pak mohou být porovnány s daty z experimentu. Cílem této práce je poskytnout informace o výpočtu fluktuací multiplicity a vyšších momentů rozdělení multiplicity za použití centrálních statistických momentů. Budou představeny metody výpočtů fluktuací multiplicity ve statistickém modelu nejprve pro chemickou rovnováhu, poté i pro chemickou nerovnováhu, při které předpokládáme generování chemických potenciálů pro každý stabilní druh částic v závislosti na teplotě. Závěrem budou představeny výsledky výpočtu momentů rozdělení protonového čísla v závislosti na teplotě pro scénáře chlazení relevantní pro ultrarelativistické jaderné srážky z programu RHIC BES.

Klíčová slova: Těžko-iontové srážky, statistický model, centrální momenty, fluktuace multiplicity, chemická nerovnováha

Contents

List of Figures

Introduction

The number of particles produced in ultra-relativistic nucleus-nucleus collisions is well described by the statistical model. In this model, the particle yields depend on temperature and chemical potentials. In this thesis, we will describe the computation of higher moments of the multiplicity distribution along with their implementation in the heavy-ion collisions. For this, we will use a method based on central statistical moments. Furthermore, we will provide the temperature dependence of the moments of the proton number distribution at chemical non-equilibrium for relevant cool-down scenarios based on the data from the RHIC BES programme.

In **Chapter 1**, the concept of the Quark-Gluon Plasma (QGP) will be introduced and the main motivation for using multiplicity fluctuations along with the statistical approach will be laid down.

In **Chapter 2**, the statistical moments will be formally introduced, defined and elaborated. We will focus on the first four central moments especially, as those are the most important ones when considering the heavy-ion collisions. They are called **mean (M), variance (σ^2), skewness (S) and kurtosis (κ)** and they - along with the respective products of said moments - contribute significantly to a better understanding of the heavy-ion collisions and the subsequent particle production, which will also be emphasized in the text. Also, the canonical and grandcanonical formalism will be introduced as well as the so-called "scaled variance" which is widely used when describing fluctuations specifically.

In **Chapter 3**, the topic of chemical equilibrium and the fluctuations therein will be elaborated. Subsequently, the fluctuations in a hadron resonance gas model will be introduced and the corresponding thermodynamic susceptibilites will be defined and the first four cumulants in the ideal hadron gas will be written down. At the end of this Chapter, the loss of chemical equilibrium and the chemical freeze-out parametrization will be dealt with and the effect of resonance decays will be taken into account, which includes the generalization of the first four cumulants in the ideal hadron gas for the case that the effect of resonance decays is assumed.

In **Chapter 4**, the formalism laid down in Chapter 3 will be further generalized in order to account for the case of chemical non-equilibrium, which is characterized by all stable particle species having their own chemical potential. The calculation of said potentials will be introduced. We will reintroduce the formula for the particle pressure and adjust it to the state of chemical non-equilibrium. Furthermore, we will write down the formulae for the (net)-baryon and (net-)proton number density as well as particle fluctuations thereof expressed as the scaled variance along with the products $S\sigma$ and $\kappa\sigma^2$, all while accounting for the state of chemical non-equilibrium using the generalized particle pressure formula. These formulae will be presented as functions of temperature.

In **Chapter 5**, the results of the performed calculations will be introduced for the first four moments of the proton number distribution. The temperature dependence of the proton number density, the scaled variance σ^2/M and the products $S\sigma$ and $\kappa\sigma^2$ will be plotted for the most central collisions (centralities 0-5, 5-10) using data from the beam energy scan program (BES) at RHIC. The calculations will be performed for seven collision energies for both centralities, which are characterized by their respective freeze-out parametres.

Chapter 1

Quark-Gluon Plasma and Heavy Ion Collisions within the Statistical Model

The main goal of Heavy Ion Collisions is the study of nuclear matter at high energy density. This is of particular interest when investigating the properties of hadronic matter and of the Quark-Gluon Plasma region (QGP), which is assumed to have existed during the first few microseconds after the Big Bang, for which the existence of a highly dense region is necessary within the laboratory.

The term "Heavy Ions" means that extremely heavy atomic nuclei are used, whereas "ultrarelativistic energy" stands for the energy regime where the kinetic energy exceeds the rest energy significantly [1]. This energy range makes high energy collisions a perfect tool for studying smaller objects, i. e. subatomic particles, successfully providing the basis for **particle physics**. On the other hand, low energy collisions are suitable for describing more complex compound object, i. e. nuclei, thus laying ground for **nuclear physics**.

The main aim of this Chapter is to introduce the concept of the QGP with the emphasis on its **thermodynamical** or **statistical** approach.

1.1 Quark-Gluon Plasma

The Quark-Gluon Plasma (QGP) is a state of matter where partons are *deconfined*, i. e. not confined in hadrons. Deconfinement is phenomenologically (i. e. within the QCD framework) defined as a phase transition. Furthermore, this state of matter is believed to have existed during the earliest state of the Universe ($\sim 10\ \mu$s after the Big Bang [19]). Under certain special circumstances, said state may also emerge in ultrarelativistic heavy-ion collisions. However, its existence is limited to a period of the order of few fm/c. Speaking in terms of physics, such a collision can be considered similar, which is why it is often referred to as a *little-bang* or *micro-bang* [19].

In Figure 1.1 the spacetime evolution of a fireball induced after a collision of two nuclei A and B is depicted, while nuclei with a large proton number, such as ^{82}Pb or

^{79}Au, are usually used. Such a collision results in a formation of dense hadronic matter, whose energy density ϵ approximately corresponds to a value $\epsilon \geqslant 1$ GeV fm^{-3} and the corresponding pressure P of the relativistic matter approximately equals to $P \simeq \frac{1}{3}\epsilon$ [19].

The character of the phase transition mentioned above, the normal position of nuclear matter in the QCD phase diagram along with relevant scales of the nuclear many-body problem is shown in Figure 1.2. As can be seen in the aforementioned Figures, the phase transition is characterized by two free parameters - the freeze-out temperature $T_{(fo)}$ and the baryo-chemical potential μ_B.

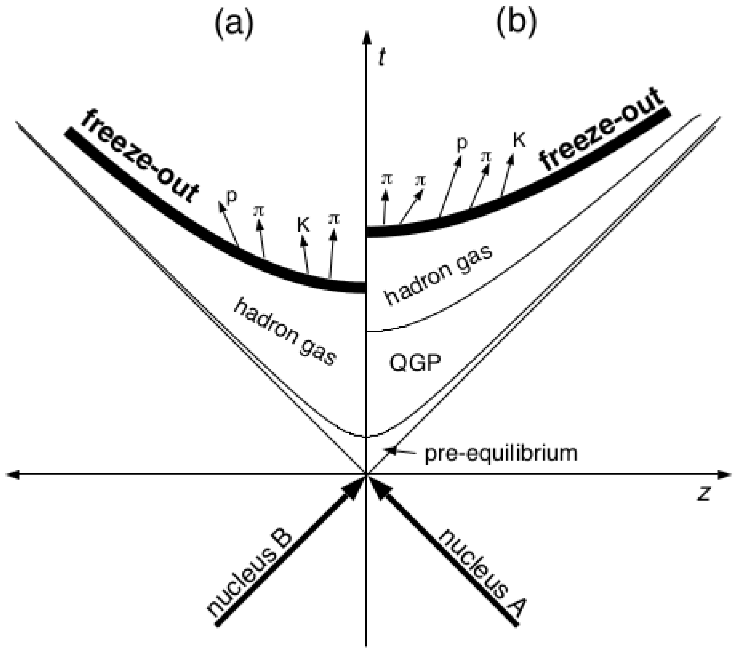

Figure 1.1: Spacetime evolution of a fireball: (a) without QGP, (b) with QGP (taken from [18]).

Due to a high pressure the fireball will continue to expand until it has reached the so called *freeze-out*. The life expectancy of the fireball τ (meaning the time that passed between the collision and the freeze-out) depends on the volume of the system and is approximately given by

$$\tau \approx \frac{2R}{c} \tag{1.1}$$

where R is the radius of the sphere used to approximate the fireball, c is the speed of light in a vacuum.

After the freeze-out, a large abundance of low-energy hadrons can be observed. This is typical for a heavy-ion collision, since it is characterized by the fact that the collision energy is partitioned among a large number of hadrons, contrary to elementary interactions (see [19]). It is the high particle yield that justifies the assumption that heavy-ion collisions can be well described by using the methods of statistical physics. A considerable advantage of these methods is the fact that they do not require the description of every single particle in the system, but describe the system as a whole.

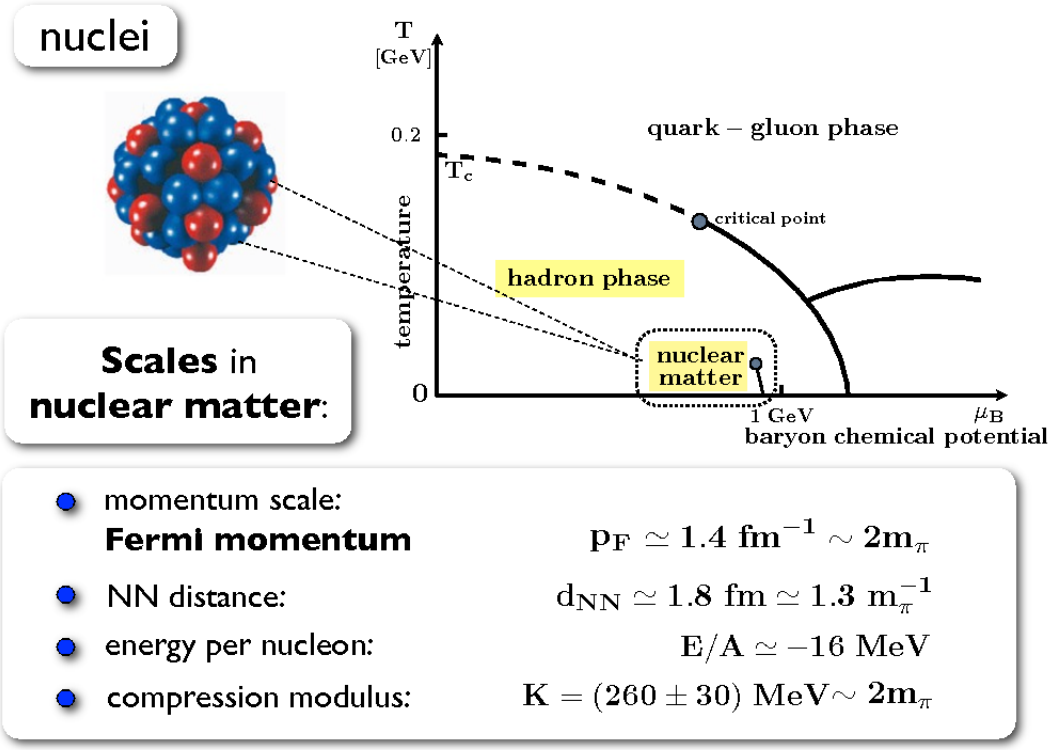

Figure 1.2: Illustration of the position of nuclear matter in the QCD phase diagram, outlining relevant scales of the nuclear many-body problem. Taken from [20].

1.1.1 Comparison of the Big-Bang and the Micro-Bang

As we have already mentioned the similarity between the *micro-bang* and the Big Bang, it seems only fitting to point out that these two theoretical phenomena are neither entirely equivalent, as the reader may have acquired the impression of a certain similarity based on the previous description. In Figure 1.3 we can see two nuclei, which are subject to Lorentz contraction in the direction of movement. The collision is depicted in the centre of mass reference frame. The collision of these two nuclei results in the formation of a highly dense matter - the *fireball*, which subsequently expands according to Figure 1.1,until the final state is reached, where individual particles which were formed after the chemical freeze-out are present. In Figure 1.3, these particles are depicted as arrows.

This brings us to the conclusion that even though the conditions immediately after the collision are very similar to those during the earliest stages of the universe, it is impossible to compare these two events. The main reason is that the life expectancy of the QGP in the Universe and that in a heavy-ion collision are different by a factor of 10^{18}.

The time scale of the expansion of the Universe is defined by the mutual conformity of gravitational forces and the radiation and Fermi pressure of hot matter, whereas in the case of a micro-bang, there is no gravitational interaction that would slow down the expansion of the fireball, which justifies the already mentioned difference between the times of expansion of the fireball and of the Universe. One must also consider the fact that

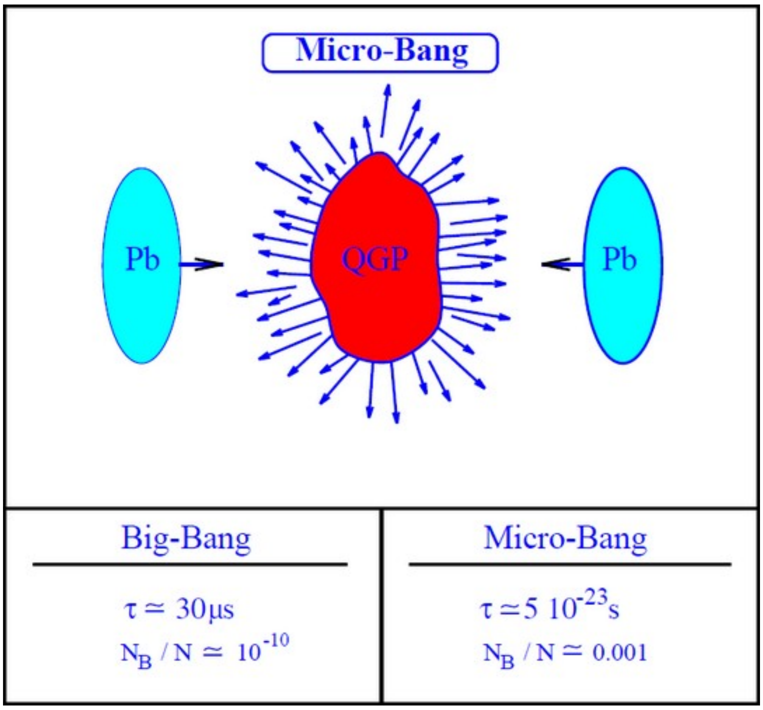

Figure 1.3: Lead nuclei in the state of Lorentz Contraction (taken from [19]).

the properties of the fireball as well as its size change rapidly with the fireball's expansion, quite unlike during the early stages of the Universe. The time expansion constant of the Universe τ_U can be expressed as

$$\tau_U = \sqrt{\frac{3c^2}{32\pi GB}} \tag{1.2}$$

where B is the vacuum energy (the so called "bag constant" - see Chapter 1.2) and G is the gravitational constant.

In the early Universe, the baryon number density was extremely low, which was caused by the presence of baryons and almost exactly the same number of antibaryons. Contrary to that, in laboratory conditions, a dense fireball with an non-negligible baryon number N_b emerges. The term "unnegligible" means that the ratio of the difference of the number of baryons and that of antibaryons to the number of baryons, which can be expressed as

$$\frac{N_b - \bar{N}_b}{N_b},$$

is much much greater than 0 in heavy-ion collisions (in the case of energies in the order of MeV, this ratio is almost equal to 1; in the early Universe, it was almost 0). For this reason, a considerable matter-antimatter asymmetry is assumed within a micro-bang.

The numerical value of the constant B is approximately 145 MeV $< B^{\frac{1}{4}} <$ 235 MeV and that of the time constant τ_U approximately 66 μs $> \tau_U >$ 25 μs (taken from [19]).

The time evolution of the Universe is depicted in Figure 1.4, which shows the time dependence of typical particle energies. Likewise, the values of energy of individual colliders (in a decreasing order - LHC, RHIC a SPS) are depicted. Here we can see that after

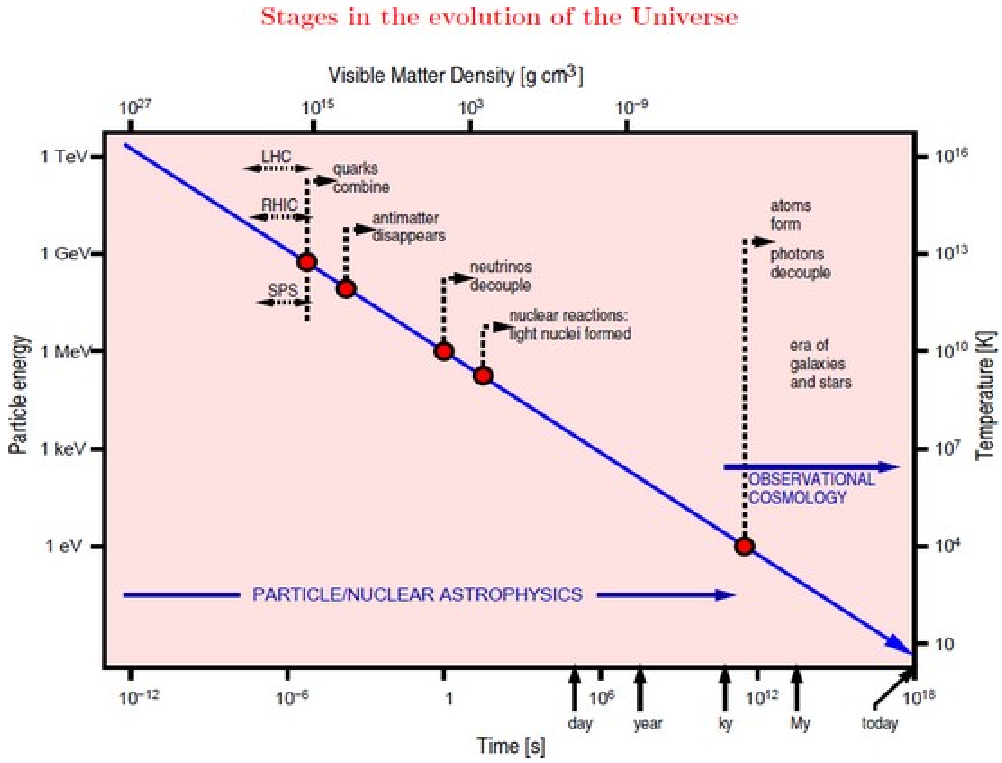

Figure 1.4: Time dependence of the particle energy in the Universe (taken from [19]).

the neutrino separation, the subsequent evolution of the Universe is well known and documented. The same however does not apply for earlier stages. As already mentioned, in a period of approximately 10 μs after the Big Bang, the transformation of the deconfined parton phase into a hot gas comprised of hadrons, more specifically of mesons, baryons and antibaryons, takes place. Immediately after that, the baryon-antibaryon annihilation is believed to have taken place in the early Universe as well as a possible separation of baryons from antibaryons.

The lattice QCD calculations proved [24] that the transformation of the QGP into a hadron gas occurs at a temperature of approximately $T \simeq 170$ MeV. If the methods of statistical physics are used, it can be found out that the baryons and antibaryons make up approximately 25 % of the energy of the early Universe, half of which comprises of heavy baryons and antibaryons. It is also assumed that the strong interaction did not play any role at and after the point of nucleosynthesis.

1.2 Statistical properties of nuclear matter

The main source of information about the nature, composition and size of the original medium are the **hadron multiplicities**. The main focus is the question, to what extent the measured particle yields are in the state of equilibrium. According to the theoretical apparatus which e. g. sources such as [17] and [23] base upon, the main quality able to prove the existence of the QGP is the chemical equilibrium of all emerging hadron constituents, which can lead to a high level of chemical saturation - mostly considering strange particles - which is connected with the existence of a deconfined phase during the earliest moments of a heavy-ion collision.

In the Gibbs' approximation, the behaviour of thermodynamical observables can be quantified as an average over all statistical samples (not as one may think as a time average for a specific state). Therefore, the distribution is obtained by averaging over the whole phase space. Furthermore, the sample corresponding to thermodynamical equilibrium is such a sample, in which the phase density is equal to the density of the whole available phase space.

1.2.1 Energy distribution

We will now sum up the mathematical apparatus used for describing of statistical ensembles. This apparatus does not differ from that used in classical statistical physics, e. g. [17].

Let N be the number of identical bound systems, which are distinguishable from one another e. g. by their respective energy states E_i. In order to simplify the whole situation, we shall assume that the energy states E_i only possess discrete values and that there are K different "macro" states. It can be generally assumed that some energy states E_i will be occupied more than once, therefore let n_i represent the occupation of the i-th energy state. The total energy $E^{(N)}$ can then be written as

$$E^{(N)} = \sum_{i=1}^{K} n_i E_i \tag{1.3}$$

and the total number of states as

$$N = \sum_{i=1}^{K} n_i. \tag{1.4}$$

If we do not consider any other quantum numbers, the states E_i are equivalent, which means **indistinguishable** in terms of statistical physics. A distribution such that the n_i-th state possesses energy E_i, can be reached by various means. Let us consider

$$K^N = (x_1 + x_2 + \cdots + \cdots + x_K)^N|_{x_i=1} = \sum_n \frac{N!}{n_1! n_2! \cdots n_K!} x_1^{n_1} x_2^{n_2} \cdots x_K^{n_K}|_{x_i=1}, \tag{1.5}$$

then the normalized coefficients expressing the relative probability of reaching an i-th state in ensemble $\mathbf{n}$ with n_i equivalent elements are given by

$$W(\mathbf{n}) = \frac{K^{-N} N!}{\prod_{i=1}^{K} n_i!}. \tag{1.6}$$

Our goal is to find the most probable distribution $\bar{n}$, which means having to find the maximal value of the logarithm $\ln W$, where W is given by Eq. (1.6) with respect to conditions (1.3) and (1.4). The whole problem now transforms into the search for **bound extremes**. The Lagrange function of such system $A(n_1, n_1, \cdots, n_K)$ is given by

$$A(n_1, n_1, \cdots, n_K) = \ln W(\mathbf{n}) - a \sum_i n_i - \beta \sum_i n_i E_i. \tag{1.7}$$

where a and β are the corresponding Lagrange multipliers.

We may now partially differentiate the whole equation according to the variable n_i and set it equal to zero. By neglecting the influence of constants K and N, we obtain the equation for the i-th state

$$\frac{\partial}{\partial n_i}[-\ln(n_i!) - n_i a - \beta n_i E_i]|_{n_m} = 0 \tag{1.8}$$

and now searching for the value of $\bar{n}_m$. If furthermore $\bar{n}_i >> 1$, we may - using the Lagrange theorem -approximate the derivative of the logarithm of the factorial of an arbitrary number k as

$$\frac{d}{dk}[\ln(k!)] \approx \frac{\ln(k!) - \ln(k-1)!}{k-(k-1)} = \ln k. \tag{1.9}$$

The maximal value $\bar{n}_i$ of (1.6) can therefore be written as

$$\bar{n}_i = \gamma e^{-\beta E_i}. \tag{1.10}$$

The inverse value of the parameter β has the meaning of temperature T, which is expressed as

$$T = \frac{1}{\beta}. \tag{1.11}$$

From Eq. (1.4) we may now deduce the relation for the total number of particles

$$\sum_{i=1}^{K} \bar{n}_i = \gamma \sum_{i=1}^{K} e^{-\beta E_i} = N. \tag{1.12}$$

The meaning of the parameter γ is to regulate the total number of particles in the ensemble N. It can be rewritten in an exponential form

$$\gamma = e^{-a}. \tag{1.13}$$

If we insert (1.10) into (1.3), we obtain the total energy $E^{(N)}$

$$E^{(N)} = \sum_{i=1}^{K} \bar{n}_i E_i = \gamma \sum_i E_i e^{-\beta E_i}. \tag{1.14}$$

If we divide $E^{(N)}$ by the number of ensembles N, it leads to

$$\frac{E^{(N)}}{N} = \bar{E}^{(N)} = \frac{\gamma \sum_i E_i e^{-\beta E_i}}{\gamma \sum_i e^{-\beta E_i}} = -\frac{d}{d\beta} \ln Z. \tag{1.15}$$

The symbol Z stands for the **canonical partition function**, which we may express as

$$Z = \sum_i \gamma e^{-\beta E_i}. \tag{1.16}$$

Contrary to the microcanonical approach, where the energy is fixed for each member of the ensemble, the statistical "canonical" approach serves for studying the most probable energy distribution and other physical interactions between the members of the ensemble. These properties only depend on parameters β and γ, the Lagrange multipliers representing the energy conservation and the particle number conservation, respectively.

1.2.2 Grandcanonical formalism

Let us now assume that energy is equally distributed, as energy transfer occurs among macrosystems. In the grandcanonical approach we will again search for the most probable distribution, yet this time we will take another quantum number corresponding to the change among individual members of the statistical ensemble, into account. The methodics will be equivalent to the one used in the case of the canonical approach, but as there is another (discrete) quantum number, it is necessary to characterize said number by another (discrete) parameter, which will be called the **baryon number**. The condition of the baryon number conservation is expressed as follows

$$\sum_{i=1}^{N} n_i^b b_i = b^{(N)} = N\bar{b}_i \tag{1.17}$$

where $\bar{b_i}$ is the average number of baryons in each sample we take into account. Apart from conditions (1.3) and (1.4), we therefore have another condition given by (1.17).

Let us now consider the conditions (1.3), (1.4) and (1.17). The condition (1.17) requires another Lagrange multiplier to be assigned, which we for the sake of simplicity rewrite as $\kappa = -\ln\lambda$. We may now proceed to searching for the extremes of the corresponding Lagrange function. If we perform equivalent calculations as in the previous Section, we obtain the derivative of the Lagrange function with respect to parameter n_i^b:

$$\frac{\partial}{\partial n_i^b}[-\ln(n_i^b!) - n_i^b a - \beta n_i^b E_i + \ln\lambda n_i^b\ b_i]|_{\bar{n}_m} = 0. \tag{1.18}$$

The derivative is set equal to zero in order to find the extreme value.

An equivalent method as in the previous Section can be used to obtain the most probable distribution $\bar{n}_i$, given by

$$\bar{n}_i^b = \gamma\lambda^{b_i}e^{-\beta E_i}. \tag{1.19}$$

Let us now redefine the chemical potential μ as

$$\mu = T\ln\lambda. \tag{1.20}$$

Then the quantity λ can be rewritten as

$$\lambda = e^{\beta\mu} = e^{\frac{\mu}{T}}, \tag{1.21}$$

which enables us to express it as a function of temperature T and the chemical potential μ - the two quantities essential (and sufficient) for determining the point where the **phase transition** occurs. This quantity is called **fugacity**.

The chemical potentials elaborated above have the meaning of energy necessary to add or remove a particle at a fixed pressure, energy and entropy. Using the same formalism as in the case of the canonical potential, by which we obtained Eq. (1.15), we obtain

$$\bar{E}_{(N)} = \gamma \frac{\sum_{i;b} E_i \lambda^{b_i} e^{-\beta E_i}}{\gamma \sum_{i;b} \lambda^{b_i} e^{-\beta E_i}} = -\frac{d}{d\beta} \ln Z. \tag{1.22}$$

The quantity Z then represents the grandcanonical partition function given by

$$Z(V, \beta, \lambda) = \gamma \sum_{i;b} \lambda^{b_i} e^{-\beta E_i}. \tag{1.23}$$

We may also write a relation for the average value of b with respect to the grandcanonical partition function. This is given by

$$\bar{b} = \frac{\sum_{i;b} b_i \lambda^{b_i} e^{-\beta E_i}}{\sum_{i;b} \lambda^{b_i} e^{-\beta E_i}} = \lambda \frac{d}{d\lambda} \left(\ln \sum_{i;b} \gamma \lambda^{b_i} e^{-\beta E_i} \right) = \lambda \frac{d}{d\lambda} \ln Z(\beta, \lambda). \tag{1.24}$$

1.2.3 Independent (quasi)particles

In terms of quantum mechanics, the grandcanonical ensemble can be looked upon as an ensemble with hamiltonian $\hat{H}$ with eigenvalues E_i, which correspond to discrete energy states $|i\rangle$. This fact can be written as

$$\hat{H} \left| i \right\rangle = E_i \left| i \right\rangle . \tag{1.25}$$

With the operator $\hat{b}$ (according to the correspondence principle assigned to baryon number b) commutes with the Hamiltonian, we may also write

$$\hat{b} \left| i, b \right\rangle = b \left| i, b \right\rangle . \tag{1.26}$$

The values b then correspond to eigenvalues of $\hat{b}$.

The grandcanonical partition function, which we have derived as (1.23), may in the operator representation be rewritten as

$$Z = \sum_{i,b} \left\langle i, b \right| \gamma e^{-\beta(\hat{H} - \mu\hat{b})} \left| i, b \right\rangle = Tr\ \gamma e^{-\beta(\hat{H} - \mu\hat{b})} \tag{1.27}$$

where Tr symbolizes the trace of the matrix.

This relation is very important, since the trace of a quantum operator **does not depend on the representation**. This means that we may choose any arbitrary set $|n\rangle$ of basic states and always find a corresponding (quantum) canonical or grandcanonical partition function. We can thus obtain information about the properties of quantum gases, which are often approximated as an ensemble of independent (quasi)particles. In the same way, the interactions between said particles can be included using the perturbation expansion.

We speak about quasiparticles, if there are objects in the medium similar to particles, whose mass is different from that of elementary particles. Generally speaking, states of collective excitation characterized by a mass spectrum will be observed. The hadronic matter can thus be described as another system with a high mass density. If the excitation states are well defined, it does not matter if we take particles or quasiparticles while performing the calculation of the trace (1.27).

Let us now choose the basis of the occupation number of "one quasiparticle". In this case, each macrostate $|n\rangle$ is described by a set of occupation numbers n_i with corresponding baryon numbers b_i, energy ε_i and the energy of state $E_n = \sum_i n_i \varepsilon_i$. The sum over all states corresponds to the sum over all enabled sets n_i: For fermions, we have $n_i \in 0, 1$ and for bosons we have $n_i \in 0, 1, 2, \cdots, \infty$. The partition function Z can thus be expressed as

$$\begin{aligned} Z = \sum_n e^{-\sum_{i=1}^{\infty} n_i \beta(\varepsilon_i - \mu b_i - \beta^{-1} \ln \gamma)} &= \sum_n \prod_i e^{-n_i \beta(\varepsilon_i - \mu b_i - \beta^{-1} \ln \gamma)} \\ &= \prod_i \sum_{n_i = 0, 1 \cdots} e^{-n_i \beta(\varepsilon_i - \mu b_i - \beta^{-1} \ln \gamma)}. \end{aligned} \tag{1.28}$$

In the last modification, we have taken advantage of the possibility of interchanging the sum and product signs, which follows from equivalent summing over all states and summing over all enabled sets n_i. The logarithm of the partition function can then be expressed as

$$\ln Z_{F/B} = \ln \prod_i \left(1 \pm \gamma e^{-\beta(\varepsilon_i - \mu b_i)}\right)^{\pm 1} = \pm \sum_i \ln(1 \pm \gamma \lambda_i^b e^{-\beta \varepsilon_i}) \tag{1.29}$$

where "+" corresponds to fermions F and "-" corresponds to bosons B.

It is also necessary to verify the values we obtain, if antiparticles instead of particles are used. The eigenvalue of the operator $\hat{b}$ in Eq. (1.29) will be the opposite value of that obtained for particles. This means that the fugacity $\lambda_{\bar{f}}$ for antiparticles is equal to

$$\lambda_{\bar{f}} = \lambda_f^{-1}.$$

Chemical potentials are then expressed as

$$\mu_f = -\mu_{\bar{f}}.$$

For a homogenous spacetime, the energy of an i-th state ε_i is given by

$$\varepsilon_i = \sqrt{m_i^2 + \vec{p}^2}. \tag{1.30}$$

1.2.4 Fermi and Bose quantum gases

Let us now consider a particle of mass m and degeneration g. Then Eq. (1.29) can be rewritten as

$$\ln Z_{F/B}(V, \beta, \lambda, \gamma) = \pm g V \int \frac{d^3 p}{(2\pi)^3} \left[\ln(1 \pm \gamma \lambda e^{-\beta \sqrt{p^2 + m^2}}) + \ln(1 \pm \gamma \lambda^{-1} e^{-\beta \sqrt{p^2 + m^2}})\right]. \tag{1.31}$$

The second logarithm in Eq. (1.31) was added to account for the presence of antiparticles. If we perform the classical Boltzmann limit, which means, that the term within the exponential function is much smaller than one, we obtain

$$\ln Z_{cl} = gV \int \frac{d^3p}{(2\pi)^3} \gamma(\lambda + \lambda^{-1}) e^{-\beta\sqrt{p^2+m^2}}. \tag{1.32}$$

The normalized partice spectrum which is represented as a relative probability of finding a particle on an energy level E_i, may - using Eq. (1.10) and (1.12) - be rewritten as

$$\bar{w}_i = \frac{\bar{n}_i}{N} = \frac{e^{-\beta E_i}}{\sum_j e^{-\beta E_j}} = -\frac{1}{\beta} \frac{\partial}{\partial E_i} \left(\ln \sum_j \gamma e^{-\beta E_j} \right). \tag{1.33}$$

The relation for a one-particle spectrum is the following

$$f_{F/B}(\varepsilon; \beta, \lambda, \gamma) = \frac{1}{\gamma^{-1}\lambda^{-1}e^{\beta\varepsilon} \pm 1} \tag{1.34}$$

where (+) symbolizes fermions, (-) bosons.

1.2.5 Towards the role and the motivation of using multiplicity fluctuations in the QGP research

In the next Chapters, we will elaborate on multiplicity fluctuations as an efficient tool for characterizing the QGP region. As we have mentioned before, the phase transition is fully described (at sufficiently high collision energies) by a set of two parameters, these being the temperature T and the baryo-chemical potential μ_b.

As the HRG models reproduce the equilibrium lQCD results for the lowest order susceptibilities and their ratios (see further text) reasonably well [3] [8], we may further restrict on using the HRG model only. Statistical hadronization models have been successfully used to describe the data on hadron multiplicities in relativistic nucleus-nucleus (A+A) collisions [2]. In A+A collisions, the grand canonical ensemble (GCE) is preferred, whereas the canonical ensemble (CE) or the microcanonical ensemble (MCE) have been used for describing the $pp, p\bar{p}$ and e^+e^- collisions.

It has been shown that the moments of net-particle multiplicity distributions from the experiment can be related to susceptibilities of conserved charges calculated on the lattice [3]. Therefore, chemical freeze-out parameters can be directly determined in the thermally equilibrated GCE approach on the lattice without having to rely on statistical models. This makes said moments - which immediately lead to said fluctuations - a powerful tool in determination of the freeze-out parameters.

Chapter 2

Calculation of the statistical moments within the Statistical Model

Statistical moments are an important mathematical tool used to describe and calculate multiplicity fluctuations in the statistical model. The m-th central moment $\varphi_m(X)$, where $m \in \mathbb{N}$ is defined as follows:

$$\varphi_m(X) = E(X - EX)^m$$

where EX is the mean value of the statistical quantity X. We will further concentrate on the quantities defined by the first four moments only, as those are of great significance. They are defined and called as follows:

mean: $M = \varphi_1$
variance: $\sigma^2 = \varphi_2$
skewness: $S = \varphi_3/\varphi_2^{3/2}$
kurtosis: $\kappa = \varphi_4/\varphi_2^2 - 3$

The constant -3 may or may not be added to kurtosis, which depends on whether we want the kurtosis of the Gauss distribution to be equal to zero. In our calculations, this factor is accounted for. The meaning of skewness and kurtosis becomes obvious from Figure 2.1, where also the meaning of those two moments is depicted: skewness measures the assymetry of the probability distribution, kurtosis its "tailedness".

2.1 Grandcanonical and canonical formalism

We usually assume that we work with grandcanonical or canonical ensemble, whose event-by-event distributions of conserved quantities are characterized by the quantities (M, σ, S, κ) defined above. In order to be able to directly compare theoretical predictions and experimental measurements, we also introduce the following:

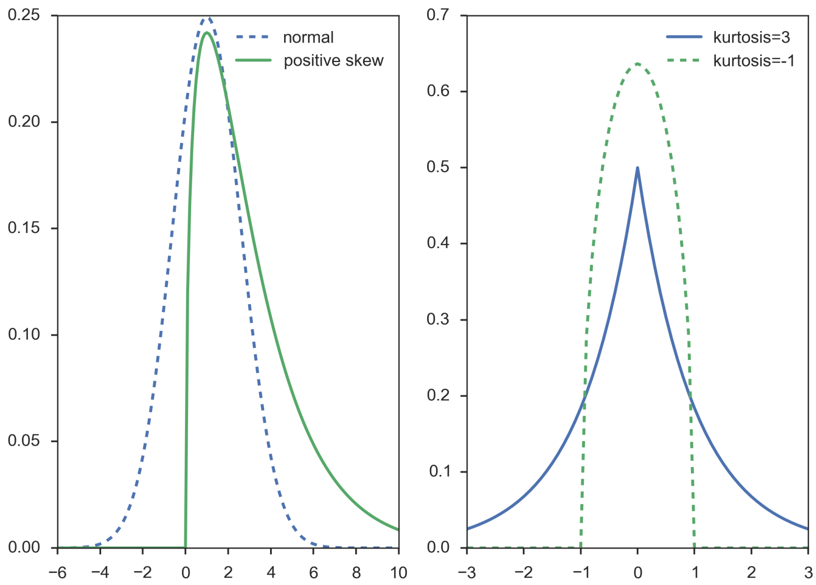

Figure 2.1: Explanation of skewness and kurtosis [1].

$$S\sigma = \varphi_3/\varphi_2 \tag{2.1}$$

$$\kappa\sigma^2 = \varphi_4/\varphi_2 \tag{2.2}$$

$$M/\sigma^2 = \varphi_1/\varphi_2 \tag{2.3}$$

$$S\sigma^3/M = \varphi_3/\varphi_1 \tag{2.4}$$

Specifically, fluctuations can be described by means of the so-called "scaled variance" ω [7] of a multiplicity distribution:

$$\omega = \frac{\langle N^2\rangle - \langle N\rangle^2}{\langle N\rangle} = \frac{\sigma^2}{M} \tag{2.5}$$

defined in accordance with [9] where N is the multiplicity distribution of any hadron species, which includes primary or final (i.e. after resonance decays [7]) hadrons or the sum of an arbitrary number of hadron species (see further text). Obviously, this is the inverse value of the ratio given by Eq. (2.3).

The grandcanonical partition (GC) function is given by

$$Z_{GC}(\lambda_j) = \prod_j \exp\left[\sum_{n_j=1}^{+\infty} \frac{z_j(n_j)\lambda_j^{n_j}}{n_j}\right] \tag{2.6}$$

and the single particle partition function by

$$z_j(n_j) = (\mp 1)^{n_j+1} \frac{g_j V}{2\pi^2 n_j} T m_j^2 K_2 \left(\frac{n_j m_j}{T} \right). \tag{2.7}$$

The products runs over all types of hadrons and the sum is necessary due to the quantum statistical distribution.

Furthermore, K_2 is the modified Bessel function (see Appendix A), V is the volume of the hadron gas,

$$\lambda_j = \exp\left(\frac{\mu_j}{T}\right)$$

is the fugacity for each particle species j, m_j is the hadron mass, μ_j is the chemical potential of a particle species j,

$$g_j = 2J_j + 1$$

is the spin degeneracy and the upper sign holds for fermions, lower sign for bosons.

Canonical formalism is a little more complicated, as it cannot be factorized into one-species expressions, as is the case for the GC formalism. We will now introduce the vector of total charges

$$\vec{Q} = (Q_1, Q_2, Q_3) = (B, S, Q)$$

and the vector of charges of the hadron species j

$$\vec{q_j} = (q_{1,j}, q_{2,j}, q_{3,j}) = (b_j, s_j, q_j)$$

where Q, B, S denote the charge, the baryon number and the strangeness, respectively.

As such, three conservation laws are imposed within the canonical formalism. We introduce an **exact conservation law** as the restriction on the sets of the occupation numbers $\{n_{p,i}\}$, which means only those sets satisfying

$$\Delta Q = \sum_{p,i} q_i \Delta n_{p,i} = 0$$

can be realized and the equilibrium probability distribution $W_{c.e.}(\Delta n_{p,i})$ can be introduced as follows:

$$W_{c.e.}(\Delta n_{p,i}) \propto \prod_{p,i} \exp\left[-\frac{(\Delta n_{p,i})^2}{2v_{p,i}^2}\right] \cdot \delta\left(\sum_{p,i} q_i \Delta n_{p,i}\right) \cdot \delta\left(\sum_{p,i} b_i \Delta n_{p,i}\right) \cdot \delta\left(\sum_{p,i} s_i \Delta n_{p,i}\right)$$

whereas for the GC formalism, this would be

$$W_{g.c.e.}(\Delta n_{p,i}) \propto \prod_{p,i} \exp\left[-\frac{(\Delta n_{p,i})^2}{2v_{p,i}^2}\right].$$

Furthermore, if we introduce the Wick-rotated fugacities:

$$\lambda_j = \exp[i \sum_i q_{i,j}\phi_i]$$

where $\phi_i, i \in \{1,2,3\}$ is the rotation angle and $q_{i,j}$ the vector of charges of the hadron species j.

The canonical partition function will now be expressed as:

$$Z_{\vec{Q}} = \left[\prod_{i=1}^{3} \frac{1}{2\pi} \int_0^{2\pi} d\phi_i e^{-iQ_i\phi_i}\right] Z_{GC}(\lambda_j) \tag{2.8}$$

where Z_{GC} is the GC partition function given by Eq. (2.6).

Let h be a set of hadron species with the corresponding fugacity factor λ_h. We may then write

$$\lambda_j \to \lambda_h \lambda_j$$

and have now everything we need to write down the explicit form of the first four statistical moments:

$$\langle N_h \rangle = \frac{1}{Z_{\vec{Q}}} \frac{\partial Z_{\vec{Q}}}{\partial \lambda_h}|_{\lambda_h=1} = \sum_{j\in h} \sum_{n_j=1}^{\infty} z_j(n_j) \frac{Z_{\vec{Q}-n_j\vec{q_j}}}{Z_{\vec{Q}}} \tag{2.9}$$

$$\begin{aligned}\langle N_h^2 \rangle = \frac{1}{Z_{\vec{Q}}} \left[\frac{\partial}{\partial \lambda_h}\left(\lambda_h \frac{\partial Z_{\vec{Q}}}{\partial \lambda_h}\right)\right]|_{\lambda_h=1} = \\ \sum_{j\in h} \sum_{n_j=1}^{+\infty} n_j z_j(n_j) \frac{Z_{\vec{Q}-n_j\vec{q_j}}}{Z_{\vec{Q}}} + \\ \sum_{j\in h} \sum_{n_j=1}^{+\infty} z_j(n_j) \sum_{k\in h} \sum_{n_k=1}^{+\infty} z_k(n_k) \frac{Z_{\vec{Q}-n_j\vec{q_j}-n_k\vec{q_k}}}{Z_{\vec{Q}}}\end{aligned} \tag{2.10}$$

$$\left\langle N_h^3 \right\rangle = \frac{1}{Z_{\vec{Q}}} \left[\frac{\partial}{\partial \lambda_h} \left(\lambda_h \frac{\partial}{\partial \lambda_h} \left(\lambda_h \frac{\partial Z_{\vec{Q}}}{\partial \lambda_h} \right) \right) \right] |_{\lambda_h = 1} =$$

$$\sum_{j \in h} \sum_{n_j=1}^{+\infty} n_j^2 z_j(n_j) \frac{Z_{\vec{Q}-n_j\vec{q_j}}}{Z_{\vec{Q}}} +$$

$$3 \left[\sum_{j \in h} \sum_{n_j=1}^{+\infty} n_j z_j(n_j) \sum_{k \in h} \sum_{n_k=1}^{+\infty} z_k(n_k) \frac{Z_{\vec{Q}-n_j\vec{q_j}-n_k\vec{q_k}}}{Z_{\vec{Q}}} \right] +$$

$$\sum_{j \in h} \sum_{n_j=1}^{+\infty} z_j(n_j) \sum_{k \in h} \sum_{n_k=1}^{+\infty} z_k(n_k)$$

$$\sum_{l \in h} \sum_{n_l=1}^{+\infty} z_l(n_l) \frac{Z_{\vec{Q}-n_j\vec{q_j}-n_k\vec{q_k}-n_l\vec{q_l}}}{Z_{\vec{Q}}} \quad (2.11)$$

$$\left\langle N_h^4 \right\rangle =$$

$$\frac{1}{Z_{\vec{Q}}} \left[\frac{\partial}{\partial \lambda_h} \left(\lambda_h \frac{\partial}{\partial \lambda_h} \left(\lambda_h \frac{\partial}{\partial \lambda_h} \left(\lambda_h \frac{\partial Z_{\vec{Q}}}{\partial \lambda_h} \right) \right) \right) \right] |_{\lambda_h = 1} =$$

$$\sum_{j \in h} \sum_{n_j=1}^{+\infty} n_j^3 z_j(n_j) \frac{Z_{\vec{Q}-n_j\vec{q_j}}}{Z_{\vec{Q}}} +$$

$$4 \left[\sum_{j \in h} \sum_{n_j=1}^{+\infty} n_j^2 z_j(n_j) \sum_{k \in h} \sum_{n_k=1}^{+\infty} z_k(n_k) \frac{Z_{\vec{Q}-n_j\vec{q_j}-n_k\vec{q_k}}}{Z_{\vec{Q}}} \right]$$

$$+ 3 \left[\sum_{j \in h} \sum_{n_j=1}^{+\infty} n_j z_j(n_j) \sum_{k \in h} \sum_{n_k=1}^{+\infty} n_k z_k(n_k) \frac{Z_{\vec{Q}-n_j\vec{q_j}-n_k\vec{q_k}}}{Z_{\vec{Q}}} \right]$$

$$+ 6 \left[\sum_{j \in h} \sum_{n_j=1}^{+\infty} n_j z_j(n_j) \sum_{k \in h} \sum_{n_k=1}^{+\infty} z_k(n_k) \sum_{l \in h} \sum_{n_l=1}^{+\infty} z_l(n_l) \right.$$

$$\left. \frac{Z_{\vec{Q}-n_j\vec{q_j}-n_k\vec{q_k}-n_l\vec{q_l}}}{Z_{\vec{Q}}} \right]$$

$$+ \left[\sum_{j \in h} \sum_{n_j=1}^{+\infty} z_j(n_j) \sum_{k \in h} \sum_{n_k=1}^{+\infty} z_k(n_k) \sum_{l \in h} \sum_{n_l=1}^{+\infty} z_l(n_l) \right.$$

$$\left. \sum_{m \in h} \sum_{n_m=1}^{+\infty} z_m(n_m) \frac{Z_{\vec{Q}-n_j\vec{q_j}-n_k\vec{q_k}-n_l\vec{q_l}-n_m\vec{q_m}}}{Z_{\vec{Q}}} \right] \quad (2.12)$$

2.2 Asymptotic fluctuations in the canonical ensemble

The canonical partition function is given by Eq. (2.8). We will now introduce a way to compute this integral using the so-called "saddle-point expansion" (see Appendix B). The integration is performed on the complex $\mathbf{w}$ unit circle parametrized as:

$$w_i = \exp[i\phi_i].$$

The canonical partition function may then be written as

$$Z_{\vec{Q}} = \frac{1}{(2\pi i)^3} \oint dw_B \oint dw_S \oint dw_Q w_B^{-B-1} w_S^{-S-1} w_Q^{-Q-1} \exp \sum_j z_{j(1)} w_B^{b_i} w_S^{s_i} w_Q^{q_i} \quad (2.13)$$

where $z_j(1)$ is the one-particle partition function given by

$$z_j(1) = (2J_j + 1) \frac{V}{(2\pi)^3} \int d^3p \exp\left[-\sqrt{p^2 + m_j^2}\right]. \quad (2.14)$$

Obviously:

$$w_B^{-B} = \exp[-B \ln w_B], \quad (2.15)$$

$$w_Q^{-Q} = \exp[-Q \ln w_Q], \quad (2.16)$$

and

$$w_S^{-S} = \exp[-S \ln w_S] \quad (2.17)$$

where Q, B, S denote the charge, the baryon number and the strangeness, respectively. Let

$$g(\vec{w}) = w_B^{b_j-1} w_S^{s_j-1} w_Q^{q_j-1}, \quad (2.18)$$

$$\rho_B = \frac{B}{V}, \quad (2.19)$$

$$\rho_S = \frac{S}{V}, \quad (2.20)$$

$$\rho_Q = \frac{Q}{V} \quad (2.21)$$

and

$$f(\vec{w}) = -\rho_B \ln w_B - \rho_S \ln w_S - \rho_Q \ln w_Q + \sum_k \frac{z_{k(1)}}{V} w_B^{b_k} w_S^{s_k} w_Q^{q_k}. \quad (2.22)$$

We may now write

$$Z_{\vec{Q}-\vec{q_j}} = \frac{1}{(2\pi i)^3} \oint dw_B \oint dw_S \oint dw_Q g(\vec{w}) \exp[V f(\vec{w})] \quad (2.23)$$

Once the quantum statistics is neglected and in the absence of any other dynamical effects, the multiplicity distribution of any primary hadron is a Poisson, which means

$\omega = 1$, where ω is the scaled variance defined by Eq. (2.5).

Having performed the calculations in Eq. (2.9) and Eq. (2.10), we can rewrite the scaled variance as the sum of a Poissonian term, which means 1, and a canonical correction term:

$$\omega = 1 + \frac{\sum_{j \in h} \langle N_j \rangle \sum_{k \in h} z_{k(1)} \left(\frac{Z_{\vec{Q}-\vec{q_k}-\vec{q_j}}}{Z_{\vec{Q}-\vec{q_j}}} - \frac{Z_{\vec{Q}-\vec{q_k}}}{Z_{\vec{Q}}} \right)}{\sum_{j \in h} \langle N_j \rangle} \tag{2.24}$$

Chapter 3

Multiplicity fluctuations for a resonance gas model with chemical equilibrium

Since we have at this point presented all the necessary formalism concerning the calculation of multiplicity fluctuations, it seems only fitting that we now proceed towards systems where chemical equilibrium is a priori assumed. At first, we will present a certain generalization of what we laid down above.

As statistical models provide a valid description of hadron multiplicities in relativistic nucleus-nucleus collisions [2], we may further concentrate on multiplicity fluctuations in **high energy** nuclear collisions.

3.1 Fluctuations in a hadron resonance gas model

We may describe fluctuations in the number of particles of species i in a thermally and chemically equilibrated Hadron Resonance Gas (HRG) using the corresponding susceptibilities defined as

$$\chi_l^{(i)} = \frac{\partial^l (P/T^4)}{\partial(\mu_i/T)^l}\,|_T \tag{3.1}$$

where $l \in \mathbb{N}$.

The susceptibilities can be related to the cumulants of the multiplicity distribution of particle i via

$$\chi_1^{(i)} = \frac{1}{VT^3}\left\langle N_i \right\rangle_c = \frac{1}{VT^3}\left\langle N_i \right\rangle \tag{3.2}$$

$$\chi_2^{(i)} = \frac{1}{VT^3}\left\langle (\Delta N_i)^2 \right\rangle_c = \frac{1}{VT^3}\left\langle (\Delta N_i)^2 \right\rangle \tag{3.3}$$

$$\chi_3^{(i)} = \frac{1}{VT^3}\left\langle (\Delta N_i)^3 \right\rangle_c = \frac{1}{VT^3}\left\langle (\Delta N_i)^3 \right\rangle \tag{3.4}$$

$$\chi_4^{(i)} = \frac{1}{VT^3}\left\langle (\Delta N_i)^4 \right\rangle_c = \frac{1}{VT^3}\left(\left\langle (\Delta N_i)^4 \right\rangle - 3\left\langle (\Delta N_i)^2 \right\rangle^2\right) \tag{3.5}$$

where $\Delta N_i = N_i - \langle N_i \rangle$ and the subscript c denotes the corresponding cumulant value.

It is obvious that the first three cumulants are equal to the corresponding central moments, but the fourth cumulant is given by a combination of fourth and second central moments. The cumulants will be discussed later on in this Chapter. If we assume an equilibrium HRG model in the GCE formulation, thermally produced and non-interacting particles and anti-particles are uncorrelated [8]. The susceptibilities of the net-distributions can thus be written as:

$$\chi_l^{net,i} = \chi_l + (-1)^l \chi_l^{\bar{i}} \tag{3.6}$$

where $\bar{i}$ denotes the species of the antiparticle and i the species of the particle.

As we have already mentioned in Chapter 2, some ratios of the susceptibilities can be expressed in terms of the first four central moments, those being the mean M, the variance σ, and in terms of the skewness S and the kurtosis κ, as we can see in Eq. (2.1), (2.2), (2.3), (2.4).

The dependence of susceptibility ratios (2.1), (2.2) and (2.3) on the collision energy $\sqrt{s}$ is depicted in Fig. 3.1-3.3. The **full squares** depict experimental data on net proton fluctuations as measured by the STAR collaboration for the two most central collision classes (0-10%). **Empty circles** stand for the susceptibility ratios for the net baryon number fluctuations in the full HRG model, the **empty triangles** show the corresponding ratios for the net proton fluctuations with respect to primordial protons and anti/protons.

We may now write down the specific equilibrium pressure P, which is given by the sum of the partial pressures of all particle species i included in the model [8]:

$$P/T^4 = \frac{1}{VT^3} \sum_i \ln Z_{m_i}^{M/B}(V, T, \mu_B, \mu_Q, \mu_S), \tag{3.7}$$

where

$$\ln Z_{m_i}^{M/B} = \mp \frac{V g_i}{(2\pi)^3} \int d^3k \ln(1 \mp z_i \exp(-\epsilon_i/T)). \tag{3.8}$$

The single-particle energy is equal to

$$\epsilon_i = \sqrt{k^2 + m_i^2}$$

with m_i being the particle mass, g_i the degeneracy factor, V the volume and z_i being the fugacity given by

$$z_i = \exp((B_i\mu_B + Q_i\mu_Q + S_i\mu_S)/T) \equiv \exp(\mu_i/T). \tag{3.9}$$

We may also perform the partial derivative of the pressure with respect to the particle chemical potential μ_i, which gives us the density of particles i:

$$n_i(T, \mu_i) = \frac{g_i}{(2\pi)^3} \int d^3k f_{FD/BE}(T, \mu_i) \tag{3.10}$$

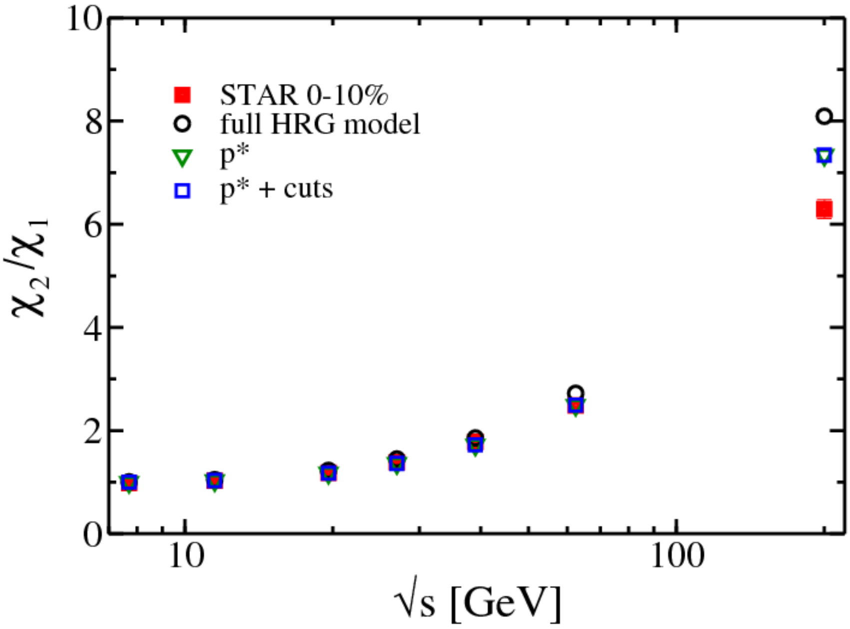

Figure 3.1: Ratios of susceptibilities as function of the collision energy. Taken from [8].

where $f_{FD/BE}$ is the Fermi-Dirac/Bose-Einstein distribution function for (anti-)baryons or mesons.

3.1.1 The first four cumulants in the ideal hadron gas

In this subsection, the aforementioned cumulants of primary particles i will be discussed [9]. We may plug Eq. (3.9) into Eq. (3.8), thus immediately obtaining

$$\ln Z_i(T, V, \mu_i) = \frac{V g_i}{2\pi^2} \int_0^{+\infty} \pm p^2 dp \ln[1 \pm \exp(-(E_i - \mu_i)/T)], \tag{3.11}$$

where $E_i = \sqrt{p^2 + m_i^2}$ is the single particle energy.

Using Eq.(3.11), we may now calculate the first four cumulants. The mean number of primary particles i is calculated (see formalism in Chapter 2) as follows:

$$C_1 = M = \langle N_i \rangle = \left[\left(T \frac{\partial}{\partial \mu_i} \right) \ln Z_i \right]_{T,V} = \frac{V g_i}{2\pi^2} \int_0^{+\infty} p^2 dp \; n_i \tag{3.12}$$

where

$$n_i = \frac{1}{\exp[(E_i - \mu_i)/T] \pm 1}.$$

The variance and higher order cumulants have the following form:

$$\begin{aligned} C_2 &= \sigma^2 = \left\langle (\Delta N_i)^2 \right\rangle = \left[\left(T \frac{\partial}{\partial \mu_i} \right)^2 \ln Z_i \right]_{T,V} && (3.13) \\ &= \frac{V g_i}{2\pi^2} \int_0^{+\infty} p^2 dp \; n_i (1 \mp n_i), && (3.14) \end{aligned}$$

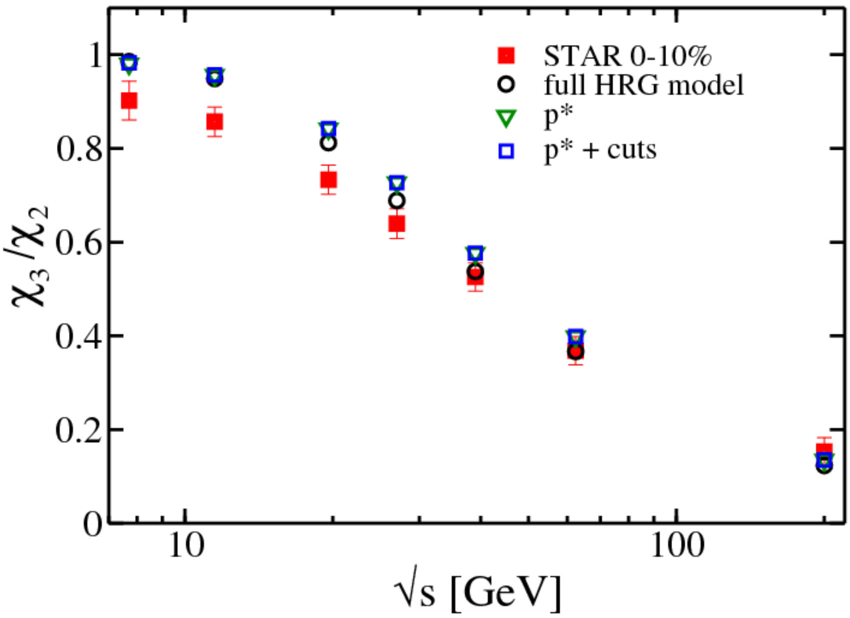

Figure 3.2: Ratios of susceptibilities as function of the collision energy. Taken from [8].

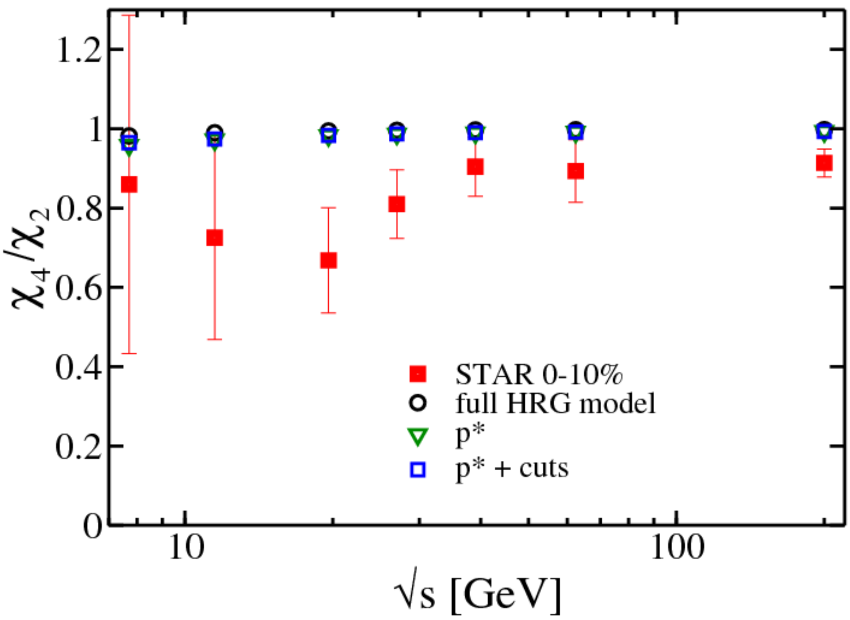

Figure 3.3: Ratios of susceptibilities as function of the collision energy. Taken from [8].

$$C_3 = \left\langle (\Delta N_i)^3 \right\rangle = \left[\left(T \frac{\partial}{\partial \mu_i} \right)^3 \ln Z_i \right]_{T,V} \tag{3.15}$$

$$= \frac{V g_i}{2\pi^2} \int_0^{+\infty} p^2 dp \; n_i (1 \mp 3n_i + 2n_i^2), \tag{3.16}$$

$$C_4 = \left\langle (\Delta N_i)^4 \right\rangle - 3 \left\langle (\Delta N_i)^2 \right\rangle^2 = \left[\left(T \frac{\partial}{\partial \mu_i} \right)^4 \ln Z_i \right]_{T,V} \tag{3.17}$$

$$= \frac{V g_i}{2\pi^2} \int_0^{+\infty} p^2 dp \; n_i (1 \mp 7n_i + 12n_i^2 \mp 6n_i^3). \tag{3.18}$$

3.2 Loss of chemical equilibrium and chemical freeze-out parametrization

The chemical composition of a HRG in local thermal and chemical equilibrium is determined by the conserved quantum charges [8]. However, the created matter expands rapidly, causing the density to decrease and leading to an enhancement of the particle mean free path. Consequently, there must be a specific set of parameters $(T^{fo}, \mu_B^{fo}, \mu_S^{fo}, \mu_Q^{fo})$, where reactions like baryon-antibaryon annihilation ($p\bar{p} \to \pi\pi\pi\pi\pi$) become too rare to maintain chemical equilibrium among different particle species [8]. This particular set of parameters describes the chemical freeze-out. The chemical freeze-out is an instant at which chemical equilibrium is lost, the chemical composition of the gas is frozen-out and after which only elastic scatterings occur frequently enough to maintain local thermal equilibrium until even these become too rare and the particles start to stream freely after the kinetic freeze-out [8].

We may assume that chemical equilibrium is not completely lost just after the chemical freeze-out. If the temperature T is high enough, specific reactions in form of resonance regenerations and decays (e.g. $\pi\pi \to \rho \to \pi\pi$) continue to occur, which means that resonances are still in chemical equilibrium with their decay products.

We may assume the hadronic matter to be in a state of partial chemical equillibrium, which means that the chemical potentials of all stable hadrons μ_h become $T-$dependent, while the chemical potentials of the resonances (whose effects will be discussed in the next Section) μ_R become functions of the μ_h:

$$\mu_R = \sum_h \mu_h \left\langle n_h \right\rangle_R .$$

The sum runs over all stable hadrons and

$$\left\langle n_h \right\rangle_R \equiv \sum_r b_r^R n_{h,r}^R$$

is the decay-channel averaged number of hadrons h produced in the decay of resonance R, where b_r^R is the branching ratio of the decay-channel and $n_{h,r}^R = 0, 1, \dots$ is the number of hadrons h formed in that specific decay-channel.

In accordance with [8], the chemical freeze-out parameters are taken as an input and the freeze-out temperature is parametrized - for different collision energies - by a polynomial function of μ_B:

$$T^{fo}(\mu_B^{fo}) = a - b(\mu_B^{fo})^2 - c(\mu_B^{fo})^4 \tag{3.19}$$

where $a = (0.166 \pm 0.002)$ GeV, $b = (0.139 \pm 0.016)$ GeV^{-1}, $c = (0.053 \pm 0.021)$ GeV^{-3}.

The baryon-chemical potential can be given as a function of $\sqrt{s}$:

$$\mu_B^{fo}(\sqrt{s}) = \frac{d_B}{1 + e_B\sqrt{s}} \tag{3.20}$$

where $d_B = (1.308 \pm 0.028)$ GeV, $e_B = (0.273 \pm 0.008)$ GeV^{-1}.

All the parameter values are taken from [8]. If we want to investigate the $\sqrt{s}-$dependence of the electric charge and strangeness chemical potentials -μ_B and μ_S- we have to require the following [8]:

$$n_S^{(net)}(T, \mu_B, \mu_S, \mu_Q) = 0, \tag{3.21}$$

$$n_Q^{(net)}(T, \mu_B, \mu_S, \mu_Q) = x n_B^{(net)}(T, \mu_B, \mu_S, \mu_Q). \tag{3.22}$$

where $x \in \langle 0, 1 \rangle$., e. g. $x \simeq 0.4$ for Au + Au and Pb + Pb collisions [8].

Just as in case of Eq. (3.20), μ_Q^{fo} and μ_S^{fo} can be parametrized as functions of $\sqrt{s}$. Here, the parameters are $d_Q = -0.0202$ GeV, $e_Q = 0.125$GeV^{-1} and $d_s = 0.224$ GeV, $e_S = 0.184$ GeV^{-1}.

3.3 The effect of resonance decays

We will now finally take the resonance decays into account. As we have already mentioned, the chemical potential of the resonances μ_R depends on the chemical potential of stable hadron species μ_h. As such, the resonances significantly affect the evolution of the created strongly interacting hadronic matter and their decays exercise a major influence on the final numbers of the stable hadrons and fluctuations [8]. We may now consider the derivative of P/T^4 with respect to μ_h/T as defined in Eq. (3.1). Considering that only the chemical potentials μ_h are independent of each other (while the μ_R depend on μ_h), we obtain

$$VT^3 \frac{\partial(P/T^4)}{\partial(\mu_h/T)}|_T = \langle N_h \rangle + \sum_R \langle N_R \rangle \langle n_h \rangle_R \tag{3.23}$$

where $\langle N_h \rangle$ and $\langle N_R \rangle$ are the means of the primordial numbers of hadrons and resonances, respectively. The sum runs over all the resonances in the model.

In agreement with the QCD equations of state [8], there are 26 particle species we consider stable, those being: $\pi^0, \pi^+, \pi^-, K^+, K^-, K^0, \bar{K_0}, \eta$ and $p, n, \Lambda^0, \Sigma^+, \Sigma^0, \Sigma^-, \Xi^0, \Xi^-, \Omega^-$ and their respective anti-baryons.

We will now demonstrate this using the example of fluctuations in the final numbers of **protons**. Since μ_R is μ_p-dependent and under assumption of fixed average numbers of produced protons as determined by the branching ratios of the resonance decays, we may write:

$$\left\langle \hat{N}_p \right\rangle = \langle N_p \rangle + \sum_R \langle N_R \rangle \langle n_p \rangle_R \tag{3.24}$$

$$\left\langle (\Delta \hat{N}_p)^2 \right\rangle = \left\langle (\Delta N_p)^2 \right\rangle + \sum_R \left\langle (\Delta N_R)^2 \right\rangle \langle n_p \rangle_R^2 \tag{3.25}$$

$$\left\langle (\Delta \hat{N}_p)^3 \right\rangle = \left\langle (\Delta N_p)^3 \right\rangle + \sum_R \left\langle (\Delta N_R)^3 \right\rangle \langle n_p \rangle_R^3 \tag{3.26}$$

$$\left\langle (\Delta \hat{N}_p)^4 \right\rangle_c = \left\langle (\Delta N_p)^4 \right\rangle_c + \sum_R \left\langle (\Delta N_R)^4 \right\rangle_c \langle n_p \rangle_R^4 . \tag{3.27}$$

The same holds for antiprotons; p is then replaced by $\bar{p}$. The related susceptibilities are given by

$$\hat{\chi}_l^{(p)} = \chi_l^{(p)} + \sum_R \chi_l^{(R)} \langle n_p \rangle_R^l . \tag{3.28}$$

In reality though, the actual numbers of decay products follow a multinomial distribution, since resonance decays are probabilistic processes. Said multinomial distribution results in fluctuations on the final particle numbers, which makes it necessary for them to be taken into account. If we assume a grandcanonical ensemble, the corresponding cumulants of the final proton distribution read as follows [8]:

$$\left\langle \hat{N}_p \right\rangle = \langle N_p \rangle + \sum_R \langle N_R \rangle \langle n_p \rangle_R \tag{3.29}$$

$$\left\langle (\Delta \hat{N}_p)^2 \right\rangle = \left\langle (\Delta N_p)^2 \right\rangle + \sum_R \left\langle (\Delta N_R)^2 \right\rangle \langle n_p \rangle_R^2 + \sum_R \langle N_R \rangle \left\langle (\Delta n_p)^2 \right\rangle_R , \tag{3.30}$$

$$\begin{aligned} \left\langle (\Delta \hat{N}_p)^3 \right\rangle &= \left\langle (\Delta N_p)^3 \right\rangle + \sum_R \left\langle (\Delta N_R)^3 \right\rangle \langle n_p \rangle_R^3 \\ &+ 3 \sum_R \left\langle (\Delta N_R)^2 \right\rangle \langle n_p \rangle_R \left\langle (\Delta n_p)^2 \right\rangle_R + \sum_R \langle N_R \rangle \left\langle (\Delta n_p)^3 \right\rangle_R \end{aligned} \tag{3.31}$$

$$\begin{aligned} \left\langle (\Delta \hat{N}_p)^4 \right\rangle_c &= \left\langle (\Delta N_p)^4 \right\rangle_c + \sum_R \left\langle (\Delta N_R)^4 \right\rangle \langle n_p \rangle_R^4 \\ &+ 6 \sum_R \left\langle (\Delta N_R)^3 \right\rangle \langle n_p \rangle_R^2 \left\langle (\Delta n_p)^2 \right\rangle_R + \sum_R \left\langle (\Delta N_R)^2 \right\rangle \Big[3 \left\langle (\Delta n_p)^2 \right\rangle_R^2 \\ &+ 4 \langle n_p \rangle_R \left\langle (\Delta n_p)^3 \right\rangle_R \Big] + \sum_R \langle N_R \rangle \left\langle (\Delta n_p)^4 \right\rangle_{R,c} . \end{aligned} \tag{3.32}$$

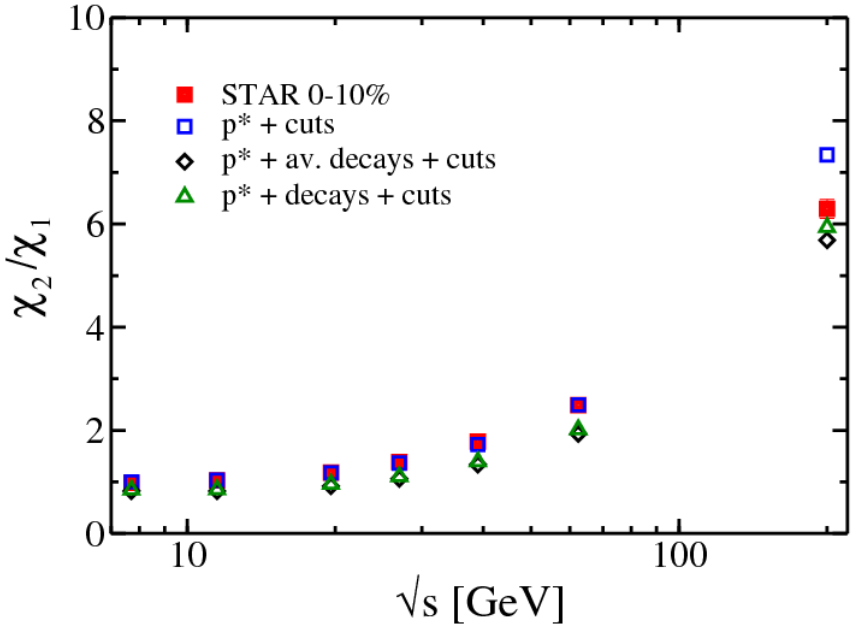

Figure 3.4: Ratios of susceptibilities as function of the collision energy with resonance decays taken into account. Taken from [8].

The factors $\langle(\Delta n_h)^2\rangle_R$, $\langle(\Delta n_h)^2\rangle_R$ and $\langle(\Delta n_h)^4\rangle_{R,c}$ vanish for those resonances which have only one decay-channel or for which the number of formed hadrons $n_{h,r}^R$ of species h is the same in each decay-chanel r. As mentioned before, the subscript c denotes the value of the corresponding cumulant. The first three cumulants are equal to the corresponding central moments, which is why we can omit the subscript, whereas we cannot omit if we consider the fourth cumulant, which differs from the fourth central moment. That is why we retained the subscript c in both Eq. (3.27) and Eq. (3.32).

We may now - exactly as in the previous Section - compute the ratios of susceptibilities as defined before. We should mention that in our framework primordial protons and anti-protons are uncorrelated and no baryonic or anti-baryonic resonance decays into an anti-proton or proton, the formula given by Eq.(3.28) remains valid for the susceptibilities of the net proton distribution even when resonance decays are included.

In Fig. 3.4-3.6, we see the dependence of ratios of susceptibilities as function of the collision energy $\sqrt{s}$ and the comparison with Fig. 3.1-3.3, where the resonance decays were not taken into account. The **empty squares** show the same as in Fig. 3.1-3.3, the **empty diamonds** show the average influence of the resonance decays on the net-proton fluctuations. The **empty triangles** depict the full impact of resonance decays and include the probabilistic contribution.

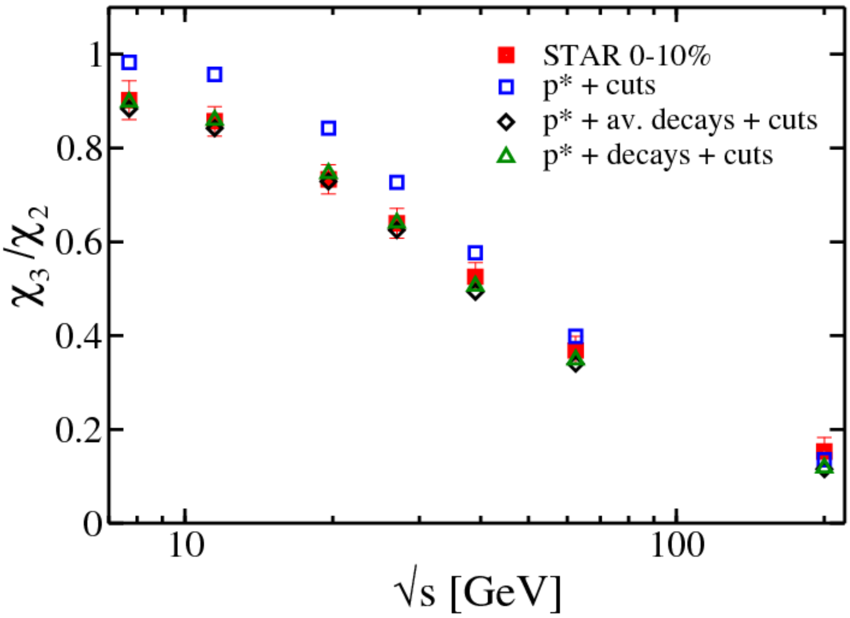

Figure 3.5: Ratios of susceptibilities as function of the collision energy with resonance decays taken into account. Taken from [8].

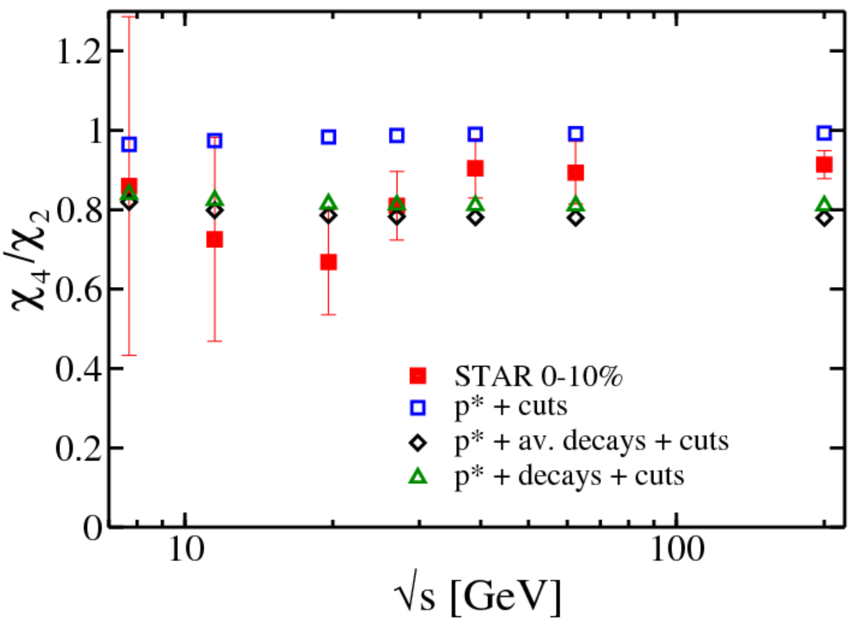

Figure 3.6: Ratios of susceptibilities as function of the collision energy with resonance decays taken into account. Taken from [8].

3.3.1 Particle correlation after resonance decays and the Generating Function

As we have already mentioned, the resonance decay has a probabilistic character, which causes the particle number fluctuations in the final state. The main goal of this subsection is to provide information on how to determine the particle correlation. The statistical central moments can be found from the following function called the **generating function**:

$$G \equiv \prod_R \left(\sum_r b_r^R \prod_i \lambda_i^{n_{i,r}^R} \right)^{N_R} \tag{3.33}$$

where b_r^R is the branching ratio of the $r-$th branch, $n_{i,r}^R$ the number of $i-$th particles produced in that decay mode and r runs over all branches with requirement $\sum_r b_r^R = 1$. The λ_i are auxiliary parameters set to one in the final formulae.

The averages from resonance decays can expressed as:

$$\bar{N}_i \equiv \sum_R \langle N_i \rangle_R = \lambda_i \frac{\partial}{\partial \lambda_i} G = \sum_R N_R \sum_r b_r^R n_{i,r}^R \equiv \sum_R N_R \langle n_i \rangle_R \,, \tag{3.34}$$

$$\begin{aligned} \overline{N_i N_j} \quad &\equiv \quad \sum_R \langle N_i N_j \rangle_R = \lambda_i \frac{\partial}{\partial \lambda_i} \left(\lambda_j \frac{\partial}{\partial \lambda_j} G \right) \\ &= \quad \sum_R [N_R (N_R - 1) \langle n_i \rangle_R \langle n_j \rangle_R + N_R \langle n_i n_j \rangle_R], \end{aligned} \tag{3.35}$$

where $\langle n_i n_j \rangle \equiv \sum_r b_r^R n_{i,r}^R n_{j,r}^R$.

The origin of the formula defined by Eq. (3.33) is given by the fact that the normalized probability distribution $P(N_R^r)$ for the decay of N_R resonances is the following:

$$P(N_R^r) = N_R! \prod_r \frac{(b_r^R)^{N_R^r}}{N_R^r!} \delta \left(\sum_r N_R^r - N_R \right) , \tag{3.36}$$

where N_R^r denotes the numbers of $R-$th resonances decaying via $r-$th branch.

The scaled variance ω_R^{i*} due to decays of $R-$th resonances will then read

$$\omega_R^{i*} \equiv \frac{\langle N_i^2 \rangle_R - \langle N_i \rangle_R^2}{\langle N_i \rangle_R} = \frac{\langle n_i^2 \rangle_R - \langle n_i \rangle_R^2}{\langle n_i \rangle_R} \equiv \frac{\sum_r b_r^R (n_{i,r}^R)^2 - (\sum_r b_r^R n_{i,r}^R)^2}{\sum_r b_r^R n_{i,r}^R} . \tag{3.37}$$

We can immediately see that Eq. (3.37) is equal to 0, if either $n_{i,r}^R$ are the same in all decay channels or if there is only one decay channel, which would mean $b_1^R = 1$.

Also, Eq. (3.34) and (3.35) assume fixed values of N_R, while in reality, N_R fluctuates, due to which we finally arrive at

$$\omega_R^i \equiv \frac{\langle\langle N_i^2\rangle\rangle_T - \langle\langle N_i\rangle_R\rangle_T^2}{\langle\langle N_i\rangle_R\rangle_T} = \omega_R^{i*} + \langle n_i\rangle_R\,\omega_R, \tag{3.38}$$

where the scaled variance

$$\omega_R = \frac{\langle N_R^2\rangle_T - \langle N_R\rangle_T^2}{\langle N_R\rangle_T} \tag{3.39}$$

corresponds to the thermal fluctuation of the number of resonances [2].

3.4 Experimental cuts

In Fig. 3.1-3.3 and Fig. 3.4-3.6, a reference to "(experimental) cuts" has been made. This means that the experimental phase-space coverage is limited in rapidity y and transverse momentum k_T according to the detector design and the demands from reconstruction efficiency and particle identification [8]. The following kinematic acceptance cuts have been considered by the STAR collaboration: $|y| \leq 0.5$ and $0.4 \leq k_T \leq 0.8$ GeV with full azimuthal coverage ($\phi = 2\pi$).

For our purposes, the acceptance cuts can be modelled by limiting the integration range in Eq. (3.8) and Eq. (3.10) accordingly [8]. This means that the momentum variables (k_x, k_y, k_z) are transformed into (k, y, ϕ), which implies replacing the integration measure d^3k by $k_T\sqrt{k_T^2 + m_i^2}\cosh(y)\ dk_T dy d\phi$ and the single-particle energies ϵ_i by $\cosh(y)\sqrt{k_T^2 + m_i^2}$. Thus, the results for the net-proton fluctuations as shown in the mentioned figures can (and could) be obtained.

Chapter 4

Multiplicity fluctuations for a resonance gas model with chemical non-equilibrium

The main aim of this chapter is to provide formulae for the temperature dependence of the (net-)baryon and (net-)proton number multiplicity along with that of the ratios of higher thermodynamic susceptibilities, while chemical potentials, whose calculation will also be summarized, will appear for each stable particle species. Before we do that, we will summarize some of the facts we have stated in the previous Chapters. The effect of resonance decays will also be taken into account. As such, we approximate the hadron gas by a collection of free particles [6], distributed according to

$$dN_i = \frac{d^3x d^3p}{(2\pi)^3} g_i \left\{ \exp\left(\frac{E-\mu_i}{T}\right) \pm 1 \right\}^{-1} \tag{4.1}$$

where μ_i is the chemical potential of level $i, i = \pi, K, \rho, N, \dots$ and $E = \sqrt{m_i^2 + p^2}$ and $\pm$ depends on whether the particle is a fermion or a boson, $g_i = 2J_i + 1$ is the isospin degeneration factor corresponding to the statistical weight, providing $(g_\pi = 3, g_K = 4, g_\rho = 9, \dots)$.

The pressure generated by the distribution (4.1) is given by

$$P = T \sum_i \pm g_i \int \frac{d^3p}{(2\pi)^3} \ln\left\{ 1 \pm \exp\left(\frac{\mu_i - E}{T}\right) \right\}. \tag{4.2}$$

where we assumed $V = 1$.

4.1 Chemical potentials in a HRG model with chemical non-equilibrium

In order to be able to lay down the formalism describing the state of chemical non-equilibrium, we have to consider the chemical potentials first. All performed calculations are in accordance with [6]. They start building up once the chemical equilibrium is lost. We assume that the population of the excited states remains in equilibrium with the particles formed in their decay [6]. Furthermore, we set the chemical potential of the mother equal to the sum of the chemical potentials of the daughters. If there are several decay channels (i. e. more than one) open, we multiply the various final state configurations with the corresponding branching ratio.

Let us for example consider the states $\rho(770)$, $\Delta(1231)$ and $a_2(1320)$. Considering the aforementioned assumptions, this leads to

$$\mu_\rho = 2\mu_\pi,$$

$$\mu_\Delta = \mu_\pi + \mu_N$$

and

$$\mu_{a_2} = 2.8\mu_\pi + 0.1\mu_K + 0.15\mu_\eta.$$

The condition for partial equilibrium determines the chemical potentials of the excited states as functions of the potentials corresponding to the stable particles

$$\sigma = \{\pi, K, \eta, N, \Lambda, \Sigma, \Xi, \Omega\}$$

, which occur as end products of the decay chain

$$\mu_i = \sum_\sigma d_i^\sigma \mu_\sigma \tag{4.3}$$

where d_i^σ is the mean number of stable particles emerging in the decay of the level i, e. g., d_i^π. is the mean number of pions emerging in the decay of the level i.

If we want to obtain the temperature dependence of chemical potentials of hadron species by assuming fixed adundancies after a chemical freeze-out (as is our case, see Figure E.1, which is characterized by a freeze-out temperature $T^{(fo)}$ and chemical potentails for baryon number μ_B and strangeness μ_S, we perform this recursively using the formalism above, with the initial potentials being calculated as

$$\mu_\sigma = B_\sigma \mu_B + S_\sigma \mu_S$$

where B_σ is the baryon number and S_σ the strangeness of the stable particle σ, while including every resonance in the model decaying into the respective stable particle. This allows us to account for several collision energies $\sqrt{s_{NN}}$ (see further text), as these are characterized by the set $\{T^{(fo)}, \mu_B, \mu_S\}$.

4.2 The partition function and higher moments of particle distributions at chemical non-equilibrium

We now have everything we need to introduce the full-scale formalism of multiplicity fluctuations within systems in chemical non-equilibrium. Let us now perform the following denotations:

· $i \ldots$ all particles (resonances) included in the model
· $j \ldots$ j-th stable particle
· $A \ldots$ set of all stable particles
· $A_B \ldots$ set of stable baryons
· $N_{ji} \ldots$ average number of the j-th stable particle produced by channel i, equivalent to d_i^σ in 4.1
· $\mu_j \ldots$ chemical potential of stable particle j obtained as described in 4.1
· $m_i \ldots$ mass of resonance i
· $d_i \ldots$ isospin degeneracy of the i-th particle

As we shall further concentrate on baryons only, we may write the logarithm of the partition function for the i-th resonance as

$$\ln Z^B_{m_i}(V,T,\vec{\mu}) = \frac{V d_i}{(2\pi)^3} \int d^3k \ln\left(1+\exp\left(\frac{\sum_{j\in A} N_{ji}\mu_j}{T}\right)\exp\left(-\frac{\sqrt{k^2+m_i^2}}{T}\right)\right). \quad (4.4)$$

Transforming into spherical coordinates using

$$k_1 = p\sin\vartheta\cos\varphi,$$

$$k_2 = p\sin\vartheta\sin\varphi,$$

$$k_3 = p\cos\vartheta$$

with

$$p \in <0,+\infty),$$

$$\vartheta \in <0,\pi>,$$

$$\varphi \in <0,2\pi>,$$

one obtains

$$\begin{aligned}
\ln Z^B_{m_i}(V,T,\vec{\mu}) &= \frac{V d_i}{(2\pi)^3}\int_0^{+\infty}\int_0^{\pi}\int_0^{2\pi} p^2 \times \qquad (4.5)\\
&\times \ln\left(1+\exp\left(\frac{\sum_{j\in A} N_{ji}\mu_j}{T}\right)\exp\left(-\frac{\sqrt{p^2+m_i^2}}{T}\right)\right) dp\sin\vartheta d\vartheta d\varphi = \\
&= \frac{V d_i}{2\pi^2}\int_0^{+\infty} p^2 \ln\left(1+\exp\left(\frac{\sum_{j\in A} N_{ji}\mu_j}{T}\right)\exp\left(-\frac{\sqrt{p^2+m_i^2}}{T}\right)\right) dp := \\
&:= \frac{V d_i}{2\pi^2} I(p,m_i).
\end{aligned}$$

where $I(p, m_i)$ represents the integral.

In order to conveniently compute the integral $I(p, m_i)$, we shall use the Taylor expansion. At first, we will define

- $u(p) := \exp\left(-\frac{\sqrt{p^2+m_i^2}}{T}\right)$
- $z^{ineq.} := \exp\left(\frac{\sum_{j\in A} N_{ji}\mu_j}{T}\right)$,

thus $u(+\infty) = 0$. Since all the baryon masses i are above 1 GeV, it is convenient (and justified) to perform the Taylor equation of $I(p, m_i)$ at infinity. The function

$$f(p) = \ln\left(1 + \exp\left(\frac{\sum_{j\in A} N_{ji}\mu_j}{T}\right)\exp\left(-\frac{\sqrt{p^2+m_i^2}}{T}\right)\right)$$

then transforms into

$$f(u) = \ln(1 + z^{ineq.}u),$$

where we perform the Taylor expansion at 0. We may therefore use the following MacLaurin series:

$$\ln(1 + z^{ineq.}u) = \sum_{k=1}^{+\infty}(-1)^{k+1} z^{ineq.k}\frac{u^k}{k}, \tag{4.6}$$

therefore, Eq. (4.5) transforms into

$$\ln Z^B_{m_i}(V, T, \vec{\mu}) = \frac{Vd_i}{2\pi^2}\sum_{k=1}^{+\infty}\frac{(-1)^{k+1}}{k} z^{ineq.k}\int_0^{+\infty} p^2u^k(p)dp. \tag{4.7}$$

We may now perform the following parametrization for

$$\int_0^{+\infty} p^2u^k(p)dp :$$

- $p = m_i \sinh\eta$
- $dp = m_i \cosh\eta d\eta.$

Using the relation

$$\cosh^2\eta - \sinh^2\eta = 1,$$

one arrives at

$$\int_0^{+\infty} p^2u^k(p) = \int_0^{+\infty} m_i^3 \exp\left(-\frac{k}{T}m_i\cosh\eta\right)\cosh\eta\sinh^2\eta d\eta,$$

which can be recast as

$$\int_0^{+\infty} p^2u^k(p) = m_i^3\left(\int_0^{+\infty}\cosh^3\eta\exp\left(-\frac{k}{T}m_i\cosh\eta\right)d\eta - \int_0^{+\infty}\cosh\eta\exp\left(-\frac{k}{T}m_i\cosh\eta\right)d\eta\right).$$

We use the identity

$$\cosh^3\eta = \frac{1}{4}\cosh(3\eta) + \frac{3}{4}\cosh(\eta),$$

which leads to

$$\int_0^{+\infty} p^2 u^k(p) = \frac{1}{4}m_i^3\left(\int_0^{+\infty}\cosh(3\eta)\exp\left(-\frac{k}{T}m_i\cosh\eta\right)d\eta - \right.$$
$$\left. - \int_0^{+\infty}\cosh\eta\exp\left(-\frac{k}{T}m_i\cosh\eta\right)d\eta\right)$$

In accordance with with Appendix A and with [26], we may write

$$\int_0^{+\infty} p^2 u^k(p) = \frac{1}{4}m_i^3\left(K_3\left(\frac{km_i}{T}\right) - K_1\left(\frac{km_i}{T}\right)\right)$$

where K_1, K_3 are modified Bessel functions of the second kind (see Appendix A). This - in accordance with the corresponding recurrence relation given by Eq. (A.14) - immediately leads to

$$\int_0^{+\infty} p^2 u^k(p) = \frac{m_i^2}{k}TK_2\left(\frac{km_i}{T}\right).$$

Therefore, Eqs. (4.4-4.7) can be recast as

$$\ln Z^B_{m_i}(V,T,\vec{\mu}) = VT\frac{d_i m_i^2}{2\pi^2}\sum_{k=1}^{+\infty}\frac{(-1)^{k+1}}{k^2}\exp\left(\frac{k}{T}\sum_{j\in A}N_{ji}\mu_j\right)K_2\left(\frac{km_i}{T}\right). \tag{4.8}$$

4.3 (Net-)baryon and (net-)proton number densities

We shall also - for the coming Chapter to be more straightforward - explicitly mention the relations expressing the (anti)baryon number density

$$\begin{aligned} n_B &= \frac{\langle N_B\rangle}{V} = \frac{T}{2\pi^2}\sum_i\sum_{k=1}^{+\infty}\sum_{a\in A_B}N_{ai}d_i m_i^2\frac{(-1)^{k+1}}{k}\cdot \\ &\cdot\exp\left(\frac{k}{T}\sum_{j\in A}N_{ji}\mu_j\right)K_2\left(\frac{km_i}{T}\right)\end{aligned} \tag{4.9}$$

$$\begin{aligned} n_{\bar{B}} &= \frac{\langle N_{\bar{B}}\rangle}{V} = \frac{T}{2\pi^2}\sum_i\sum_{k=1}^{+\infty}\sum_{a\in A_B}N_{\bar{a}i}d_i m_i^2\frac{(-1)^{k+1}}{k}\cdot \\ &\cdot\exp\left(\frac{k}{T}\sum_{j\in A}N_{ji}\mu_j\right)K_2\left(\frac{km_i}{T}\right)\end{aligned} \tag{4.10}$$

and the (anti)proton number density

$$n_p = \frac{\langle N_p \rangle}{V} = \frac{T}{2\pi^2}\sum_i \sum_{k=1}^{+\infty} N_{pi} d_i m_i^2 \frac{(-1)^{k+1}}{k} \exp\left(\frac{k}{T}\sum_{j\in A} N_{ji}\mu_j\right) K_2\left(\frac{km_i}{T}\right) \quad (4.11)$$

$$n_{\bar{p}} = \frac{\langle N_{\bar{p}} \rangle}{V} = \frac{T}{2\pi^2}\sum_i \sum_{k=1}^{+\infty} N_{\bar{p}i} d_i m_i^2 \frac{(-1)^{k+1}}{k} \exp\left(\frac{k}{T}\sum_{j\in A} N_{ji}\mu_j\right) K_2\left(\frac{km_i}{T}\right) \quad (4.12)$$

which for net-quantities obviously lead to terms included in the denominators of Eq. (4.20) and Eq. (4.21), respectively, in the following Section:

$$\begin{aligned} n_{B-\bar{B}} &= n_B - n_{\bar{B}} \quad (4.13) \\ &= \frac{T}{2\pi^2}\sum_i \sum_{k=1}^{+\infty} \sum_{a\in A_B} (N_{ai} - N_{\bar{a}i}) d_i m_i^2 \frac{(-1)^{k+1}}{k} \exp\left(\frac{k}{T}\sum_{j\in A} N_{ji}\mu_j\right) K_2\left(\frac{km_i}{T}\right) \end{aligned}$$

$$\begin{aligned} n_{p-\bar{p}} &= n_p - n_{\bar{p}} \quad (4.14) \\ &= \frac{T}{2\pi^2}\sum_i \sum_{k=1}^{+\infty} (N_{pi} - N_{\bar{p}i}) d_i m_i^2 \frac{(-1)^{k+1}}{k} \exp\left(\frac{k}{T}\sum_{j\in A} N_{ji}\mu_j\right) K_2\left(\frac{km_i}{T}\right) \end{aligned}$$

4.4 Net-baryon number and net-proton number variances

In accordance with Eq. (C.10) in Appendix C and for

$$Cov(N_a, N_b) = T^2 \frac{\partial^2 \ln[Z(V,T,\vec{\mu}]}{\partial\mu_a \partial\mu_b},$$

we obtain

$$\begin{aligned} Var(N_{B-\bar{B}}) &= \sum_{a,b\in A_B} (Cov(N_a, N_b) + Cov(N_{\bar{a}}, N_{\bar{b}}) \quad (4.15) \\ &- Cov(N_{\bar{a}}, N_b) - Cov(N_a, N_{\bar{b}})) \\ &= \frac{VT}{2\pi^2}\sum_i \sum_{k=1}^{+\infty} \sum_{a,b\in A_B} (N_{ai}N_{bi} + N_{\bar{a}i}N_{\bar{b}i} - N_{\bar{a}i}N_{bi} - N_{a_i}N_{\bar{b}i}) \cdot \\ &\cdot \ d_i m_i^2 (-1)^{k+1} \exp\left(\frac{k}{T}\sum_{j\in A} N_{ji}\mu_j\right) K_2\left(\frac{km_i}{T}\right) \\ &= \frac{VT}{2\pi^2}\sum_i \sum_{k=1}^{+\infty} \sum_{a,b\in A_B} (N_{ai} - N_{\bar{a}i})(N_{bi} - N_{\bar{b}i}) \cdot \\ &\cdot \ d_i m_i^2 (-1)^{k+1} \exp\left(\frac{k}{T}\sum_{j\in A} N_{ji}\mu_j\right) K_2\left(\frac{km_i}{T}\right), \end{aligned}$$

which specifically for protons (which for the Eq. above means $a = b = p$) results in

$$\begin{aligned} Var(N_{p-\bar{p}}) &= \frac{VT}{2\pi^2}\sum_i \sum_{k=1}^{+\infty}(N_{pi} - N_{pi})^2 \cdot \\ &\cdot \quad d_i m_i^2 (-1)^{k+1} \exp\left(\frac{k}{T}\sum_{j\in A} N_{ji}\mu_j\right) K_2\left(\frac{km_i}{T}\right). \end{aligned} \tag{4.16}$$

4.5 Scaled variance of the (net-)baryon number and (net-)proton multiplicity distribution

In accordance with the definition of the scaled variance written down in chapter 2 which we will - entirely for the sake of clarity - once again mention here

$$\omega = \frac{\langle N^2\rangle - \langle N\rangle^2}{\langle N\rangle}, \tag{4.17}$$

combined with

$$\langle N_{B-\bar{B}}\rangle = T\sum_{a\in A_B}\left(\frac{\partial \ln Z}{\partial \mu_a} - \frac{\partial \ln Z}{\partial \mu_{\bar{a}}}\right) \tag{4.18}$$

for the whole set of net-baryons and

$$\langle N_{p-\bar{p}}\rangle = T\left(\frac{\partial \ln Z}{\partial \mu_p} - \frac{\partial \ln Z}{\partial \mu_{\bar{p}}}\right) \tag{4.19}$$

specifically for net-protons, one may write

$$\begin{aligned} \omega_{B-\bar{B}} &= \frac{\left\langle N_{B-\bar{B}}^2\right\rangle - \langle N_{B-\bar{B}}\rangle^2}{\langle N_{B-\bar{B}}\rangle} \\ &= \frac{\sum_i \sum_{k=1}^{+\infty}\sum_{a,b\in A_B}(N_{ai} - N_{\bar{a}i})(N_{bi} - N_{\bar{b}i}) d_i m_i^2 (-1)^{k+1}\exp\left(\frac{k}{T}\mu_i\right) K_2\left(\frac{km_i}{T}\right)}{\sum_i \sum_{k=1}^{+\infty}\sum_{a\in A_B}(N_{ai} - N_{\bar{a}i}) d_i m_i^2 \frac{(-1)^{k+1}}{k}\exp\left(\frac{k}{T}\mu_i\right) K_2\left(\frac{km_i}{T}\right)} \end{aligned} \tag{4.20}$$

where $\mu_i = \sum_{j\in A} N_{ji}\mu_j$ for the whole set of net-baryons or specifically

$$\begin{aligned} \omega_{p-\bar{p}} &= \frac{\left\langle N_{p-\bar{p}}^2\right\rangle - \langle N_{p-\bar{p}}\rangle^2}{\langle N_{p-\bar{p}}\rangle} \\ &= \frac{\sum_i \sum_{k=1}^{+\infty}(N_{pi} - N_{\bar{p}i})^2 d_i m_i^2 (-1)^{k+1}\exp\left(\frac{k}{T}\sum_{j\in A} N_{ji}\mu_j\right) K_2\left(\frac{km_i}{T}\right)}{\sum_i \sum_{k=1}^{+\infty}(N_{pi} - N_{\bar{p}i}) d_i m_i^2 \frac{(-1)^{k+1}}{k}\exp\left(\frac{k}{T}\sum_{j\in A} N_{ji}\mu_j\right) K_2\left(\frac{km_i}{T}\right)} \end{aligned} \tag{4.21}$$

for net-protons. Separately for protons and antiprotons, we may write

$$\begin{aligned} \omega_p &= \frac{\left\langle N_p^2\right\rangle - \langle N_p\rangle^2}{\langle N_p\rangle} \\ &= \frac{\sum_i \sum_{k=1}^{+\infty} N_{pi}^2 d_i m_i^2 (-1)^{k+1}\exp\left(\frac{k}{T}\sum_{j\in A} N_{ji}\mu_j\right) K_2\left(\frac{km_i}{T}\right)}{\sum_i \sum_{k=1}^{+\infty} N_{pi} d_i m_i^2 \frac{(-1)^{k+1}}{k}\exp\left(\frac{k}{T}\sum_{j\in A} N_{ji}\mu_j\right) K_2\left(\frac{km_i}{T}\right)}, \end{aligned} \tag{4.22}$$

$$
\begin{aligned}
\omega_{\bar{p}} &= \frac{\left\langle N_{\bar{p}}^2\right\rangle - \left\langle N_{\bar{p}}\right\rangle^2}{\left\langle N_{\bar{p}}\right\rangle} \\
&= \frac{\sum_i \sum_{k=1}^{+\infty} N_{\bar{p}i}^2 d_i m_i^2 (-1)^{k+1} \exp\left(\frac{k}{T}\sum_{j\in A} N_{ji}\mu_j\right) K_2\left(\frac{km_i}{T}\right)}{\sum_i \sum_{k=1}^{+\infty} N_{\bar{p}i} d_i m_i^2 \frac{(-1)^{k+1}}{k} \exp\left(\frac{k}{T}\sum_{j\in A} N_{ji}\mu_j\right) K_2\left(\frac{km_i}{T}\right)}.
\end{aligned}
\tag{4.23}
$$

The definition of the scaled variance given by Eq. (2.5) and Eq. (4.17) corresponds to the following ratio of susceptibilities

$$\frac{\chi_2}{\chi_1} = \frac{\sigma^2}{M},$$

where M is the mean value. This is entirely in accordance with [8] and Appendix C.

4.6 Third and fourth moment of the (net-)baryon number and (net-)proton distribution

In accordance with the formalism laid down above and with Appendix C, we may now write down the relations for skewness (S) and kurtosis (κ), which we will do - for the sake of transparency - in the form of *ratios of susceptibilities*

$$\frac{\chi_3}{\chi_2} = S\sigma$$

and

$$\frac{\chi_4}{\chi_2} = \kappa\sigma^2,$$

whose definitions are in accordance with [8] and with Appendix C.

For the whole set of stable baryons, the formulae - see Appendix C - are as follows:

$$S\sigma \mid_B = \frac{\sum_i \sum_{k=1}^{+\infty} \sum_{a,b,c\in A_B} d_i m_i^2 (-1)^{k+1} k N_{ai} N_{bi} N_{ci} \exp\left(\frac{k}{T}\sum_{j\in A} N_{ji}\mu_j\right) K_2\left(\frac{km_i}{T}\right)}{\sum_i \sum_{k=1}^{+\infty} \sum_{a,b\in A_B} d_i m_i^2 (-1)^{k+1} N_{ai} N_{bi} \exp\left(\frac{k}{T}\sum_{j\in A} N_{ji}\mu_j\right) K_2\left(\frac{km_i}{T}\right)} \tag{4.24}$$

$$\kappa\sigma^2 \mid_B = \frac{\sum_i \sum_{k=1}^{+\infty} \sum_{a,b,c,d\in A_B} d_i m_i^2 (-1)^{k+1} k^2 N_{ai} N_{bi} N_{ci} N_{di} \exp\left(\frac{k}{T}\sum_{j\in A} N_{ji}\mu_j\right) K_2\left(\frac{km_i}{T}\right)}{\sum_i \sum_{k=1}^{+\infty} \sum_{a,b\in A_B} d_i m_i^2 (-1)^{k+1} N_{ai} N_{bi} \exp\left(\frac{k}{T}\sum_{j\in A} N_{ji}\mu_j\right) K_2\left(\frac{km_i}{T}\right)} \tag{4.25}$$

for baryons, for antibaryons we obtain

$$S\sigma \mid_{\bar{B}} = \frac{\sum_i \sum_{k=1}^{+\infty} \sum_{a,b,c\in A_B} d_i m_i^2 (-1)^{k+1} k N_{\bar{a}i} N_{\bar{b}i} N_{\bar{c}i} \exp\left(\frac{k}{T}\sum_{j\in A} N_{ji}\mu_j\right) K_2\left(\frac{km_i}{T}\right)}{\sum_i \sum_{k=1}^{+\infty} \sum_{a,b\in A_B} d_i m_i^2 (-1)^{k+1} N_{\bar{a}i} N_{\bar{b}i} \exp\left(\frac{k}{T}\sum_{j\in A} N_{ji}\mu_j\right) K_2\left(\frac{km_i}{T}\right)} \tag{4.26}$$

$$\kappa\sigma^2 \mid_{\bar{B}} = \frac{\sum_i \sum_{k=1}^{+\infty} \sum_{a,b,c,d \in A_B} d_i m_i^2 (-1)^{k+1} k^2 N_{\bar{a}i} N_{\bar{b}i} N_{\bar{c}i} N_{\bar{d}i} \exp\left(\frac{k}{T} \sum_{j \in A} N_{ji}\mu_j\right) K_2\left(\frac{km_i}{T}\right)}{\sum_i \sum_{k=1}^{+\infty} \sum_{a,b \in A_B} d_i m_i^2 (-1)^{k+1} N_{\bar{a}i} N_{\bar{b}i} \exp\left(\frac{k}{T} \sum_{j \in A} N_{ji}\mu_j\right) K_2\left(\frac{km_i}{T}\right)}. \tag{4.27}$$

Obviously, in accordance with Appendix C, the following formulae hold for a net-baryon distribution:

$$S\sigma \mid_{net\ B} = \frac{\sum_i \sum_{k=1}^{+\infty} \sum_{a,b,c \in A_B} \prod_{q=a}^{c} d_i m_i^2 (-1)^{k+1} k (N_{qi} - N_{\bar{q}i}) \exp\left(\frac{k}{T}\mu_i\right) K_2\left(\frac{km_i}{T}\right)}{\sum_i \sum_{k=1}^{+\infty} \sum_{a,b \in A_B} d_i m_i^2 (-1)^{k+1} (N_{ai} - N_{\bar{a}i})(N_{bi} - N_{\bar{b}i}) \exp\left(\frac{k}{T}\mu_i\right) K_2\left(\frac{km_i}{T}\right)} \tag{4.28}$$

$$\kappa\sigma^2 \mid_{net\ B} = \frac{\sum_i \sum_{k=1}^{+\infty} \sum_{a,b,c,d \in A_B} \prod_{q=a}^{d} d_i m_i^2 (-1)^{k+1} k^2 (N_{qi} - N_{\bar{q}i}) \exp\left(\frac{k}{T}\mu_i\right) K_2\left(\frac{km_i}{T}\right)}{\sum_i \sum_{k=1}^{+\infty} \sum_{a,b \in A_B} d_i m_i^2 (-1)^{k+1} (N_{ai} - N_{\bar{a}i})(N_{bi} - N_{\bar{b}i}) \exp\left(\frac{k}{T}\mu_i\right) K_2\left(\frac{km_i}{T}\right)} \tag{4.29}$$

where $\mu_i = \sum_{j \in A} N_{ji}\mu_j$ and

$$\prod_{q=a}^{c} (N_{qi} - N_{\bar{q}i}) = (N_{ai} - N_{\bar{a}i})(N_{bi} - N_{\bar{b}i})(N_{ci} - N_{\bar{c}i}),$$

$$\prod_{q=a}^{d} (N_{qi} - N_{\bar{q}i}) = (N_{ai} - N_{\bar{a}i})(N_{bi} - N_{\bar{b}i})(N_{ci} - N_{\bar{c}i})(N_{di} - N_{\bar{d}i}).$$

If we now restrict the formulae to protons (and antiprotons) only, we obtain the following formulae:

$$S\sigma \mid_p = \frac{\chi_3^{(p)}}{\chi_2^{(p)}} = \frac{\sum_i \sum_{k=1}^{+\infty} N_{pi}^3 d_i m_i^2 (-1)^{k+1} k \exp\left(\frac{k}{T} \sum_{j \in A} N_{ji}\mu_j\right) K_2\left(\frac{km_i}{T}\right)}{\sum_i \sum_{k=1}^{+\infty} N_{pi}^2 d_i m_i^2 (-1)^{k+1} \exp\left(\frac{k}{T} \sum_{j \in A} N_{ji}\mu_j\right) K_2\left(\frac{km_i}{T}\right)} \tag{4.30}$$

$$\kappa\sigma^2 \mid_p = \frac{\chi_4^{(p)}}{\chi_2^{(p)}} = \frac{\sum_i \sum_{k=1}^{+\infty} N_{pi}^4 d_i m_i^2 (-1)^{k+1} k^2 \exp\left(\frac{k}{T} \sum_{j \in A} N_{ji}\mu_j\right) K_2\left(\frac{km_i}{T}\right)}{\sum_i \sum_{k=1}^{+\infty} N_{pi}^2 d_i m_i^2 (-1)^{k+1} \exp\left(\frac{k}{T} \sum_{j \in A} N_{ji}\mu_j\right) K_2\left(\frac{km_i}{T}\right)} \tag{4.31}$$

and for antiprotons as follows

$$S\sigma \mid_{\bar{p}} = \frac{\chi_3^{(\bar{p})}}{\chi_2^{(\bar{p})}} = \frac{\sum_i \sum_{k=1}^{+\infty} N_{\bar{p}i}^3 d_i m_i^2 (-1)^{k+1} k \exp\left(\frac{k}{T} \sum_{j \in A} N_{ji}\mu_j\right) K_2\left(\frac{km_i}{T}\right)}{\sum_i \sum_{k=1}^{+\infty} N_{\bar{p}i}^2 d_i m_i^2 (-1)^{k+1} \exp\left(\frac{k}{T} \sum_{j \in A} N_{ji}\mu_j\right) K_2\left(\frac{km_i}{T}\right)} \tag{4.32}$$

$$\kappa\sigma^2 \mid_{\bar{p}} = \frac{\chi_4^{(\bar{p})}}{\chi_2^{(\bar{p})}} = \frac{\sum_i \sum_{k=1}^{+\infty} N_{\bar{p}i}^4 d_i m_i^2 (-1)^{k+1} k^2 \exp\left(\frac{k}{T} \sum_{j \in A} N_{ji}\mu_j\right) K_2\left(\frac{km_i}{T}\right)}{\sum_i \sum_{k=1}^{+\infty} N_{\bar{p}i}^2 d_i m_i^2 (-1)^{k+1} \exp\left(\frac{k}{T} \sum_{j \in A} N_{ji}\mu_j\right) K_2\left(\frac{km_i}{T}\right)}. \tag{4.33}$$

For a net-proton distribution, the formulae are the following

$$S\sigma \mid_{net\ p} = \frac{\sum_i \sum_{k=1}^{+\infty} (N_{pi} - N_{\bar{p}i})^3 d_i m_i^2 (-1)^{k+1} k \exp\left(\frac{k}{T} \sum_{j \in A} N_{ji}\mu_j\right) K_2\left(\frac{km_i}{T}\right)}{\sum_i \sum_{k=1}^{+\infty} (N_{pi} - N_{\bar{p}i})^2 d_i m_i^2 (-1)^{k+1} \exp\left(\frac{k}{T} \sum_{j \in A} N_{ji}\mu_j\right) K_2\left(\frac{km_i}{T}\right)}, \tag{4.34}$$

$$\kappa\sigma^2\mid_{net\ p}= \frac{\sum_i \sum_{k=1}^{+\infty}(N_{pi}-N_{\bar{p}_i})^4 d_i m_i^2 (-1)^{k+1} k^2 \exp\left(\frac{k}{T}\sum_{j\in A} N_{ji}\mu_j\right) K_2\left(\frac{km_i}{T}\right)}{\sum_i \sum_{k=1}^{+\infty}(N_{pi}-N_{\bar{p}i})^2 d_i m_i^2 (-1)^{k+1} \exp\left(\frac{k}{T}\sum_{j\in A} N_{ji}\mu_j\right) K_2\left(\frac{km_i}{T}\right)}. \quad (4.35)$$

As none of the terms given by Eq. (4.9)-(4.14) and Eq. (4.20) - (4.35) is volume-dependent, it is convenient to use them for further calculations, since the volume is not a priori known.

Chapter 5

Results

The derived formulae will now be implemented using data from DRAGON with the newest PDG update (see Appendix E). The calculations will be performed for the most central $Au + Au$ collisions (centrality 0-5 and 5-10) and for seven collision energies in accordance with [21], these being $\sqrt{s_{NN}} = 7.7, 11.5, 19.6, 27.0, 39.0, 62.4, 200$ GeV. For our purposes, the ratio fits (GCER) have been used, for which there are always corresponding chemical freeze-out parameters for grand canonical ensemble. All errors considered are systematic uncertainities. The statistical errors may be obtained by using the Delta theorem approach [12] [14]. For more details, see TABLE VIII in [21].

In this Chapter, the temperature dependencies of the (net-)proton number densities and the ratios of thermodynamic susceptibilities

$$\omega = \frac{\chi_2}{\chi_1},$$

$$S\sigma = \frac{\chi_3}{\chi_2}$$

and

$$\kappa\sigma^2 = \frac{\chi_4}{\chi_2}$$

will be presented for each of the collision energies and each centrality. On the top of each Figure, there is a depiction indicating which centrality and collision energy has been taken into account.

5.1 (Net-)proton number densities

The density of the particle number distribution for protons is given by Eq. 4.11, for antiprotons by Eq. 4.12 and for net-protons by Eq. 4.14. The corresponding Figures are Fig. 5.1a - 5.7a for centrality 0-5 and Fig. 5.8a - 5.14a for centrality 5-10.

One can see that for both centralities, protons, antiprotons and consequently also net-protons rise with the temperature monotonously. The density of net-protons increasingly differs from that of protons with the rising collision energy. This means that whereas for the lowest collision energy $\sqrt{s_{NN}} = 7.7$ GeV the number of antiprotons is almost zero (meaning that the proton-antiproton yield is dominated almost entirely by protons), this ceases to be the case as the collision energy increases. For $\sqrt{s_{NN}} = 200$ GeV, the density of antiprotons exceeds that of net-protons, which means that compared to the number of produced protons, also a considerable number of antiprotons emerges.

5.2 Scaled variance of the (net-)proton distribution

The scaled variance for protons is given by Eq. 4.22, for antiprotons by Eq. 4.23 and for net-protons by Eq. 4.21. The corresponding Figures are Fig. 5.1b - 5.7b for centrality 0-5 and Fig. 5.8b - 5.14b for centrality 5-10.

We can see that for both centralities, the scaled variance shows a decreasing trend with rising temperature. If we take a closer look at the individual results (i. e. for protons, antiprotons and net-protons separately), we realize that the scaled variance of protons and antiprotons remains approximately the same for all collision energies and both centralities, whereas that of the net-proton yield - while always retaining the decreasing trend characteristic for all yields - reaches an upwards shifting range of values (whose span remains approximately constant, this holds for the ranges of values of all scaled variance results for all yields) with increasing energy.

5.3 Ratio of the third and the second thermodynamic susceptibility for protons, antiprotons and net-protons

The product

$$S\sigma = \frac{\chi_3}{\chi_2}$$

is given by Eq. 4.30, for antiprotons by Eq. 4.32 and for net-protons by Eq. 4.34. The corresponding Figures are Fig. 5.1c - 5.7c for centrality 0-5 and Fig. 5.8c - 5.14c for centrality 5-10.

Again, for both centralities, a similar trend can be observed. This time, too, this means that the product $S\sigma$ shows a decreasing tendency with rising temperature. However, contrary to the scaled variance, the results for the net-proton yield show that the range of values (whose span remains approximately constant, this again holds for the ranges of values of all $S\sigma$ results for all yields) shifts downwards with rising collision energy (while always retaining the decreasing trend with rising temperature).

5.4 Ratio of the fourth and the second thermodynamic susceptibility for protons, antiprotons and netprotons

The product

$$\kappa\sigma^2 = \frac{\chi_4}{\chi_2}$$

is given by Eq. 4.31, for antiprotons by Eq. 4.33 and for net-protons by Eq. 4.35. The corresponding Figures are Fig. 5.1d - 5.7d for centrality 0-5 and Fig. 5.8d - 5.14d for centrality 5-10.

As was the case for all results before, a similar - this time again decreasing in terms of temperature dependence - trend can be observed here, again for both centralities and all collision energies. Whereas the results for protons and net-protons are very close for all energies and both centralities, those for anti-protons show a "converging" tendency towards protons and net-protons with rising collision energy. For both cetralities, the values for all three yields at $\sqrt{s_{NN}} = 200$ GeV are very close to each other.

As for the "spikes" one might observe in most of the Figures depicting the temperature dependence of $\kappa\sigma^2$, these must be entirely caused by the input values we put into the calculations, these being temperature T, the corresponding chemical potentials of stable particles μ_j and the average number of stable particles N_{ji} (see the beginning of the previous Chapter).

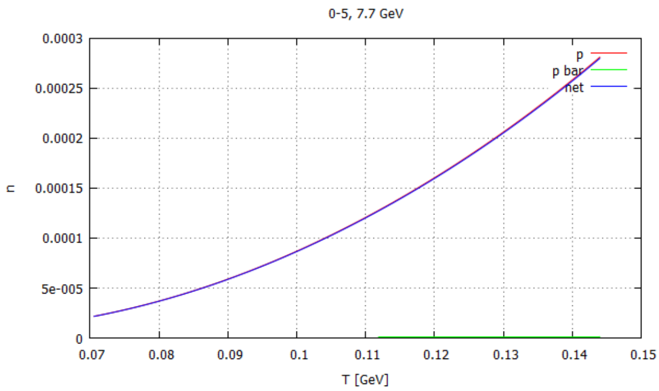

(a) Temperature dependence of the volume density.

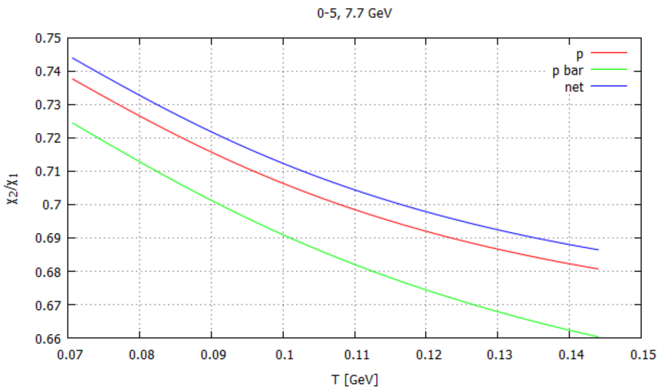

(b) Temperature dependence of the scaled variance.

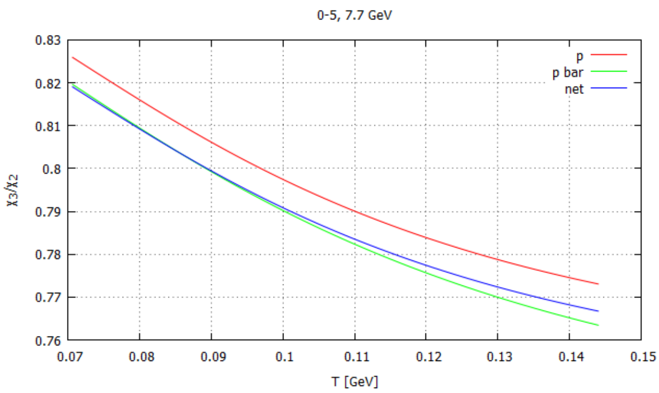

(c) Temperature dependence of $S\sigma$.

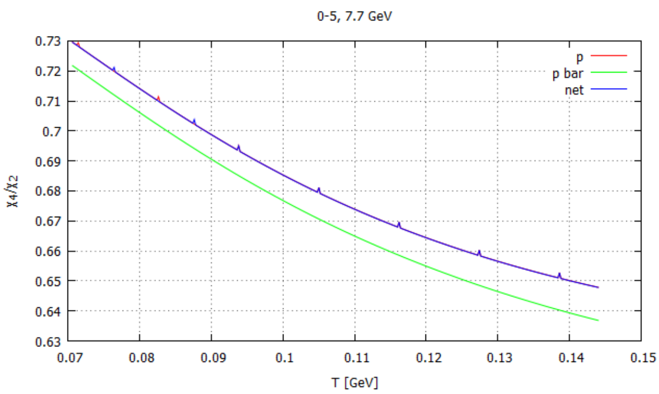

(d) Temperature dependence of $\kappa\sigma^2$.

Figure 5.1: Results for the volume density n (5.1a), scaled variance χ_2/χ_1 (5.1b) and the products of statistical moments $S\sigma$ (5.1c) and $\kappa\sigma^2$ (5.1d) of protons, antiprotons and net-protons for centrality 0-5 and collision energy $\sqrt{s_{NN}} = 7.7$ GeV.

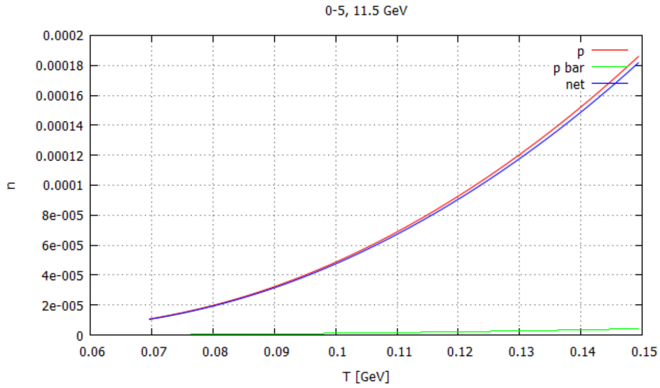

(a) Temperature dependence of the volume density.

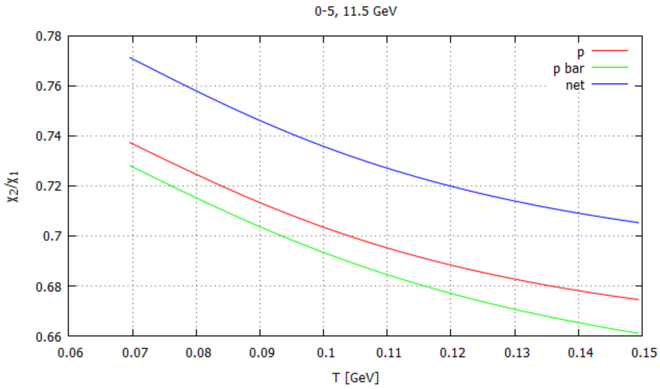

(b) Temperature dependence of the scaled variance.

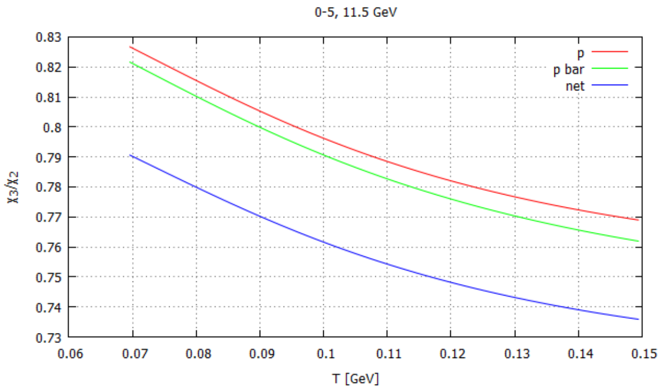

(c) Temperature dependence of $S\sigma$.

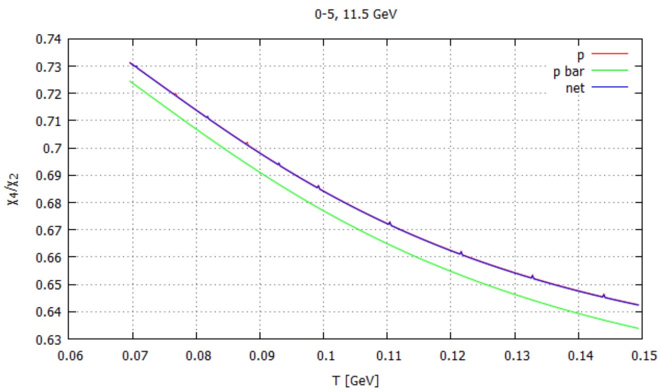

(d) Temperature dependence of $\kappa\sigma^2$.

Figure 5.2: Results for the volume density n (5.2a), scaled variance χ_2/χ_1 (5.2b) and the products of statistical moments $S\sigma$ (5.2c) and $\kappa\sigma^2$ (5.2d) of protons, antiprotons and net-protons for centrality 0-5 and collision energy $\sqrt{s_{NN}} = 11.5$ GeV.

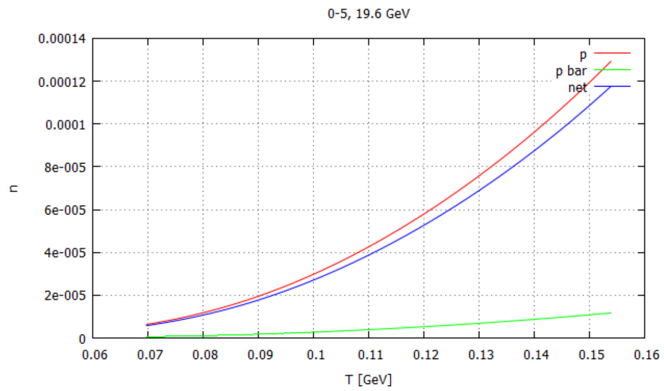

(a) Temperature dependence of the volume density.

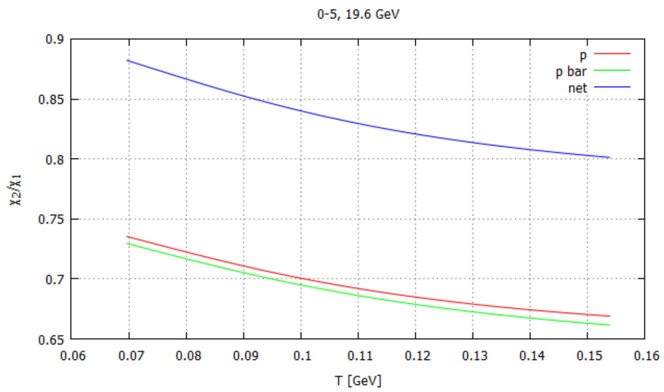

(b) Temperature dependence of the scaled variance.

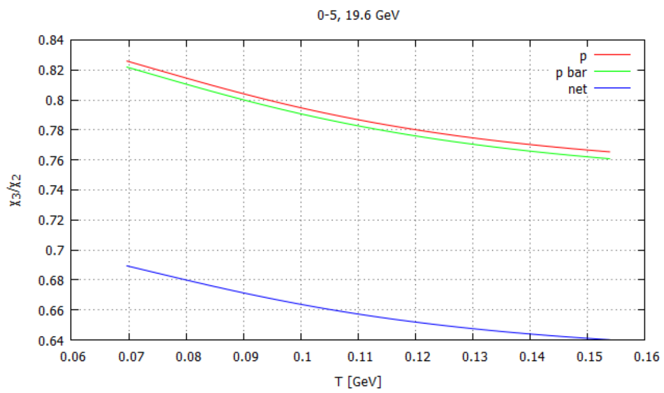

(c) Temperature dependence of $S\sigma$.

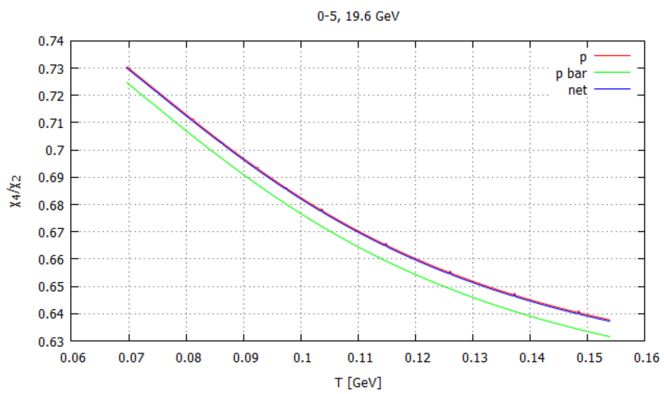

(d) Temperature dependence of $\kappa\sigma^2$.

Figure 5.3: Results for the volume density n (5.3a), scaled variance χ_2/χ_1 (5.3b) and the products of statistical moments $S\sigma$ (5.3c) and $\kappa\sigma^2$ (5.3d) of protons, antiprotons and net-protons for centrality 0-5 and collision energy $\sqrt{s_{NN}} = 19.6$ GeV.

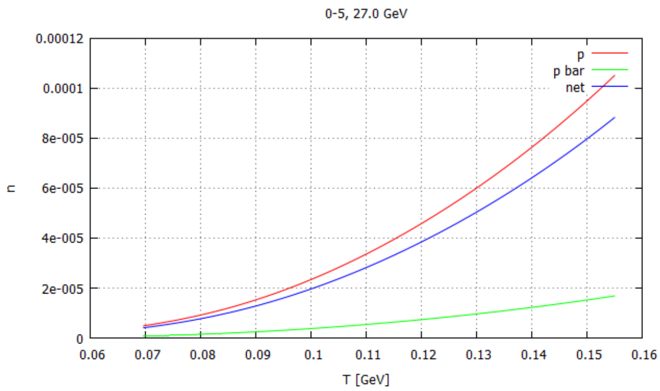

(a) Temperature dependence of the volume density.

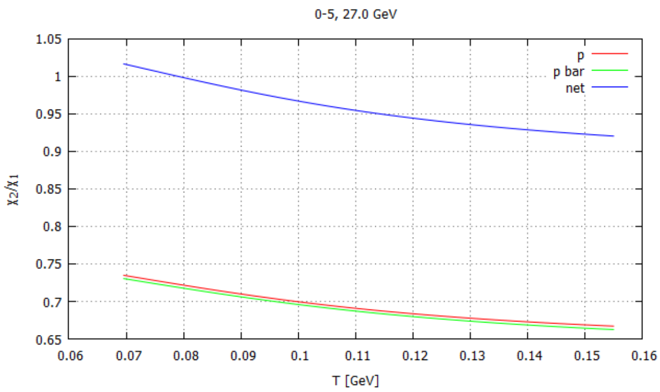

(b) Temperature dependence of the scaled variance.

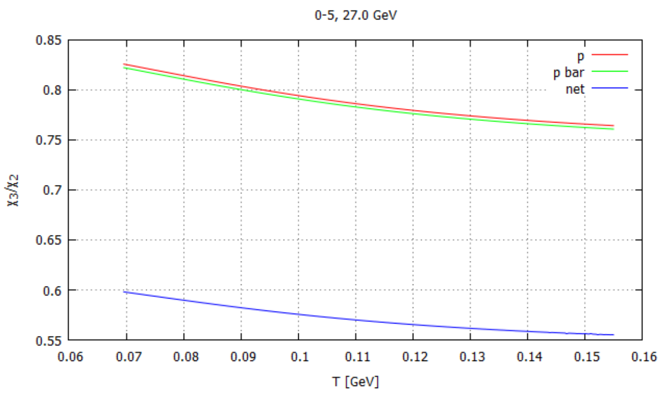

(c) Temperature dependence of $S\sigma$.

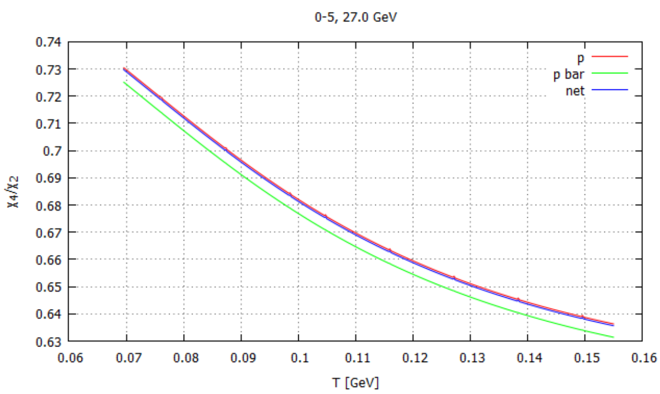

(d) Temperature dependence of $\kappa\sigma^2$.

Figure 5.4: Results for the volume density n (5.4a), scaled variance χ_2/χ_1 (5.4b) and the products of statistical moments $S\sigma$ (5.4c) and $\kappa\sigma^2$ (5.4d) of protons, antiprotons and net-protons for centrality 0-5 and collision energy $\sqrt{s_{NN}} = 27.0$ GeV.

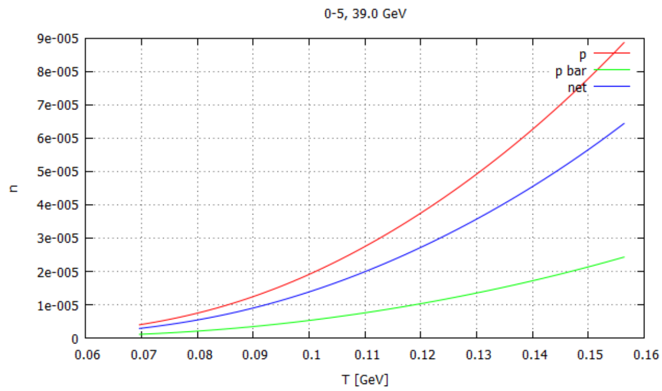

(a) Temperature dependence of the volume density.

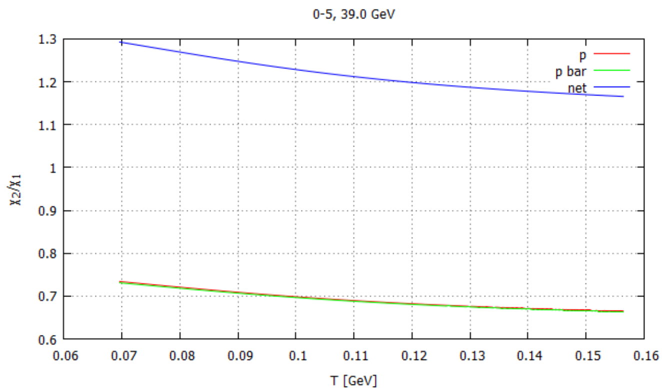

(b) Temperature dependence of the scaled variance.

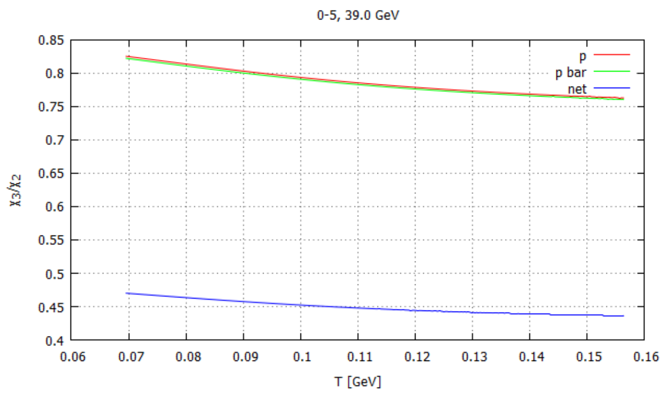

(c) Temperature dependence of $S\sigma$.

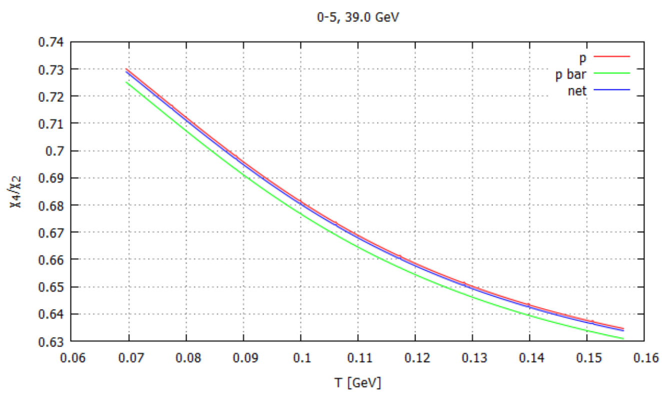

(d) Temperature dependence of $\kappa\sigma^2$.

Figure 5.5: Results for the volume density n (5.5a), scaled variance χ_2/χ_1 (5.5b) and the products of statistical moments $S\sigma$ (5.5c) and $\kappa\sigma^2$ (5.5d) of protons, antiprotons and net-protons for centrality 0-5 and collision energy $\sqrt{s_{NN}} = 39.0$ GeV.

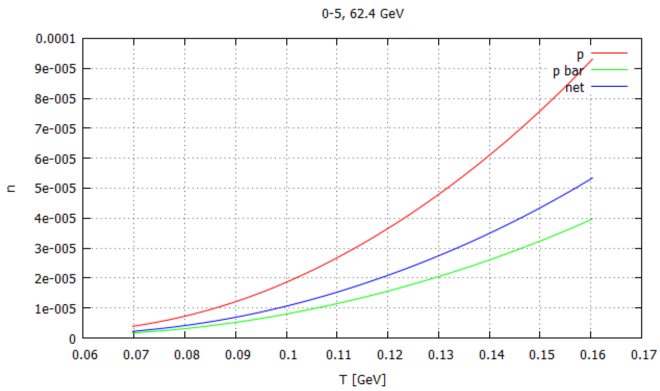

(a) Temperature dependence of the volume density.

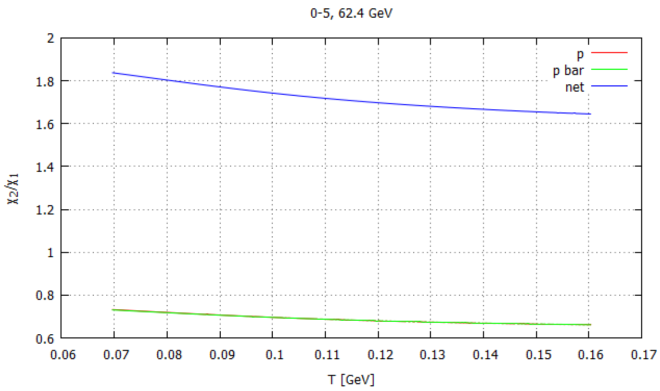

(b) Temperature dependence of the scaled variance.

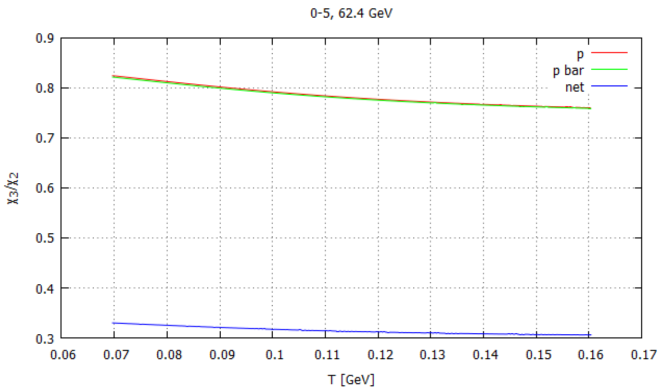

(c) Temperature dependence of $S\sigma$.

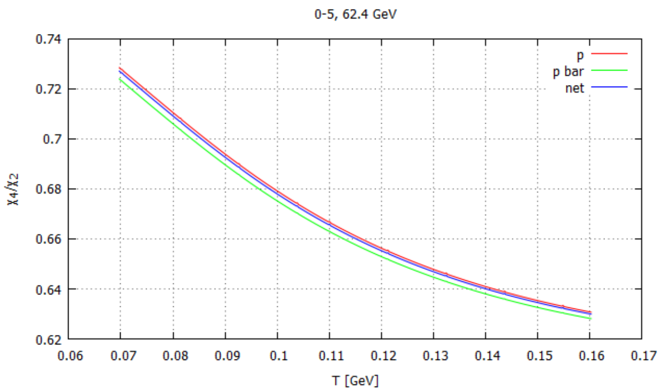

(d) Temperature dependence of $\kappa\sigma^2$.

Figure 5.6: Results for the volume density n (5.6a), scaled variance χ_2/χ_1 (5.6b) and the products of statistical moments $S\sigma$ (5.6c) and $\kappa\sigma^2$ (5.6d) of protons, antiprotons and net-protons for centrality 0-5 and collision energy $\sqrt{s_{NN}} = 62.4$ GeV.

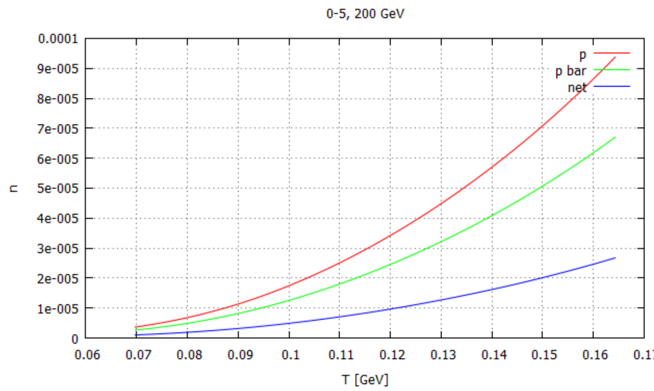

(a) Temperature dependence of the volume density.

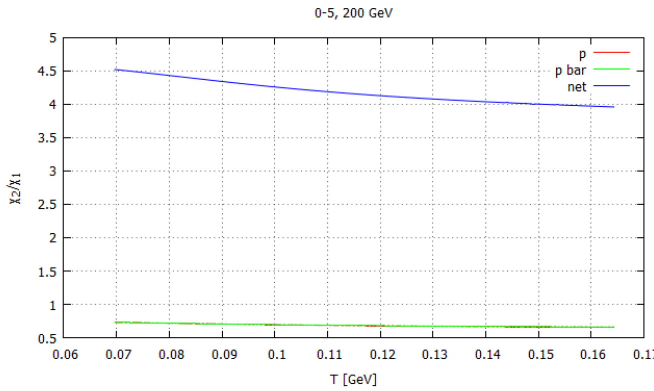

(b) Temperature dependence of the scaled variance.

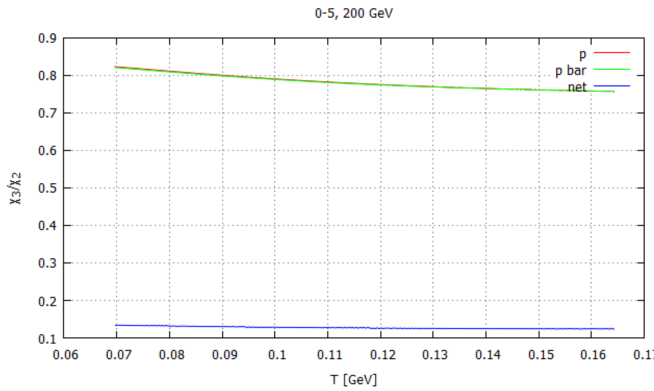

(c) Temperature dependence of $S\sigma$.

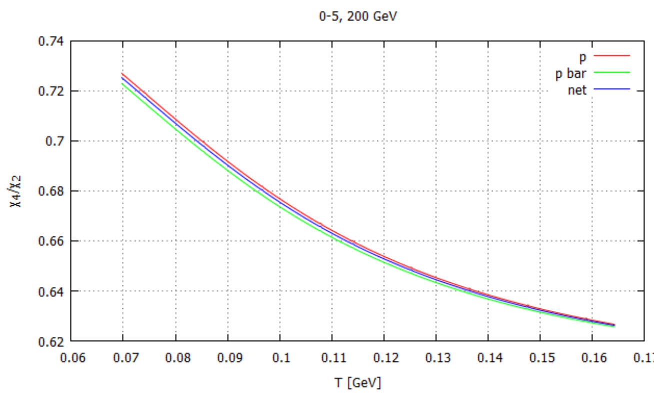

(d) Temperature dependence of $\kappa\sigma^2$.

Figure 5.7: Results for the volume density n (5.7a), scaled variance χ_2/χ_1 (5.7b) and the products of statistical moments $S\sigma$ (5.7c) and $\kappa\sigma^2$ (5.7d) of protons, antiprotons and net-protons for centrality 0-5 and collision energy $\sqrt{s_{NN}} = 200$ GeV.

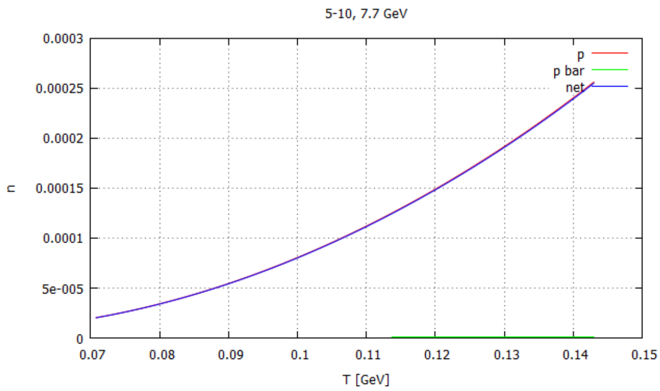

(a) Temperature dependence of the volume density.

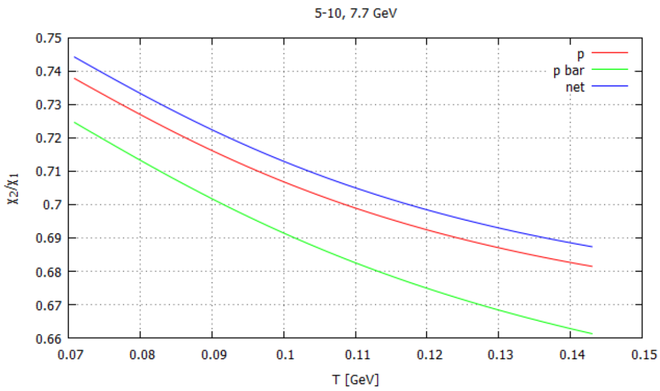

(b) Temperature dependence of the scaled variance.

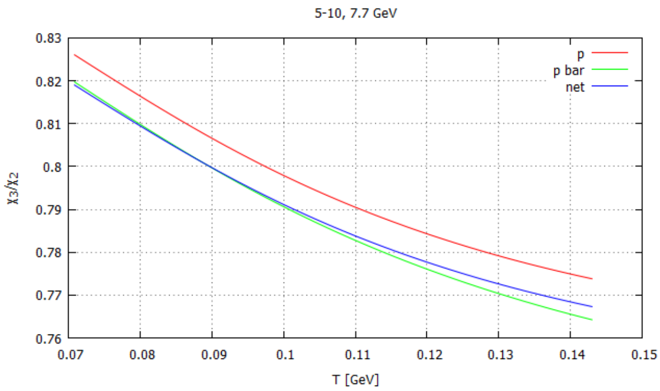

(c) Temperature dependence of $S\sigma$.

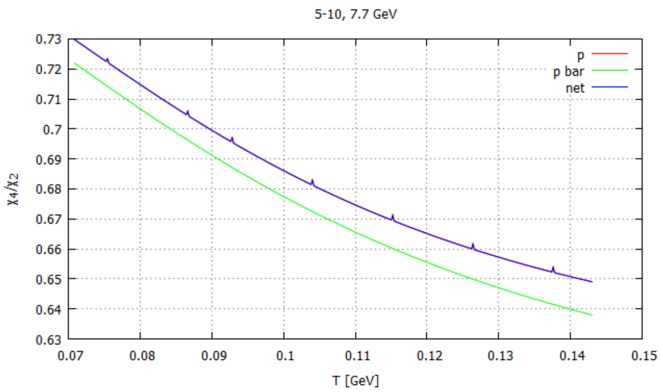

(d) Temperature dependence of $\kappa\sigma^2$.

Figure 5.8: Results for the volume density n (5.8a), scaled variance χ_2/χ_1 (5.8b) and the products of statistical moments $S\sigma$ (5.8c) and $\kappa\sigma^2$ (5.8d) of protons, antiprotons and net-protons for centrality 5-10 and collision energy $\sqrt{s_{NN}} = 7.7$ GeV.

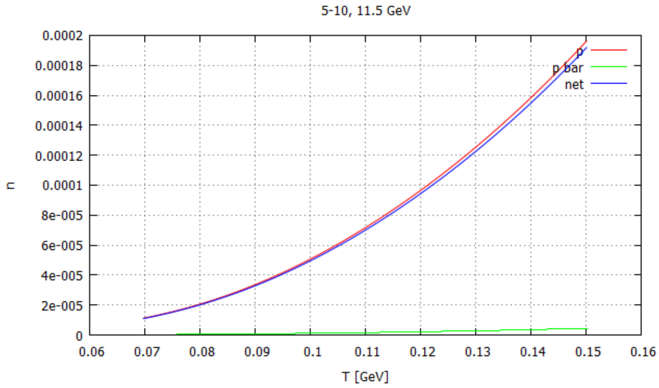

(a) Temperature dependence of the volume density.

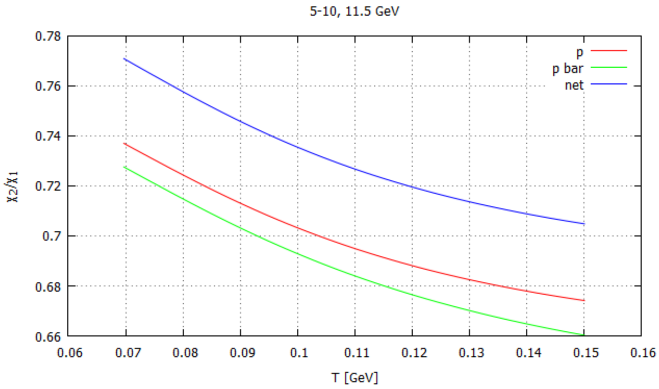

(b) Temperature dependence of the scaled variance.

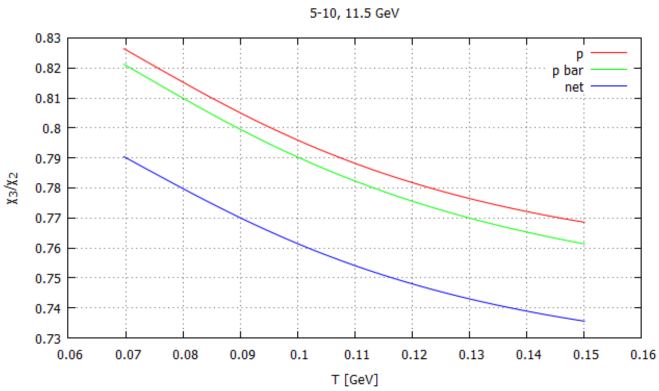

(c) Temperature dependence of $S\sigma$.

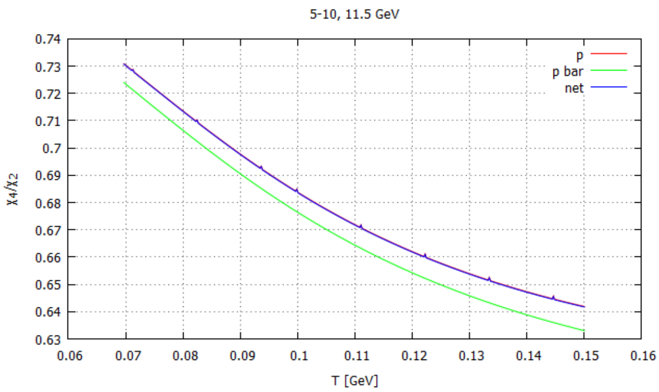

(d) Temperature dependence of $\kappa\sigma^2$.

Figure 5.9: Results for the volume density n (5.9a), scaled variance χ_2/χ_1 (5.9b) and the products of statistical moments $S\sigma$ (5.9c) and $\kappa\sigma^2$ (5.9d) of protons, antiprotons and net-protons for centrality 5-10 and collision energy $\sqrt{s_{NN}} = 11.5$ GeV.

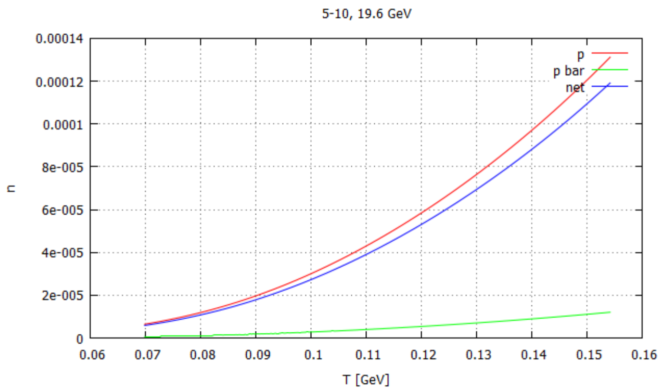

(a) Temperature dependence of the volume density.

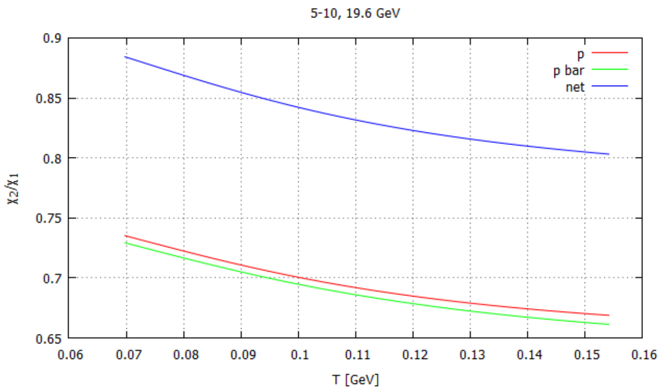

(b) Temperature dependence of the scaled variance.

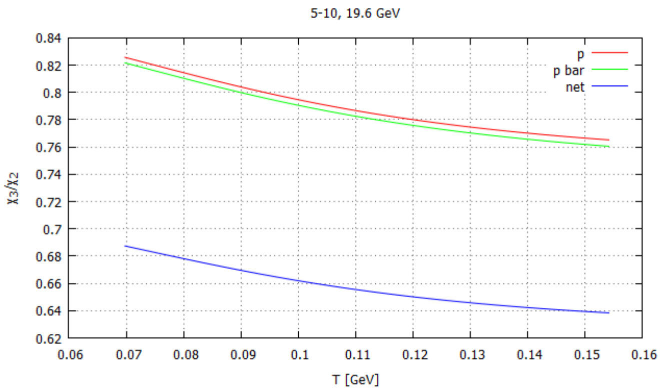

(c) Temperature dependence of $S\sigma$.

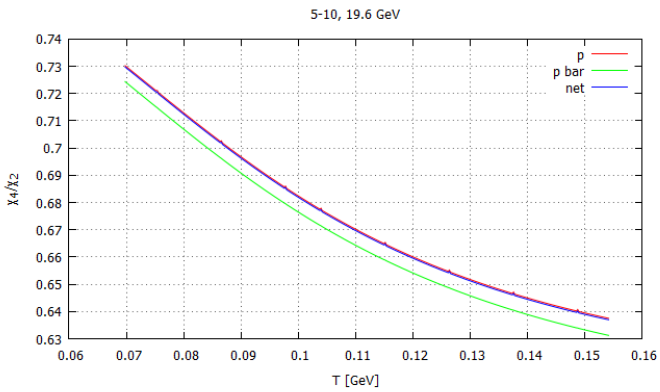

(d) Temperature dependence of $\kappa\sigma^2$.

Figure 5.10: Results for the volume density n (5.10a), scaled variance χ_2/χ_1 (5.10b) and the products of statistical moments $S\sigma$ (5.10c) and $\kappa\sigma^2$ (5.10d) of protons, antiprotons and net-protons for centrality 5-10 and collision energy $\sqrt{s_{NN}} = 19.6$ GeV.

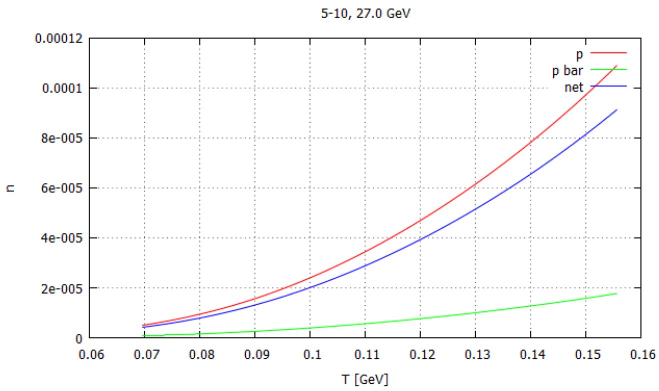

(a) Temperature dependence of the volume density.

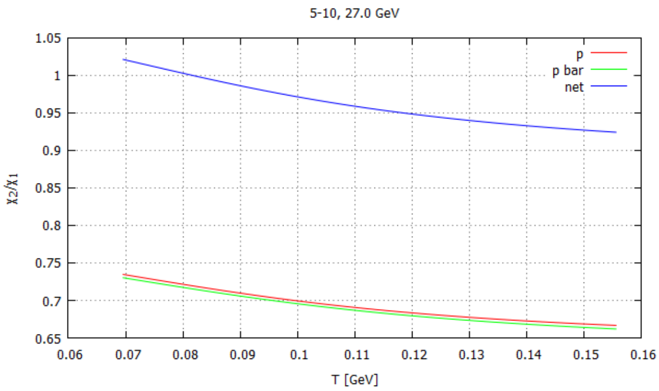

(b) Temperature dependence of the scaled variance.

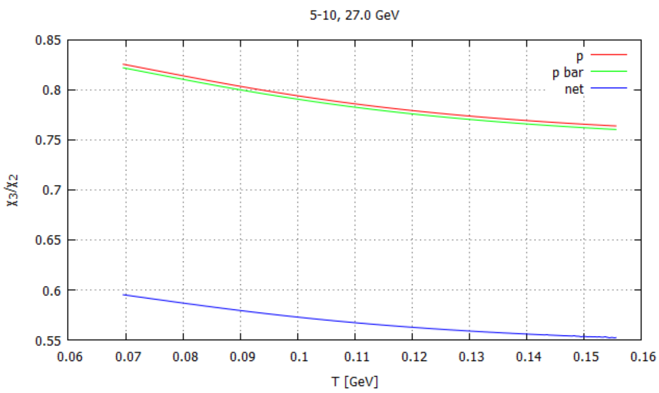

(c) Temperature dependence of $S\sigma$.

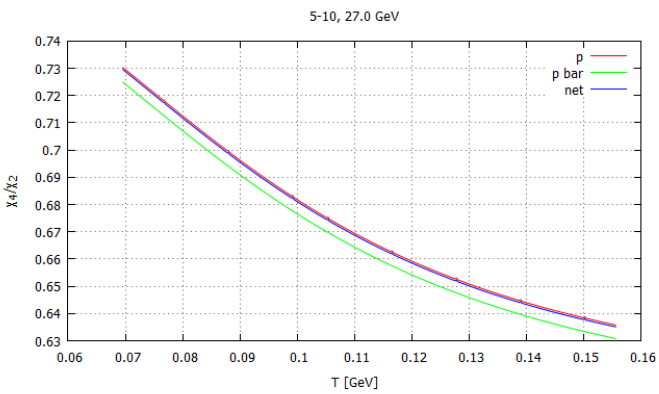

(d) Temperature dependence of $\kappa\sigma^2$.

Figure 5.11: Results for the volume density n (5.11a), scaled variance χ_2/χ_1 (5.11b) and the products of statistical moments $S\sigma$ (5.11c) and $\kappa\sigma^2$ (5.11d) of protons, antiprotons and net-protons for centrality 5-10 and collision energy $\sqrt{s_{NN}} = 27.0$ GeV.

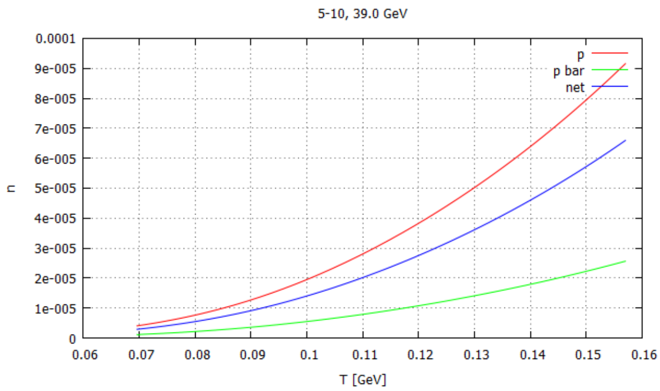

(a) Temperature dependence of the volume density.

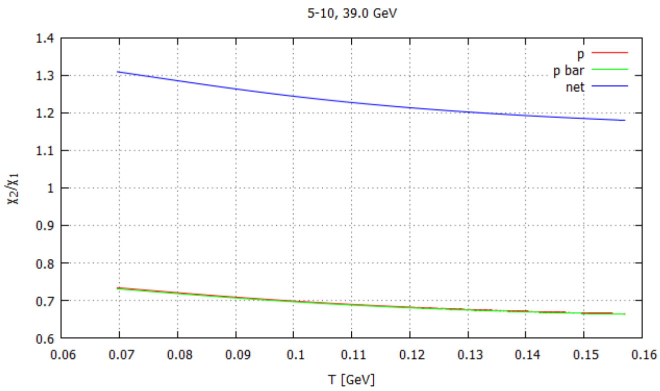

(b) Temperature dependence of the scaled variance.

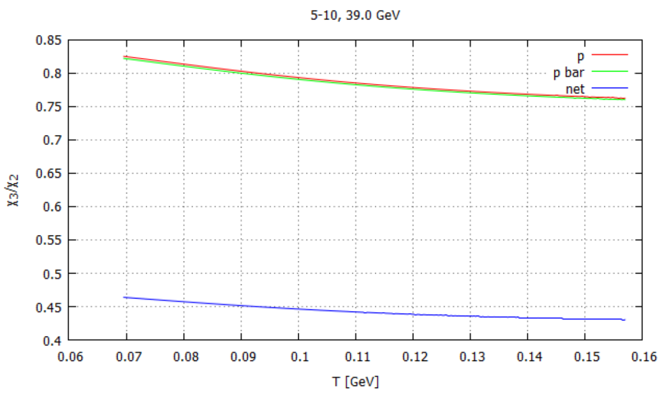

(c) Temperature dependence of $S\sigma$.

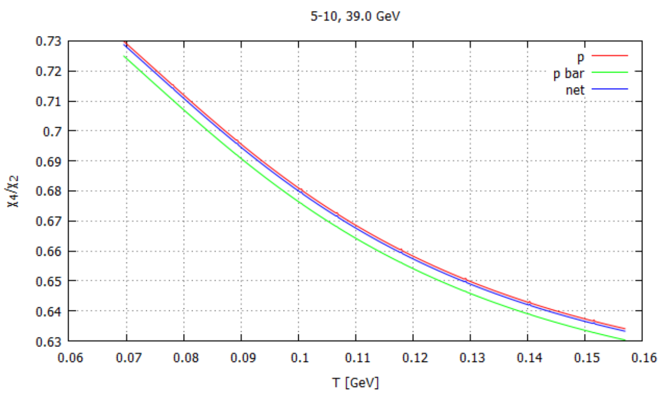

(d) Temperature dependence of $\kappa\sigma^2$.

Figure 5.12: Results for the volume density n (5.12a), scaled variance χ_2/χ_1 (5.12b) and the products of statistical moments $S\sigma$ (5.12c) and $\kappa\sigma^2$ (5.12d) of protons, antiprotons and net-protons for centrality 5-10 and collision energy $\sqrt{s_{NN}} = 39.0$ GeV.

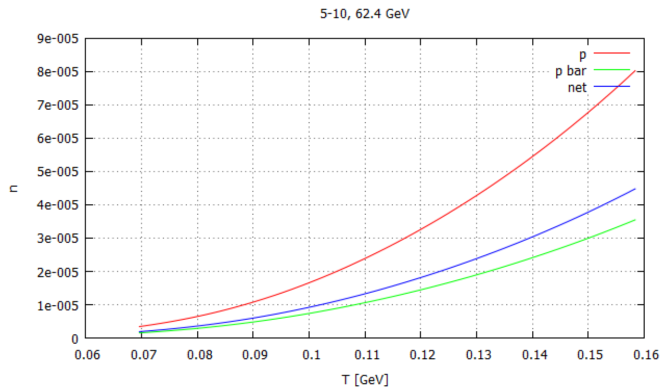

(a) Temperature dependence of the volume density.

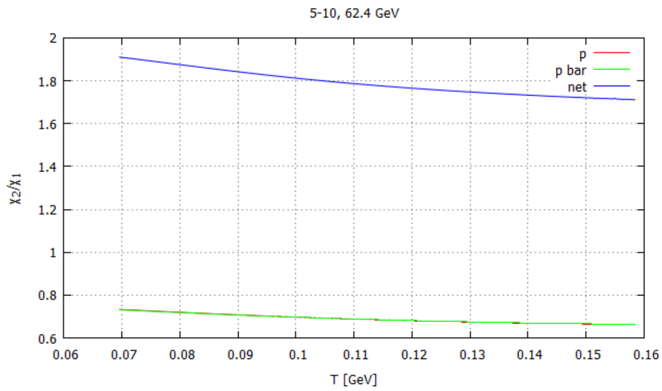

(b) Temperature dependence of the scaled variance.

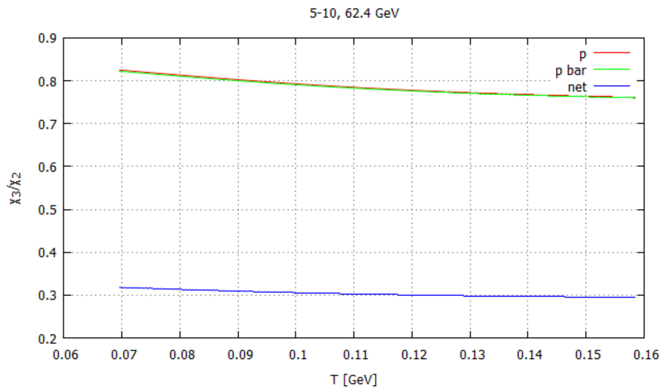

(c) Temperature dependence of $S\sigma$.

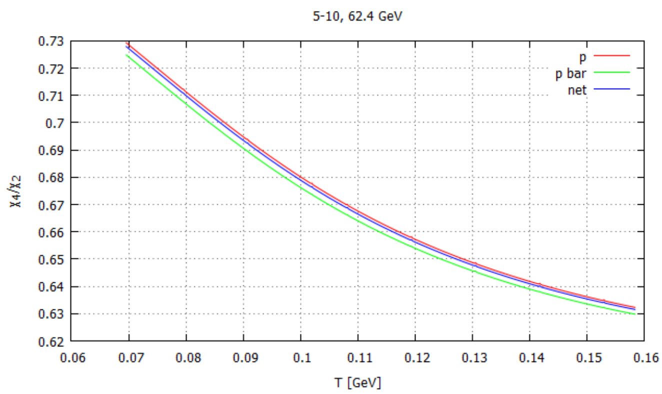

(d) Temperature dependence of $\kappa\sigma^2$.

Figure 5.13: Results for the volume density n (5.13a), scaled variance χ_2/χ_1 (5.13b) and the products of statistical moments $S\sigma$ (5.13c) and $\kappa\sigma^2$ (5.13d) of protons, antiprotons and net-protons for centrality 5-10 and collision energy $\sqrt{s_{NN}} = 62.4$ GeV.

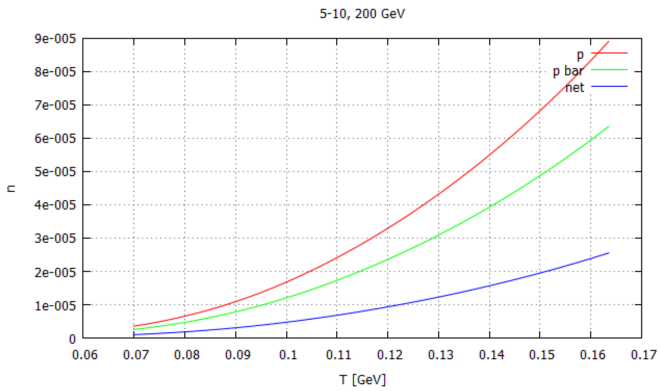

(a) Temperature dependence of the volume density.

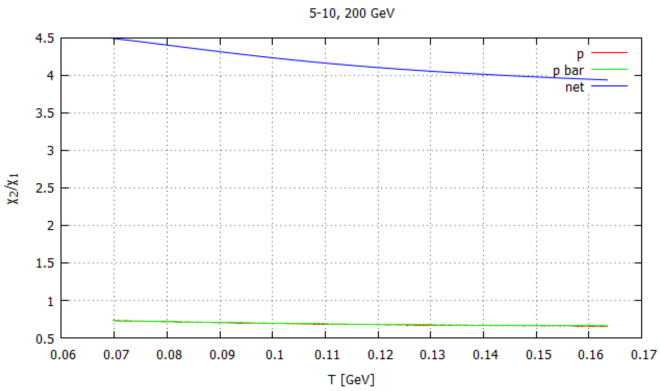

(b) Temperature dependence of the scaled variance.

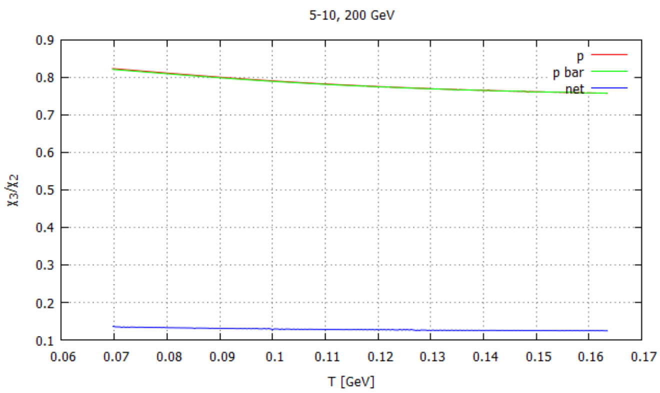

(c) Temperature dependence of $S\sigma$.

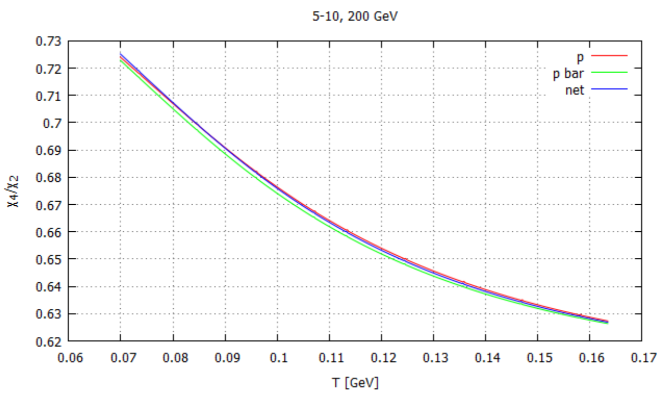

(d) Temperature dependence of $\kappa\sigma^2$.

Figure 5.14: Results for the volume density n (5.14a), scaled variance χ_2/χ_1 (5.14b) and the products of statistical moments $S\sigma$ (5.14c) and $\kappa\sigma^2$ (5.14d) of protons, antiprotons and net-protons for centrality 5-10 and collision energy $\sqrt{s_{NN}} = 200$ GeV.

5.5 Comparison to experimental data

The relevant experimental data are depicted in Fig. 5.15a ($S\sigma$, $\kappa\sigma^2$) and Fig. 5.15b (χ_2/χ_1). As the data in Fig. 5.15a were taken from RHIC - as were the data we have used to perform the calculations above - these are presented first and are also to be considered more accurate, since the collision energies are the same as those we have used. In order to account for the scaled variance χ_2/χ_1 as well, we have used the experimental results from the STAR experiment, although the collision energies there are slightly different from those used in the former case (of course, the STAR experiment is located at RHIC). The corrected data on χ_2/χ_1 mentioned in the article can be found on the public STAR webpage [22].

As can be seen in both Figures, the data relevant for us in order to perform comparison of any kind are for the case of Fig. 5.15a the filled circles, as these are the net-proton yields for centrality 0-5 in a Au + Au collision, and for the case of Fig. 5.15b the net-proton yields depicted in the Figure. As these are the most central collisions as well, we shall assume that the centrality taken into account was 0-5, as was the case for the $\S\sigma$ and $\kappa\sigma^2$ measurements in Fig. 5.15a.

Since the purpose of our research was to determine the temperature dependence of chosen ratios of thermodynamic susceptibilities and the data we have just presented depend on the collision energy $\sqrt{s_{NN}}$ only, it seems fitting that we perform a comparison between the trends of the respective temperature dependencies of said ratios for the centrality 0-5 and compare, how much the value for the chemical freeze-out (i. e. the maximal value) differs from what we can see in the mentioned Figures.

The scaled variance χ_2/χ_1 in Fig. 5.15b shows a regular increase with the rising collision energy. The same can be said about our results for the scaled variance for centrality 0-5 and the corresponding collision energies, meaning that the range of values (whose span can be considered constant) is shifted upwards with rising collision energy.

As for the $S\sigma$ product, we can see in Fig. 5.15a that for the most central collisions, the results for the net-proton yield show a decrease, ranging between the values approximately 0.9 and 0.1. If we look at our results, the same could be said about the range of values for net-protons in the individual Figures (and for the corresponding calculations, from which these Figures resulted), which varies from somewhere around 0.9 for $\sqrt{s_{NN}} = 7$ GeV and 0.1 for $\sqrt{s_{NN}} = 200$ GeV.

The $\kappa\sigma^2$ product in Fig. 5.15a shows an approximately constant value around 0.7 for the most central Au+Au collisions, however while this is the case only for the first four collision energies in the experimental measurement, our results show a range of values around 0.7 (more specifically between 0.62 and 0.74) for each of the seven collision energies.

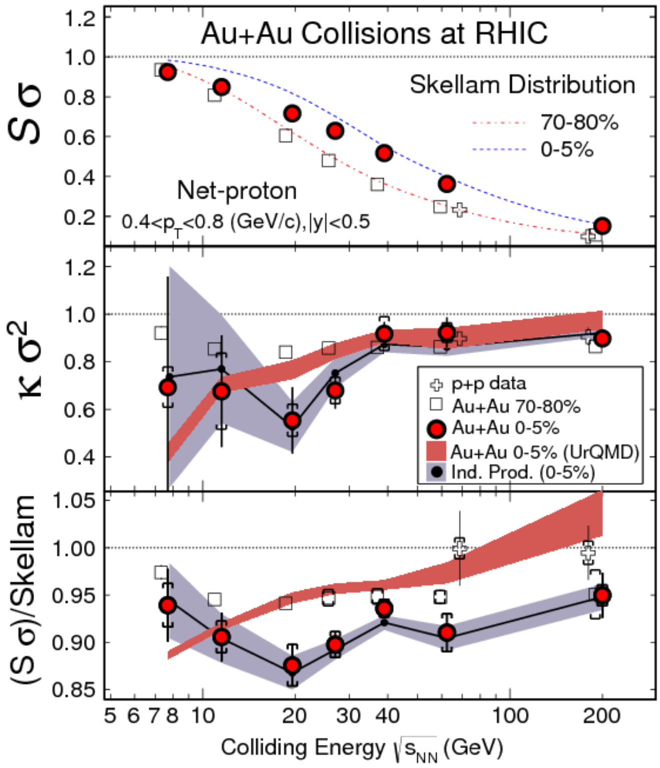

(a) Collision energy and centrality dependence of the net proton $S\sigma$ and $\kappa\sigma^2$ from Au + Au and p + p collisions at RHIC. Crosses, open squares and filled circles are for the efficiency corrected results of p+p, 70%-80%, and 0%-5% Au + Au collisions, respectively. Taken from [12].

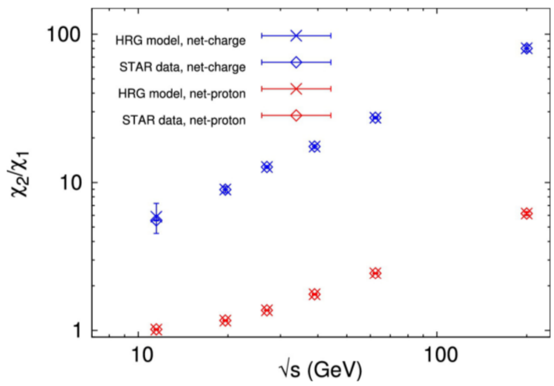

(b) Results on the comparison of the ratio χ_2/χ_1 in the HRG model and most central experimental data from STAR. Taken from [22].

Figure 5.15: Experimental results.

Conclusion

The primary aim of this thesis was to provide information on how to calculate moments of multiplicity distribution using the central statistical moments. The emphasis was laid on the first four moments and more importantly on the ratios of the related thermodynamic susceptibilities, which are of great interest when describing the QCD-predicted phase transition within heavy-ion collisions, believed to be the cause of QGP coming into existence. Subsequently, we implemented the derived formulae in exploring the temperature dependence of specific ratios of thermodynamic susceptibilities for protons, antiprotons and net protons. Finally, a brief comparison to experimental data acquired from RHIC/STAR was performed. The thesis as a whole can be summarized as follows:

In **Chapter 1**, a brief overview was given about the Quark-Gluon Plasma and the motivation of using moments of multiplicity distribution (specifically the multiplicity fluctuations described by the scaled variance) to acquire new knowledge concerning the QGP region.

In **Chapter 2**, the mathematical apparatus necessary to perform all the calculations was provided. Statistical moments in form of central moments were introduced along with close elaboration of the first four moments and the corresponding statistical quantities defined by them (mean M, variance σ, skewness S, kurtosis κ) as well as their ratios and products, which are of great importance for describing multiplicity fluctuations in the statistical model. Moreover, the basics of canonical and grandcanonical formalism, with emphasis laid on the latter, as this is the one we have used in further calculations.

Chapter 3 provided formalism for multiplicity fluctuations in a hadron resonance gas model with the assumption of chemical equilibrium. The hadron resonance gas model was introduced and the corresponding susceptibilities were defined. Using said susceptibilities, the first four cumulants in the ideal hadron gas were derived. Subsequently, the loss of chemical equilibrium and the chemical freeze-out parametrization were elaborated, which enabled us to finally lay down the formalism necessary for the resonance decays to be accounted for, which we did immediately afterwards and we also adjusted the formulae expressing the first four cumulants in the ideal hadron gas, in order to account for the resonance decays.

In **Chapter 4**, we have generalized the formalism from the previous Chapter in order to account for chemical non-equilibrium. We assumed that each stable particle species now has its own chemical potential and we have derived the corresponding formulae for the statistical moments for both baryons and specifically protons with emphasis on baryon and proton number density n, the scaled variance χ_2/χ_1 and the products $S\sigma$ and $\kappa\sigma^2$.

We have considered a total of 26 particle species stable, those being $\pi, K, \eta, N, \Lambda, \Sigma, \Xi, \Omega$. The method of calculating said potentials was also introduced. Furthermore, we have updated the tables of resonance decays and particle properties of the DRAGON programme according to the newest PDG update.

In **Chapter 5**, the calculation of said chemical potentials for corresponding sets of freeze-out parameters along with the computation of average numbers of stable particles for each resonance decay was performed. The freeze-out parameters in question concerned the most central collisions at RHIC (i. e. centrality 0-5 and 5-10) for 7 collision energies $\sqrt{s_{NN}} = 7.7, 11.5, 19.6, 27.0, 39.0, 62.4, 200$ GeV. As such, we obtained a temperature dependence for chemical potentials of all stable particles for each configuration of centrality and collision energy. These were then implemented into the derived formulae and the corresponding temperature dependencies of the number density n, the scaled variance χ_2/χ_1 and the products $S\sigma$ and $\kappa\sigma^2$ for protons, antiprotons and net-protons were plotted for each configuration of centrality and collision energy.

Finally, the obtained results were confronted with experimental data, which comprised exclusively net-protons. As these data were plotted as functions of the collision energy $\sqrt{s_{NN}}$ and not the temperature T, we have compared the shift of ranges of values for the individual quantities for net-protons up- or downwards with the trend followed by experimental data. While the scaled variance χ_2/χ_1 and $S\sigma = \chi_3/\chi_2$ agreed with the data quite well, the $\kappa\sigma^2 = \chi_4/\chi_2$ product showed an approximately constant value around 0.7 for the most central Au+Au collisions only for the first four collision energies in the experimental measurement, whereas our results showed a range of values around 0.7 (more specifically between 0.62 and 0.74) for each of the seven collision energies.

Appendix A

Bessel functions

In this Chapter, some brief trivia on Bessel functions and their practical use will be presented. A brief theoretical overview concerning the mathematical apparatus used in this master's thesis will be provided. The whole apparatus was taken from and is in accordance with [26].

A.1 Bessel functions

The Bessel functions were first defined by Daniel Bernoulli and later on generalized by Friedrich Bessel. They are defined as canonical solutions $y = y(x)$ of a differential equation better known as the "Bessel differential equation":

$$x^2 \frac{d^2y}{dx^2} + x\frac{dy}{dx} + (x^2 - \alpha^2)y = 0 \tag{A.1}$$

where the arbitrary complex number α is called the **order** of the Bessel function.

The Bessel functions can be distinguished according to the parameter α. If α is an integer, we talk about **cylinder functions** or the **cylindrical harmonics** because they appear in the solution to Laplace's equation in cylindrical coordinates. Once α is a half-integer (i.e. for each α there is an $n \in \mathbb{N}$ such that $\alpha = n + \frac{1}{2}$), then we call the functions $y = y(x)$ the **spherical Bessel functions** and they are obtained when the **Helmholtz equation** is solved in spherical coordinates.

The **Bessel functions of the first kind** are denoted as $J_\alpha(x)$. They are solutions of Bessel's differential equation that are finite at the origin ($x = 0$) for integer or positive values of α and diverge as x approaches the value $x = 0$ for negative non-integer α. They can be defined as follows:

$$J_\alpha(x) = \sum_{m=0}^{\infty} \frac{(-1)^m}{m!\Gamma(m+\alpha+1)} \left(\frac{x}{2}\right)^{2m+\alpha} \tag{A.2}$$

It is worth mentioning that for non-integer α, the functions J_α and $J_{-\alpha}$ are linearly independent, which makes them two solutions of the differential equation. If α is an integer, the following is valid:

$$J_{-n} = (-1)^n J_n(x), \tag{A.3}$$

which means that the solutions are no longer linearly independent. The second solution is then expressed as the **Bessel function of the second kind** denoted as Y_α and defined as follows:

$$Y_\alpha(x) = \frac{J_\alpha(x)\cos(\alpha\pi) - J_{-\alpha}(x)}{\sin(\alpha\pi)} \tag{A.4}$$

The plots of Bessel functions of the first and second kind for $\alpha = 0, 1, 2$ are depicted in Figure A.1 and in Figure A.2, respectively.

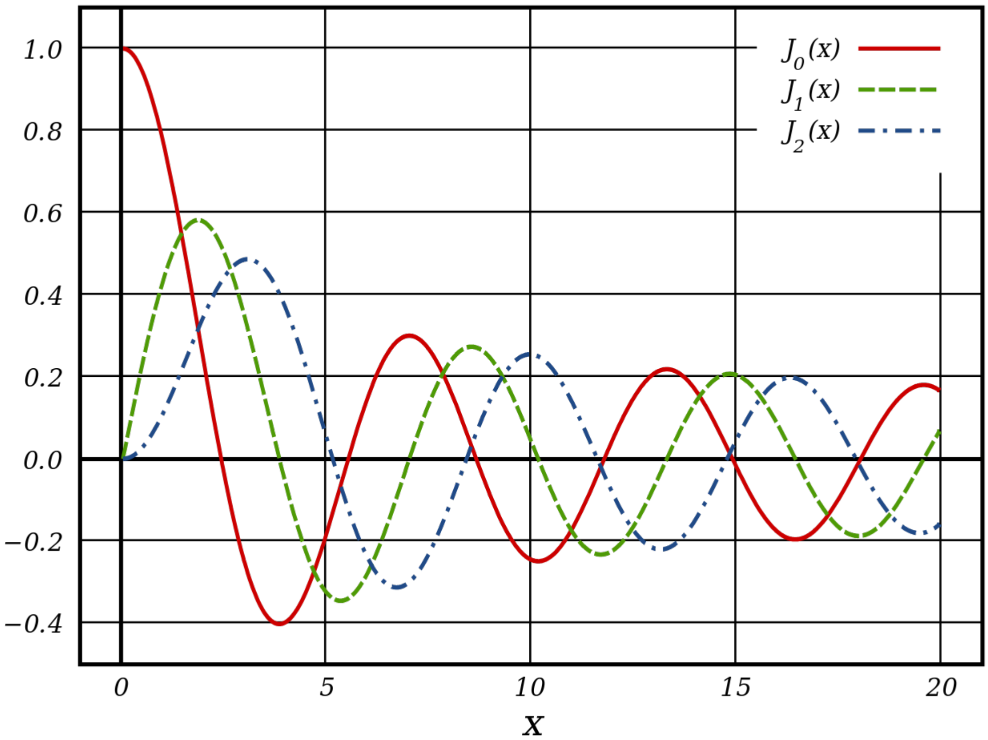

Figure A.1: Bessel Functions of the First Kind J_α. Taken from [26].

A.2 Modified Bessel functions

The Bessel functions are well defined, even though their argument x is complex. However, if a special case occurs - when this argument is purely complex - we talk about the **modified Bessel function** (also called the **hyperbolic Bessel function**) of the **first kind** (denoted as $I_\alpha(x)$) and of the **second kind** (denoted as $K_\alpha(x)$). Those are defined by the following equations:

$$I_\alpha(x) = i^{-\alpha} J_\alpha(ix) = \sum_{m=0}^{\infty} \frac{1}{m!\Gamma(m+\alpha+1)} \left(\frac{x}{2}\right)^{2m+\alpha} \tag{A.5}$$

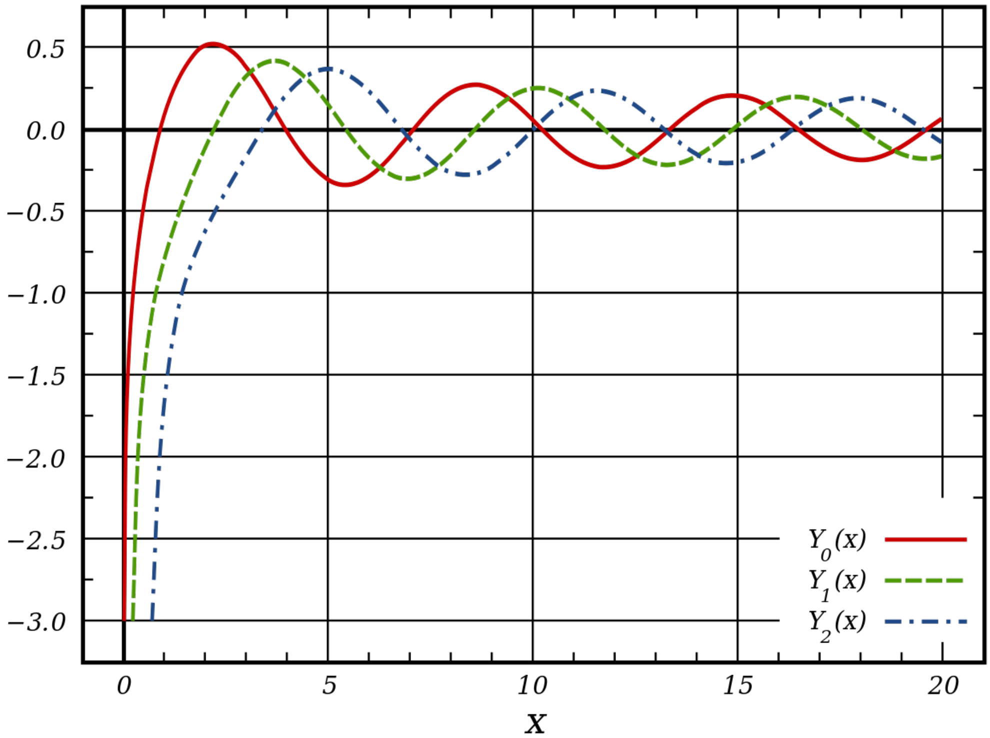

Figure A.2: Bessel Functions of the Second Kind Y_α. Taken from [26].

$$K_\alpha(x) = \frac{\pi}{2}\frac{I_{-\alpha}(x) - I_\alpha(x)}{\sin(\alpha\pi)} \tag{A.6}$$

These solutions are two independent solutions of the modified Bessel equation:

$$x^2\frac{d^2y}{dx^2} + x\frac{dy}{dx} - (x^2+\alpha^2)y = 0. \tag{A.7}$$

Unlike the classical Bessel functions, which oscillate as functions of a real argument in both $I_\alpha(x)$ and $K_\alpha(x)$, the Modified Bessel functions grow exponentially. We will now present the integral form of the Modified Bessel functions (assuming that $Re(x) > 0$):

$$I_\alpha(x) = \frac{1}{\pi}\int_0^\pi \exp(x\cos(\theta))\cos(\alpha\theta)d\theta - \frac{\sin(\alpha\pi)}{\pi}\int_0^\infty \exp(-x\cosh t - \alpha t)dt \tag{A.8}$$

$$K_\alpha(x) = \int_0^\infty \exp(-x\cosh t)\cosh(\alpha t)dt \tag{A.9}$$

The plots of Bessel functions of the first and second kind for $\alpha = 0, 1, 2$ are depicted in Figure A.3 and in Figure A.4, respectively.

A.3 Recurrence Relations

Let $Z_\nu(z)$ denote $I_\nu(z)$ **or** $e^{i\pi\nu}K_\nu(z)$ or any linear combination of these functions, the coefficients in which are independent of $z \in \mathbf{C}$ and $\nu \in \mathbf{N}$. Then the following recurrence

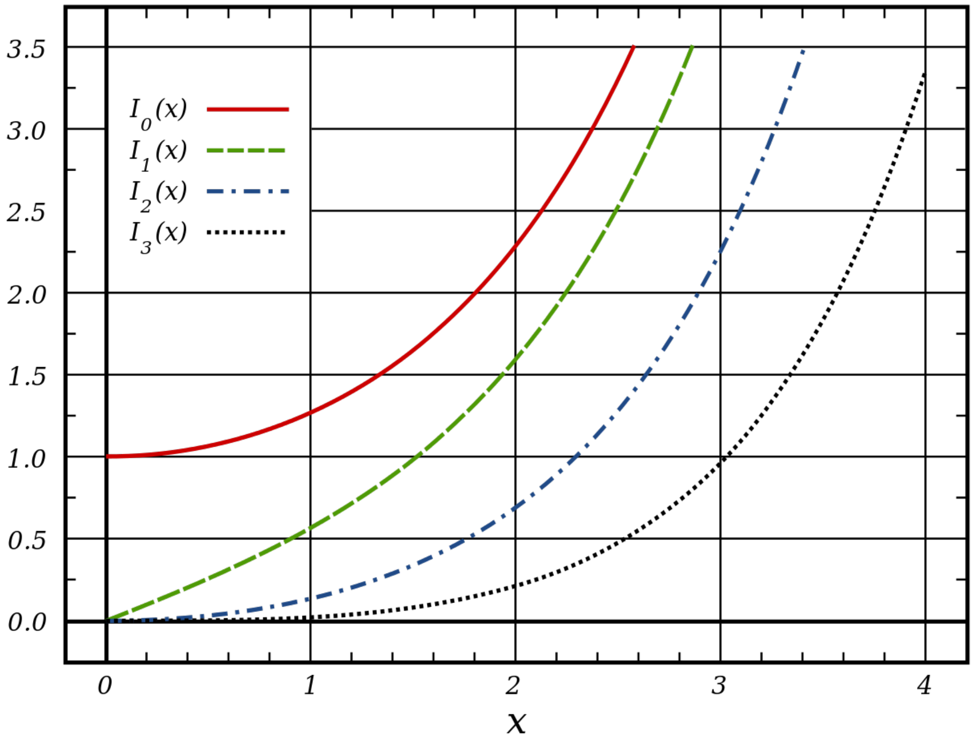

Figure A.3: Modified Bessel Functions of the First Kind. Taken from [26].

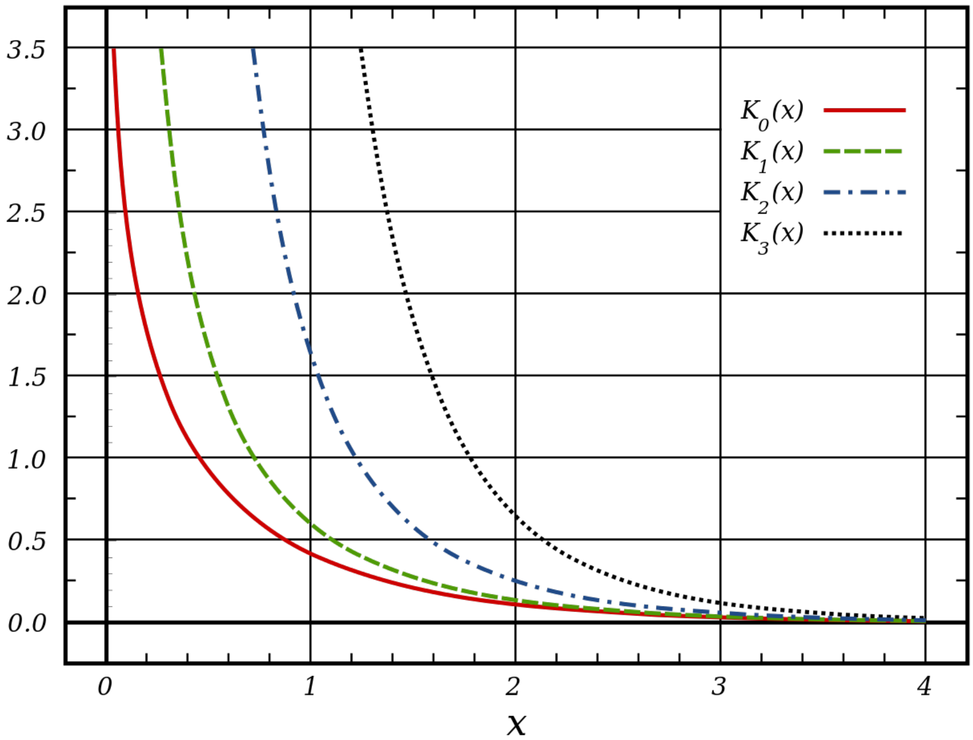

Figure A.4: Modified Bessel Functions of the Second Kind. Taken from [26].

relations can be used:

$$Z_{\nu-1}(z) - Z_{\nu+1}(z) = \frac{2\nu}{z} Z_\nu(z) \tag{A.10}$$

$$Z'_\nu(z) = Z_{\nu-1}(z) - \frac{\nu}{z} Z_\nu(z) \tag{A.11}$$

$$Z_{\nu-1}(z) + Z_{\nu+1}(z) = 2Z'_\nu(z) \tag{A.12}$$

$$Z'_\nu(z) = Z_{\nu+1}(z) + \frac{\nu}{z} Z_\nu(z) \tag{A.13}$$

For our purposes, the function $K_\nu(z)$ and Eq. (A.10) are of great importance. Since $Z_\nu(z)$ can be $Z_\nu(z) = e^{i\pi\nu} K_\nu(z)$ and

$$e^{i\pi\nu} = (-1)^\nu,$$

one may write

$$K_{\nu+1}(z) - K_{\nu-1}(z) = \frac{2\nu}{z} K_\nu(z). \tag{A.14}$$

Appendix B

Saddle-point expansion

We may now introduce the method of the saddle-point expansion. Let $\vec{w_0} = (\lambda_B, \lambda_S, \lambda_Q)$ be the saddle point. Then obviously

$$\frac{\partial f(\vec{w})}{\partial w_k}|_{\vec{w_0}} = 0.$$

We will now try to find the explicit solution of a complex d-dimensional integral

$$I(\nu) = \left[\prod_{k=1}^{d} \int_{\Gamma_k} dw_k\right] g(\vec{w}) e^{\nu f(\vec{w})}$$

where Γ_k is the k-th path of integration.

If ν is large, then only a small segment around the saddle point $\vec{w_0}$ contributes to the total integral value. We may then write

$$I(\nu) \simeq e^{\nu f(\vec{w_0})} \frac{1}{(2\pi)^d} \left[\prod_{k=1}^{d} \int_{-\infty}^{+\infty} dt_k\right] g(\vec{w(\vec{t})}) e^{-\frac{1}{2}\nu \vec{t}^T \mathbf{H} \vec{t}}$$

where $\mathbf{H}$ is the Hessian matrix of $f(\vec{w})$.

We may now summarize the procedure as follows: at first we choose a **real** integration variable t_k:

$$w_k - w_{0k} = e^{i\phi_k} t_k$$

where ϕ_k denotes the phase.

Consequently, the original path is "deformed" into a **line** in the complex plane. After that, we expand $g(\vec{w})$ into a Taylor series around $\vec{w} = \vec{w_0}$.

Finally, we assume that $\mathbf{H}$ is diagonalizable, so we can find a matrix $\mathbf{A}$ such that $\mathbf{H'} = \mathbf{A}\mathbf{H}\mathbf{A}^{\mathbf{T}}$.

The integral will now have the following expression:

$$
\begin{aligned}
I(\nu) \simeq \exp(\nu f(\vec{w_0}))\sqrt{\frac{1}{(2\pi\nu)^d det\mathbf{H}}}\Big[g(\vec{w_0})+ \\
\frac{1}{\nu}\left[-\frac{1}{2}\sum_{k,m=1}^{d}\frac{\partial^2 g(\vec{w})}{\partial w_k \partial w_m}|_{\vec{w_0}}\left(\sum_{i=1}^{d}\frac{A_{im}A_{ik}}{h_i}\right)|_{\vec{w_0}}+\right. \\
\left.\left.\sum_{k=1}^{d}\alpha_i\frac{\partial g(\vec{w})}{\partial w_i}|_{\vec{w_0}}+\gamma g(\vec{w_0})\right]\right].
\end{aligned}
\tag{B.1}
$$

where γ and α_i are constants dependent only on function f and its derivatives.

Appendix C

Calculation of the first four statistical moments for many input parameters

All calculations are performed in accordance with Chapter 2, where we defined the m-th **central statistical moment** as

$$\varphi_m(X) = E[(X - EX)^m]. \tag{C.1}$$

The m-th moment about the origin (also called the **raw moment**) can be expressed as follows:

$$\varphi'_m(X) = E[X^m]. \tag{C.2}$$

One can immediately see that for the first four moments, the following relations are fulfilled:

$$\varphi_1 = \varphi'_1 =: \varphi \tag{C.3}$$

$$\varphi_2 = \varphi'_2 - \varphi^2 \tag{C.4}$$

$$\varphi_3 = \varphi'_3 - 3\varphi\varphi'_2 + 2\varphi^3 \tag{C.5}$$

$$\varphi_4 = \varphi'_4 - 4\varphi\varphi'_3 + 6\varphi^2\varphi'_2 - 3\varphi^4 \tag{C.6}$$

C.1 First central moment - the mean value

Let A_i be a set of n arbitrary statistical quantities, $i \in \{1, \ldots, n\}$. Then using the definition of the **first** central moment, we obtain

$$\begin{aligned}\varphi_1\left(\sum_{i=1}^n A_i\right) &= E\left[\sum_{i=1}^n A_i - E\left(\sum_{i=1}^n A_i\right)\right] \\ &= E\left[\sum_{i=1}^n A_i\right] = \sum_{i=1}^n EA_i = \sum_{i=1}^n \varphi_{1i}\end{aligned} \tag{C.7}$$

which proves the linearity of the first central statistical moment. By inserting

$$A_i = N_{i-\bar{i}}$$

into Eq. (C.7), where

$$N_{i-\bar{i}} = N_i - N_{\bar{i}},$$

we obtain

$$E(N_{i-\bar{i}}) = \sum_{i \in A_B} (EN_i - EN_{\bar{i}}). \tag{C.8}$$

C.2 Second central moment - the variance

Let A_i be a set of n arbitrary statistical quantities, $i \in \{1, \ldots, n\}$. Then using the definition of the **second** central moment, we obtain

$$\begin{aligned} \varphi_2\left(\sum_{i=1}^{n} A_i\right) &= Var\left(\sum_{i=1}^{n} A_i\right) \\ &= E\left[\sum_{i=1}^{n} A_i - E\left(\sum_{i=1}^{n} A_i\right)\right]^2 \\ &= E\left[\sum_{i=1}^{n} (A_i - EA_i)\right]^2 \\ &= E\left[\sum_{i,j=1}^{n} (A_i - EA_i)(A_j - EA_j)\right] \\ &= \sum_{i,j=1}^{n} E\left[(A_i - EA_i)(A_j - EA_j)\right] \\ &= \sum_{i,j=1}^{n} Cov(A_i, A_j). \end{aligned} \tag{C.9}$$

By inserting

$$A_i = N_{i-\bar{i}}$$

into Eq. (C.9), where

$$N_{i-\bar{i}} = N_i - N_{\bar{i}},$$

we obtain

$$
\begin{aligned}
Var(N_{B-\bar{B}}) &= \sum_{i,j\in A_B} Cov(N_{i-\bar{i}}, N_{j-\bar{j}}) \qquad \text{(C.10)}\\
&= \sum_{i,j\in A_B} E\left[(N_{i-\bar{i}} - EN_{i-\bar{i}})(N_{j-\bar{j}} - EN_{j-\bar{j}})\right]\\
&= \sum_{i,j\in A_B} \left[E(N_{i-\bar{i}}N_{j-\bar{j}}) - E(N_{i-\bar{i}})E(N_{j-\bar{j}})\right]\\
&= \sum_{i,j\in A_B} \left[E[(N_i - N_{\bar{i}})(N_j - N_{\bar{j}})] - E(N_i - N_{\bar{i}})E(N_j - N_{\bar{j}})\right]\\
&= \sum_{i,j\in A_B} \left[Cov(N_i, N_j) + Cov(N_{\bar{i}}, N_{\bar{j}}) - Cov(N_{\bar{i}}, N_j) - Cov(N_i, N_{\bar{j}})\right]
\end{aligned}
$$

C.3 Third statistical moment

Let A_i be a set of n arbitrary statistical quantities, $i \in \{1, \ldots, n\}$. Then using the definition of the **third** central moment, we obtain

$$
\begin{aligned}
\varphi_3\left(\sum_{i=1}^{n} A_i\right) &= E\left[\sum_{i=1}^{n} A_i - E\left(\sum_{i=1}^{n} A_i\right)\right]^3 \qquad \text{(C.11)}\\
&= E\left[\sum_{i=1}^{n}(A_i - EA_i)\right]^3\\
&= \sum_{i,j,k=1}^{n} E\left[(A_i - EA_i)(A_j - EA_j)(A_k - EA_k)\right]\\
&= E\left[\left(\sum_{i=1}^{n} A_i\right)^3\right] - 3E\left[\left(\sum_{i=1}^{n} A_i\right)\right] E\left[\left(\sum_{i=1}^{n} A_i\right)^2\right]\\
&+ 2\left(E\left[\sum_{i=1}^{n} A_i\right]\right)^3.
\end{aligned}
$$

C.4 Fourth statistical moment

Let A_i be a set of n arbitrary statistical quantities, $i \in \{1, \dots, n\}$. Then using the definition of the **fourth** central moment, we obtain

$$\begin{aligned}
\varphi_4\left(\sum_{i=1}^{n} A_i\right) &= E\left[\sum_{i=1}^{n} A_i - E\left(\sum_{i=1}^{n} A_i\right)\right]^4 \\
&= E\left[\sum_{i=1}^{n} (A_i - EA_i)\right]^4 \\
&= \sum_{i,j,k,l=1}^{n} E\left[(A_i - EA_i)(A_j - EA_j)(A_k - EA_k)(A_l - EA_l)\right] \\
&= E\left[\left(\sum_{i=1}^{n} A_i\right)^4\right] - 4E\left[\left(\sum_{i=1}^{n} A_i\right)\right] E\left[\left(\sum_{i=1}^{n} A_i\right)^3\right] \\
&+ 6\left(E\left[\sum_{i=1}^{n} A_i\right]\right)^2 E\left[\left(\sum_{i=1}^{n} A_i\right)^2\right] - 3\left(E\left[\sum_{i=1}^{n} A_i\right]\right)^4 .
\end{aligned} \tag{C.12}$$

C.5 Ratios of susceptibilities

According to [8], the thermodynamic susceptibility χ_l of particle species a is given by

$$\chi_l^{(a)} = \frac{\partial^l (P/T^4)}{\partial(\mu_a/T)^l} = T^l \frac{\partial^l (P/T^4)}{\partial \mu_a^l}. \tag{C.13}$$

For partial pressure P/T^4, in accordance with chapter 3 given by

$$\frac{P}{T^4} = \frac{1}{VT^3} \ln Z(V, T, \vec{\mu}) \tag{C.14}$$

which - according to the calculations specifically performed above - can be recast as

$$\frac{P}{T^4} = \frac{1}{2\pi^2 T^2} \sum_i \sum_{k=1}^{+\infty} d_i m_i^2 \frac{(-1)^{k+1}}{k^2} \exp\left(\frac{k}{T} \sum_{j \in A} N_{ji}\mu_j\right) K_2\left(\frac{k m_i}{T}\right), \tag{C.15}$$

Eq. (C.13) can be rewritten as

$$\chi_l^{(a)} = \frac{1}{2\pi^2 T^2} \sum_i \sum_{k=1}^{+\infty} d_i m_i^2 (-1)^{k+1} k^{l-2} N_{ai}^l \exp\left(\frac{k}{T} \sum_{j \in A} N_{ji}\mu_j\right) K_2\left(\frac{k m_i}{T}\right). \tag{C.16}$$

Obviously, the ratio of any two thermodynamic susceptibilities of the same particle species a, denoted $\chi_l^{(a)}$ and $\chi_n^{(a)}, l \neq n$, can be written as

$$\frac{\chi_l^{(a)}}{\chi_n^{(a)}} = \frac{\sum_i \sum_{k=1}^{+\infty} d_i m_i^2 (-1)^{k+1} k^{l-2} N_{ai}^l \exp\left(\frac{k}{T} \sum_{j \in A} N_{ji}\mu_j\right) K_2\left(\frac{k m_i}{T}\right)}{\sum_i \sum_{k=1}^{+\infty} d_i m_i^2 (-1)^{k+1} k^{n-2} N_{ai}^n \exp\left(\frac{k}{T} \sum_{j \in A} N_{ji}\mu_j\right) K_2\left(\frac{k m_i}{T}\right)}. \tag{C.17}$$

If all baryons are taken into account, Eq. (C.13) and Eq. (C.16) are in accordance with [16] generalized as

$$\begin{aligned}
\chi_l^{(a_1,\ldots,a_n)} &= T^l \frac{\partial^l (P/T^4)}{\partial\mu_{a_1}\ldots\partial\mu_{a_l}} \qquad \text{(C.18)}\\
&= \frac{1}{2\pi^2 T^2}\sum_i \sum_{k=1}^{+\infty} \sum_{a_s\in A_B, s\in\hat{l}, l\leq n} d_i m_i^2 (-1)^{k+1} k^{l-2} N_{a_1 i}\ldots N_{a_l i}\exp\left(\frac{k}{T}\sum_{j\in A} N_{ji}\mu_j\right)\times\\
&\times\ K_2\left(\frac{km_i}{T}\right)
\end{aligned}$$

where $a_1,\ldots,a_n$ are stable baryons.

Obviously, Eq. (C.17) for any two thermodynamic susceptibilities denoted l and $o, l \neq o$ is then generalized as

$$\frac{\chi_l^{(a_1,\ldots,a_n)}}{\chi_o^{(a_1,\ldots,a_n)}} = \frac{\sum_i \sum_{k=1}^{+\infty} \sum_{a_s\in A_B, s\in\hat{l}, l\leq n} d_i m_i^2 (-1)^{k+1} k^{l-2} N_{a_1 i}\ldots N_{a_l i}\exp\left(\frac{k}{T}\mu_i\right) K_2\left(\frac{km_i}{T}\right)}{\sum_i \sum_{k=1}^{+\infty} \sum_{a_s\in A_B, s\in\hat{o}, o\leq n} d_i m_i^2 (-1)^{k+1} k^{o-2} N_{a_1 i}\ldots N_{a_o i}\exp\left(\frac{k}{T}\mu_i\right) K_2\left(\frac{km_i}{T}\right)} \qquad \text{(C.19)}$$

where $\mu_i = \sum_{j\in A} N_{ji}\mu_j$.

C.5.1 Ratios of susceptibilities for a net-baryon distribution

If we want to obtain the susceptibilities for a net-baryon distribution, Eq. (C.18) transforms into

$$\begin{aligned}
\chi_l^{net(a_1,\ldots,a_n)} &= T^l \frac{\partial^l (P/T^4)}{\partial\mu_{a_1}\ldots\partial\mu_{a_l}} \qquad \text{(C.20)}\\
&= \frac{1}{2\pi^2 T^2}\sum_i \sum_{k=1}^{+\infty} \sum_{a_s\in A_B, s\in\hat{l}, l\leq n} d_i m_i^2 (-1)^{k+1} k^{l-2} (N_{a_1 i} - N_{\bar{a}_1 i})\ldots(N_{a_l i} - N_{\bar{a}_l i})\times\\
&\times\ \exp\left(\frac{k}{T}\sum_{j\in A} N_{ji}\mu_j\right) K_2\left(\frac{km_i}{T}\right)
\end{aligned}$$

and Eq. (C.19) transforms accordingly.

Appendix D

Clebsch-Gordan Coefficients

In the following Chapter, the definition and basic properties of Clebsch-Gordan Coefficients will be introduced, along with a way of calculating them explicitly. All performed calculations were taken from and are in accordance with [27].

D.1 Definition and properties

A system of two mechanical angular momenta can be characterized by operators of the total angular momentum $\hat{\mathbf{J}}^{\mathbf{2}}$, $\hat{J}_z$ and operators of the individual angular momenta $\hat{\mathbf{J}}_{\mathbf{1}}^{\mathbf{2}}$, $\hat{J}_{1z}$, $\hat{\mathbf{J}}_{\mathbf{2}}^{\mathbf{2}}$, $\hat{J}_{2z}$. Thus, two groups of mutually commuting operators can be written down:

· $\hat{\mathbf{J}}_{\mathbf{1}}^{\mathbf{2}}$, $\hat{\mathbf{J}}_{\mathbf{2}}^{\mathbf{2}}$,$\hat{\mathbf{J}}^{\mathbf{2}}$, $\hat{J}_z$
· $\hat{\mathbf{J}}_{\mathbf{1}}^{\mathbf{2}}$, $\hat{\mathbf{J}}_{\mathbf{2}}^{\mathbf{2}}$,$\hat{J}_{1z}$, $\hat{J}_{2z}$,

which leads to the following basis states:

· coupled eigenstates, denoted as $\mid J_1, J_2; J, M\rangle$ or $\mid J, M\rangle$
· uncoupled eigenstates, denoted as $\mid J_1, J_2; M_1, M_2\rangle$ or $\mid (M_1, M_2)\rangle$

Since these are both **complete** basis systems, they are related to each other via a unitary transformation

$$\mid J, M\rangle = \sum_{M_1, M_2} \mid (M_1, M_2)\rangle \left\langle (M_1, M_2) \mid J, M\right\rangle . \tag{D.1}$$

The amplitudes $\langle (M_1, M_2) \mid J, M\rangle$ in Eq. (D.1) are called *Clebsch-Gordan (CG) coefficients*, whose most important properties can be summed up as follows:

· CG-coefficients vanish if $M \neq M_1 + M_2$
· The following selection rule can be applied to the total angular momentum J: $\mid J_1 - J_2 \mid \leq J \leq J_1 + J_2$
· CG-coefficients can be chosen as real.

D.2 Conventional methods of deriving the CG Coefficients and general formulae

In order to derive the specific form of the CG-coefficients, the iterative application of the lowering operator $\hat{J}_- \equiv \hat{J}_x - i\hat{J}_y$ on the maximum state is used. The maximum state can be expressed as

$$| J, M\rangle = | (M_1 = J_1, M_2 = J_2)\rangle \tag{D.2}$$

where $J = J_1 + J_2$ and $M = M_1 + M_2$. The effect of the lowering operator on $| J, M\rangle$ is given by

$$\hat{J}_- | J, M\rangle = \sqrt{(J+M)(J-M+1)}\, | J, M-1\rangle\,. \tag{D.3}$$

If we project the resulting states onto the coupled product state $\langle(M_1, M_2)$, we obtain the CG-coefficients.

The explicit formula for the CG-coefficients is given by the so called **Racah** formula

$$\begin{aligned}\langle(M_1, M_2) \mid J, M\rangle &= \sum_k (-1)^k \sqrt{2J+1} \qquad \text{(D.4)}\\ &\times \sqrt{\frac{(J_1+J_2-J)!(J_1-J_2+J)!(J_2-J_1+J)!}{(J_1+J_2+J+1)!(J_1-M_1-k)^2!(J_2+M_2-k)!^2 k!^2}}\\ &\times \sqrt{\frac{(J_1+M_1)!(J_2+M_2)!(J+M)!(J_1-M_1)!(J_2-M_2)!(J-M)!}{(J-J_2+M_1+k)!^2(J-J_1-M_2+k)!^2(J_1+J_2-J-k)!^2}}.\end{aligned}$$

Obviously, both methods are very formal, which makes the calculations even in the case of very small angular momenta quite legthy and impractical, which is why the values of CG-coefficients have been listed in tables. These tables are in Figure (D.1) and Figure (D.2).

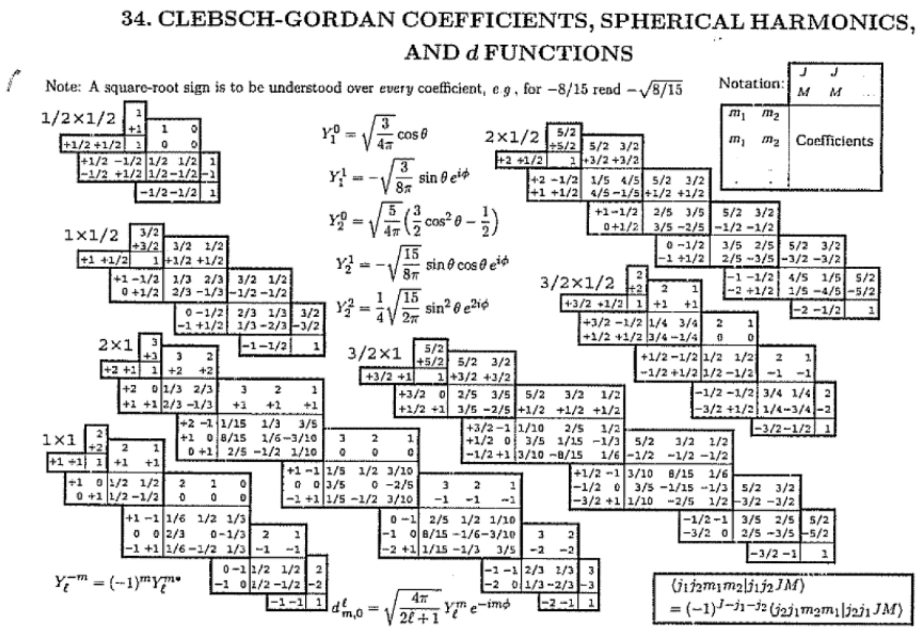

Figure D.1: Table of Clebsch-Gordan coefficients: Part 1. Taken from [28].

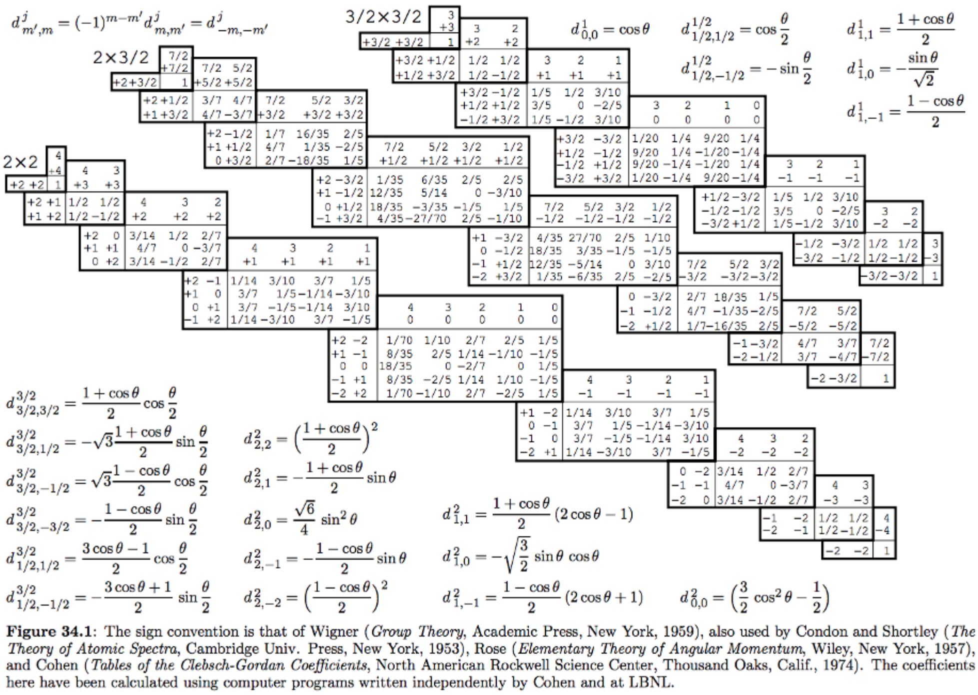

Figure D.2: Table of Clebsch-Gordan coefficients: Part 2. Taken from [28].

Appendix E

Update of the list of hadrons and the list of resonance decays within the DRAGON Monte Carlo model

One of our tasks was also to update the decay chain tables within the DRAGON programme, whose documentation can be found in [25]. All the necessary mathematical apparatus has been laid down earlier in this thesis. Here, only a brief overview will be provided with emphasis on said update, whose results have been elaborated on earlier on in the Chapter "Results". This update has been performed using PDG - measurements from 2017, yet for our purposes (meaning the measurements relevant for our aim), these are much the same even for the current update, which can be found in [15].

E.1 DRAGON

DRAGON is a Monte Carlo generator of the final state of hadrons emitted from an ultrarelativistic nuclear collision. The name DRAGON stands of DRoplet and hAdron GeneratOr for Nuclear collisions. The model upon which it is based is similar to THERMINATOR, yet in case of DRAGON, emission from fragments is included. The fragmentation at hadronisation phase transition is a result of an abrupt rise of bulk viscosity at T_c, which can make the fireball very stiff and if strong expansion - which results from pre-existing longitudinal movement of the incident nucleons and the inner pressure of the matter - is present, said fragmentation is very likely to occur. The structure of the programme is depicted in FigureE.1.

E.2 Updated particle properties

Our primary concern were the files **params.hpp** and **resonances.input**. The file **params.hpp** includes the parameters of the model and steering constants for compiling and running. This also includes the list of all species called **pproperties**, which is an array whose entries are records for individual species. The original version from 2009

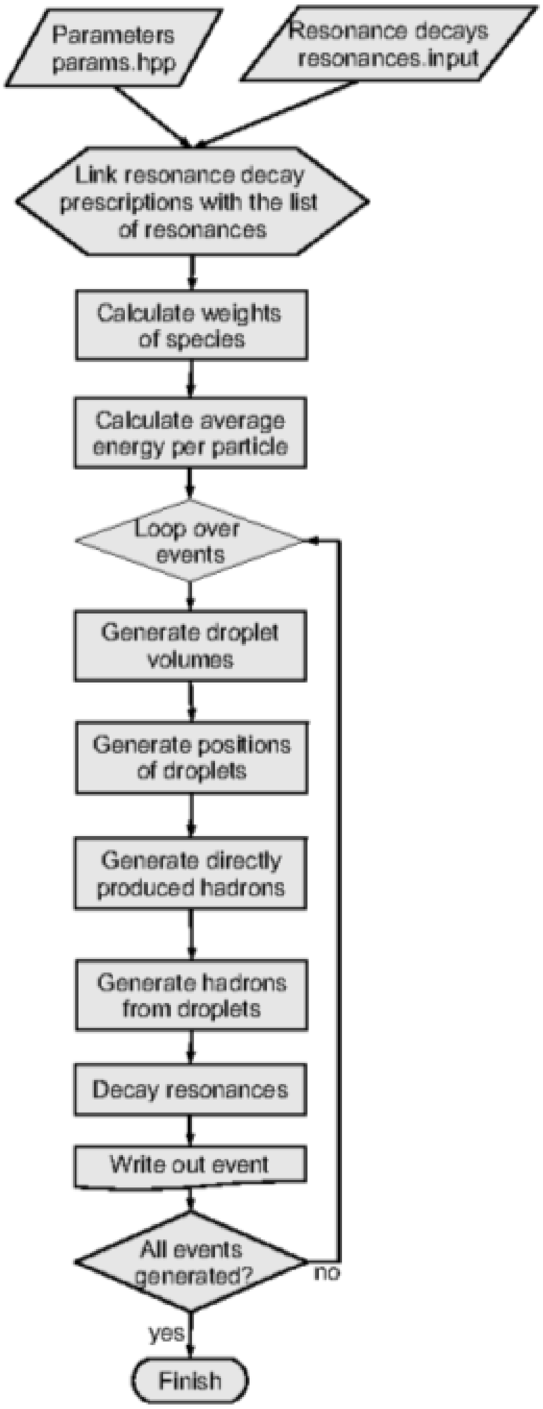

Figure E.1: The structure of DRAGON. Taken from [25].

included all baryons with masses up to 2.0 GeV/c^2 and mesons up to 1.5 GeV/c^2. After the update was performed, all baryons with masses up to 2.5 GeV/c^2 and mesons up to 2.0 GeV/c^2 are included. The file **resonances.input** is a list of resonance decays. If at least one decay mode for given species is listed in this file, that species is treated as an unstable resonance and if a species is not listed, it is treated as stable. The branching ratios can be found in [15], whilst for individual combinations (e. g. K^+K^- or $K^0\bar{K}^0$, which both result from the decay of $f_2(2300)$), this branching ratio had to be multiplied by the corresponding CG-coefficient (see Appendix D).

Before we proceed to the update tables, a few remarks concerning the syntax are in order, all of them being in full accordance with [25]. Each line of the vector **PChem pproperties**[], which are structures storing the records of properties of individual species and has as many entries as specified by **NOSpec**, represents one species and consists of the following:

(1) Monte Carlo ID number of species according to Particle Data Group [29]; integer
(2) mass in GeV/c^2; double
(3) baryon number; integer
(4) strangeness; integer
(5) 1 if the species is a boson, 0 if the species is a fermion
(6) spin degeneracy; integer
(7) 1., double (calculated later by the programme)
(8) 1., double (calculated later by the programme)
(9) -1, integer; determined by the programme, links the species to its decay prescriptions; remains -1 for stable particles.

The structure of the file **resonances.input** has been elaborated on above. An excerpt from said file can be seen in Figure E.2.

```
# rho+
213         0.766     0.150
1.          211       0.13957   111   0.13498

# rho0
113         0.769     0.151
1.          211       0.13957   -211  0.13957

# rho-
-213        -1.       0.150
1.          -211      -1.       111   -1.

# omega
223         0.782     0.00844
0.888       -211      0.13957   111   0.13498   211   0.13957
0.0221      -211      0.13957   211   0.13957
0.085       111       0.13457   22    0.

# eta'(958)
331         0.95778   0.000203
0.445       211       0.13957   -211  0.13957   221   0.54751
0.294       113       0.769     22    0.
0.208       111       0.13498   111   0.13498   221   0.54751
0.0303      223       0.782     22    0.
0.0212      22        0.        22    0.
```

Figure E.2: An excerpt from the file **resonances.input**. Taken from [25].

As one can see, the structure of this file is the following:

(1) A record of all decay modes of one resonance starts with a line with three numbers: the MC code of the resonance, its mass in GeV/c^2 and its width in GeV. If -1. is put in the position of the mass, the code automatically reads the mass from **pproperties**[].

(2) A record of a two- or three-body decay contains five or seven numbers, respectively. In both cases, there is the branching ratio for the decay channel multiplied by the CG-coefficient (if possible). This is followed by the MC code of the first daughter particle and its mass, then the same for the second or third daughter particle.

If the sum of branching ratios is not equal to 1, the program will multiply them with a common factor, so that the sum will be equal to 1. Moreover, any line starting with # - or an empty one - is considered as a comment and therefore not included in the calculations.

E.2.1 Tables of Changes

In accordance with [8], particles listed in the following Table have been considered stable in our calculations. We have used the DRAGON syntax. In total, we have 26 stable particles in contrast to the original 23, since $\eta, \Sigma^0, \bar{\Sigma}^0$ have been added. In the other Tables, the newly added **mesons, nucleon resonances, Δ-resonances, Λ-resonances, Σ-resonances and Ξ-resonances** are summed up along with their properties. For the sake of clarity, the tables are presented for each type of resonances separately.

Particle	Monte Carlo ID	Mass [GeV/c^2]	B	S	Boson (1)/Fermion(0)	Degeneracy
π^+	211	0.13957	0	0	1	1
π^-	-211	0.13957	0	0	1	1
π^0	111	0.13498	0	0	1	1
K^0	311	0.4976	0	1	1	1
$\bar{K}^0$	-311	0.4976	0	-1	1	1
K^+	321	0.4936	0	1	1	1
K^-	-321	0.4936	0	-1	1	1
η	221	0.54786	0	0	1	1
p	2212	0.93827	1	0	0	2
n	2112	0.93957	1	0	0	2
$\bar{p}$	-2212	0.93827	-1	0	0	2
$\bar{n}$	-2112	0.93957	-1	0	0	2
Λ^0	3122	1.11568	1	-1	0	2
$\bar{\Lambda}^0$	-3122	1.11568	-1	1	0	2
Σ^+	3222	1.18937	1	-1	0	2
$\bar{\Sigma}^+$	-3222	1.18937	-1	1	0	2
Σ^0	3212	1.192642	1	-1	0	2
$\bar{\Sigma}^0$	-3212	1.192642	-1	1	0	2
Σ^-	3112	1.197449	1	-1	0	2
$\bar{\Sigma}^-$	-3112	1.197449	-1	1	0	2
Ξ^0	3322	1.31483	1	-2	0	2
Ξ^-	3312	1.32131	1	-2	0	2
$\bar{\Xi}^0$	-3322	1.31483	-1	2	0	2
$\bar{\Xi}^-$	-3312	1.32131	-1	2	0	2
Ω^-	3334	1.67245	1	-3	0	4
$\bar{\Omega}^-$	-3334	1.67245	-1	3	0	4

Table E.1: Table of stable particle species.

Particle	Monte Carlo ID	Mass[GeV $/c^2$]	B	S	Boson (1)/Fermion(0)	Degeneracy
$f_2'(1525)$	335	1.525	0	0	1	5
$\pi_1^+(1600)$	9010213	1.662	0	0	1	3
$\pi_1^0(1600)$	9010113	1.662	0	0	1	3
$\pi_1^-(1600)$	-9010213	1.662	0	0	1	3
$\eta(1645)$	10225	1.617	0	0	1	5
$\omega(1650)$	30223	1.67	0	0	1	3
$\omega_3(1670)$	227	1.667	0	0	1	7
$\pi_2^+(1670)$	10215	1.6722	0	0	1	5
$\pi_2^0(1670)$	10115	1.6722	0	0	1	5
$\pi_2^-(1670)$	-10215	1.6722	0	0	1	5
$\rho_3^+(1690)$	217	1.6888	0	0	1	7
$\rho_3^0(1690)$	117	1.6888	0	0	1	7
$\rho_3^-(1690)$	-217	1.6888	0	0	1	7
$f_0(1710)$	10331	1.723	0	0	1	1
$\pi^+(1800)$	9010211	1.812	0	0	1	1
$\pi^0(1800)$	9010111	1.812	0	0	1	1
$\pi^-(1800)$	-9010211	1.812	0	0	1	1
$\phi_3(1850)$	337	1.854	0	0	1	7
$f_2(1950)$	9050225	1.944	0	0	1	5
$f_2(2010)$	9060225	2.04	0	0	1	5
$a_4^+(2040)$	219	1.995	0	0	1	9
$a_4^0(2040)$	119	1.995	0	0	1	9
$a_4^-(2040)$	-219	1.995	0	0	1	9
$f_4(2050)$	229	2.018	0	0	1	9
$f_2(2300)$	9080225	2.297	0	0	1	5
$f_2(2340)$	9090225	2.345	0	0	1	5
$K_2^+(1770)$	10325	1.773	0	1	1	5
$K_2^-(1770)$	-10325	1.773	0	-1	1	5
$K_2^0(1770)$	10315	1.773	0	1	1	5
$\bar{K}_2^0(1770)$	-10315	1.773	0	-1	1	5
$K_3^{*+}(1780)$	327	1.776	0	1	1	7
$K_3^{*-}(1780)$	-327	1.776	0	-1	1	7
$K_3^{*0}(1780)$	317	1.776	0	1	1	7
$\bar{K}_3^{*0}(1780)$	-317	1.776	0	-1	1	7
$K_2^+(1820)$	20325	1.819	0	1	1	5
$K_2^-(1820)$	-20325	1.819	0	-1	1	5
$K_2^0(1820)$	20315	1.819	0	1	1	5
$\bar{K}_2^0(1820)$	-20315	1.819	0	-1	1	5

Table E.2: Table of newly added mesons.

Particle	Monte Carlo ID	Mass [GeV/c^2]	B	S	Boson (1)/Fermion(0)	Degeneracy
$N^+(1875)$	192212	1.9	1	0	0	4
$\bar{N}^+(1875)$	-192212	1.9	-1	0	0	4
$N^0(1875)$	192112	1.9	1	0	0	4
$\bar{N}^0(1875)$	-192112	1.9	-1	0	0	4
$N^+(1900)$	202212	1.92	1	0	0	4
$\bar{N}^+(1900)$	-202212	1.92	-1	0	0	4
$N^0(1900)$	202112	1.92	1	0	0	4
$\bar{N}^0(1900)$	-202112	1.92	-1	0	0	4
$N^+(2190)$	212212	2.075	1	0	0	8
$\bar{N}^+(2190)$	-212212	2.075	-1	0	0	8
$N^0(2190)$	212112	2.075	1	0	0	8
$\bar{N}^0(2190)$	-212112	2.075	-1	0	0	8
$N^+(2220)$	222212	2.17	1	0	0	10
$\bar{N}^+(2220)$	-222212	2.17	-1	0	0	10
$N^0(2220)$	222112	2.17	1	0	0	10
$\bar{N}^0(2220)$	-222112	2.17	-1	0	0	10
$N^+(2250)$	232212	2.2	1	0	0	10
$\bar{N}^+(2250)$	-232212	2.2	-1	0	0	10
$N^0(2250)$	232112	2.2	1	0	0	10
$\bar{N}^0(2250)$	-232112	2.2	-1	0	0	10
$N^+(2600)$	242212	2.6	1	0	0	12
$\bar{N}^+(2600)$	-242212	2.6	-1	0	0	12
$N^0(2600)$	242112	2.6	1	0	0	12
$\bar{N}^0(2600)$	-242112	2.6	-1	0	0	12

Table E.3: Table of newly added Nucleon Resonances.

Particle	Monte Carlo ID	Mass [GeV/c^2]	B	S	Boson (1)/Fermion(0)	Degeneracy
$\Delta^{++}(2420)$	192224	2.42	1	0	0	12
$\Delta^{+}(2420)$	192214	2.42	1	0	0	12
$\Delta^{0}(2420)$	192114	2.42	1	0	0	12
$\Delta^{-}(2420)$	191114	2.42	1	0	0	12
$\bar{\Delta}^{++}(2420)$	-192224	2.42	-1	0	0	12
$\bar{\Delta}^{+}(2420)$	-192214	2.42	-1	0	0	12
$\bar{\Delta}^{0}(2420)$	-192114	2.42	-1	0	0	12
$\bar{\Delta}^{-}(2420)$	-191114	2.42	-1	0	0	12

Table E.4: Table of newly added Δ-Resonances.

Particle	Monte Carlo ID	Mass [GeV/c^2]	B	S	Boson (1)/Fermion(0)	Degeneracy
$\Lambda(2100)$	213122	2.1	1	-1	0	8
$\bar{\Lambda}(2100)$	-213122	2.1	-1	1	0	8
$\Lambda(2110)$	223122	2.11	1	-1	0	6
$\bar{\Lambda}(2110)$	-223122	2.11	-1	1	0	6
$\Lambda(2350)$	233122	2.35	1	-1	0	10
$\bar{\Lambda}(2350)$	-233122	2.35	-1	1	0	10

Table E.5: Table of newly added Λ-Resonances.

Particle	Monte Carlo ID	Mass [GeV/c^2]	B	S	Boson (1)/Fermion(0)	Degeneracy
$\Sigma^+(2030)$	193222	2.03	1	-1	0	8
$\Sigma^0(2030)$	193212	2.03	1	-1	0	8
$\Sigma^-(2030)$	193112	2.03	1	-1	0	8
$\bar{\Sigma}^+(2030)$	-193222	2.03	-1	1	0	8
$\bar{\Sigma}^0(2030)$	-193212	2.03	-1	1	0	8
$\bar{\Sigma}^-(2030)$	-193112	2.03	-1	1	0	8

Table E.6: Table of newly added Σ-Resonances.

Particle	Monte Carlo ID	Mass [GeV/c^2]	B	S	Boson (1)/Fermion(0)	Degeneracy
$\Xi^0(1530)$	153322	1.531	1	-2	0	4
$\Xi^-(1530)$	153312	1.531	1	-2	0	4
$\bar{\Xi}^0(1530)$	-153322	1.531	-1	2	0	4
$\bar{\Xi}^-(1530)$	-153312	1.531	-1	2	0	4

Table E.7: Table of newly added Ξ-Resonances.

Bibliography

[1] W. Florkowski: *Phenomenology of Ultrarelativistic Heavy-Ion Collisions*, World Scientific, Singapore 2010

[2] V. V. Begun et al.: *Multiplicity fluctuations in hadron resonance gas*, Phys. Rev. C **74** (2006) 044903

[3] P. Alba et al.: *Sensitivity of multiplicity fluctuations to freeze-out conditions in heavy ion collisions*, Phys. Rev. C **92** (2015) 064910

[4] G. Torrieri, J. Letessier, J. Rafelski: *SHAREv2: Fluctuations and comprehensive treatment of decay feed-down*, Comput. Phys. Commun. **175** (2006) 635

[5] G. Torrieri, S. Jeon, J. Rafelski: *Particle yield fluctuations and chemical nonequilibrium in Au+Au collisions at* $s_{NN}^{1/2} = 200\ GeV$, Phys. Rev. C **74** (2006) 024901

[6] H. Bebie, P. Gerber, J. L. Goity, H. Leutwyler: *The role of the entropy in an expanding hadronic gas*, Nucl. Phys. B378 (1992) 95

[7] F. Becattini et al.: *Multiplicity fluctuations in the hadron gas with exact conservation laws*, arXiv:nucl-th/0507039v1, 14 Jul 2005, Phys. Rev. C72 (2005) 064904

[8] M. Nahrgang et al.: *Impact of resonance regeneration and decay on the net proton fluctuations in a hadron resonance gas*, Eur. Phys. J. C(2015) 75:573, DOI 10.1140/epjc/s10052-015-3775-0, 1 Dec 2015

[9] J. Fu: *Higher moments of net-proton multiplicity distributions in heavy ion collisions at chemical freeze-out*, Phys. Let. B 722 (2013) 144-150, 9 Apr 2013

[10] F. Karsch, K. Redlich: *Probing freeze-out conditions in heavy ion collisions with moments of charge fluctuations*, arXiv:1007.2581v1 [hep-ph], 15 Jul 2010, Phys. Let. B 695 (2011) 136-142

[11] M. Kitazawa, M. Asakawa: *Revealing baryon number fluctuations from proton number fluctuations in relativistic heavy ion collisions*, arXiv:1107.2755v2 [nucl-th], 2 Mar 2012

[12] L. Adamczyk et al.: *Energy Dependence of Moments of Net-Proton Multiplicity Distributions at RHIC*, PRL 112, 032302 (2014), 24 Jan 2014

[13] M. Kitazawa, M. Asakawa: *Relation between baryon number fluctuations and experimentally observed proton number fluctuations in relativistic heavy ion collisions*, arXiv:1205.3292v1 [nucl-th], 15 May 2012, Phys. Rev. C86 (2012) 024904

[14] X. Luo: *Error Estimation for Moments Analysis in Heavy Ion Collision Experiment*, arXiv:1109.0593v2 [physics.data-an], 2 Nov 2016, J. Phys. G: Nucl. Part. Phys. 39, 025008 (2012)

[15] M. Tanabashi et al. (Particle Data Group), Phys. Rev. D 98, 030001 (2018)

[16] X. Luo, Nu Xu: *Search for the QCD Critical Point with Fluctuations of Conserved Quantities in Relativistic Heavy-Ion Collisions at RHIC: An Overview*, arXiv:1701.02105v3 [nucl-ex] 17 Oct 2017, Nucl. Sci. Tech. 28 (2017) no. 8, 112

[17] H. Kerson: *Statistical Mechanics, 2nd Edition*, Singapore, 1987

[18] F. Sanino, I. Bearden, B. Tomášik, T. Dossing: *Topics in modern nuclear physics*, Lecture Notes, University of Copenhagen, 2005

[19] J. Lettesier, J. Rafelski: *Hadrons and Quark Gluon Plasma*, Cambridge UP, 2002

[20] W. Weise: *Nuclear chiral dynamics and phases of QCD*. Prog. Part. Nucl. Phys. 67 (2012) 299-311 arXiv:1201.0950 [nucl-th]

[21] L. Adamczyk et al.: *Bulk properties of the medium produced in relativistic heavy-ion collisions from the beam energy scan program*, Phys. Rev. C 96, 044904 (2017)

[22] V. Mantovani Sarti, P. Alba et al.: *Fluctuations of conserved charges within a Hadron Resonance Gas approach: freeze-out conditions from net-proton and net-charge fluctuations at RHIC*, arXiv:1403.4903v2 [hep-ph] 21 Jul 2014, Phys. Let. B 2014.09.052

[23] P. Braun-Munzinger, K. Redlich, J. Stachel: *Particle Production in Heavy-Ion Collisions* (R.C. Hwa, X.-N. Wang ed., s. 491), World Scientific, Singapore, 2003

[24] Y. Aoki (Wuppertal U.), Z. Fodor, S.D. Katz (Wuppertal U., Eotvos U.), K.K. Szabo (Wuppertal U.), Sep 2006, 13 pp, Phys. Lett. B643 (2006) 46-54

[25] B. Tomášik: DRAGON: *Monte Carlo generator of particle production from a fragmented fireball in ultrarelativistic nuclear collisions*, arXiv:0806.4770v2 [nucl-th], 9 Jan 2009

[26] M. Abramowitz, I. Stegun: *Handbook of Mathematical Functions With Formulas, Graphs and Mathematical Tables*, U. S. Government Printing Office, Washington, D. C., June 1964

[27] K. Schertler, M. H. Thoma: *Combinatorial Computation of Clebsch-Gordan Coefficients*, arXiv:quant-ph/9504015v1 20 Apr 1995

[28] Table of Clebsch-Gordan Coefficients: http://pdg.lbl.gov/2002/clebrpp.pdf, Annalen Phys. 5 (1996) 103

[29] L. Garren et al. (Particle Data Group), pdg.lbl.gov/2006/mcdata/mc particle id contents.html .